DYSTONIA

November

Models, Mechanisms, and Maturation in Developmental Dystonia

Issue Editors

Roy Sillitoe
Baylor College of Medicine, United States

Jason Singh Gill
Baylor College of Medicine, United States

Meike E. Van Der Heijden
Baylor College of Medicine, United States

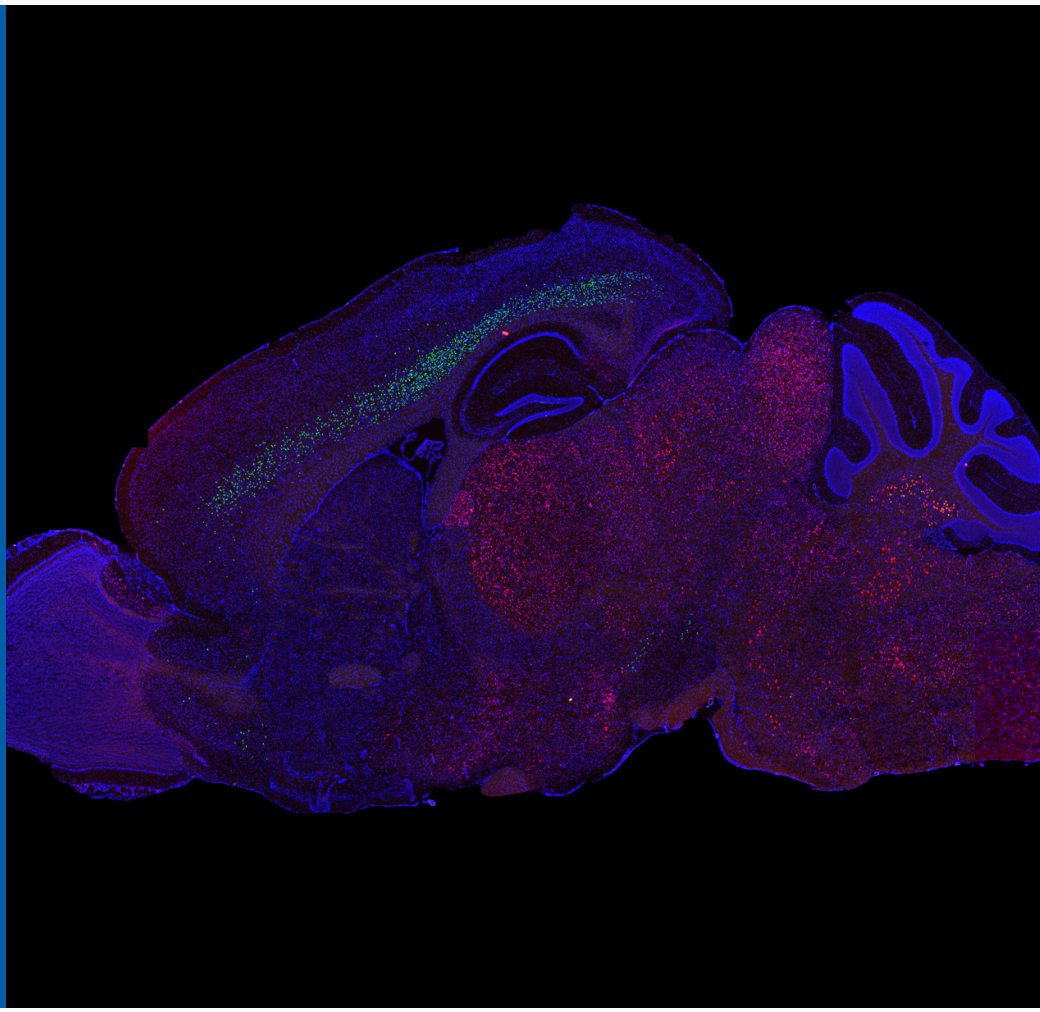

frontiers | Publishing Partnerships

Models, Mechanisms, and Maturation in Developmental Dystonia

ISSN 2813-2106
ISBN 978-2-8325-3954-5
DOI 10.3389/978-2-8325-3954-5

Dystonia, characterized by involuntary over-contractions or co-contractions of muscle groups, is the third most common movement disorder and afflicts an estimated 300-400 million individuals worldwide. Despite the convergence on abnormal muscle activity, the underlying pathophysiology of dystonia is wide-ranging, diverse, and difficult to elucidate. This reality is reflected in the clinic, where dystonia poses great diagnostic and therapeutic challenges. However, major inroads have been made in defining the causes, with mounting efforts rising to meet the demand of developing therapies to treat this group of devastating disorders. Specifically, the identification of disease-causing mutations in inherited, often childhood-onset, forms of dystonia has opened the door to generate experimental models to understand the genetic and neural network culprits that cause dystonia. However, there are still many outstanding questions in the field. Why do genetic forms of dystonia often present early in life? What protects against symptom development in non-manifesting carriers of dystonia-causing genetic mutations? Does neurodevelopmental maturation contribute to symptom acquisition, and does maturation reflect a critical therapeutic window? And importantly, can we exploit the mechanisms that underlie dystonia to design effective therapies and new treatments? This special issue covers recent perspectives on the genetic, molecular, and network mechanisms underlying developmental dystonia.

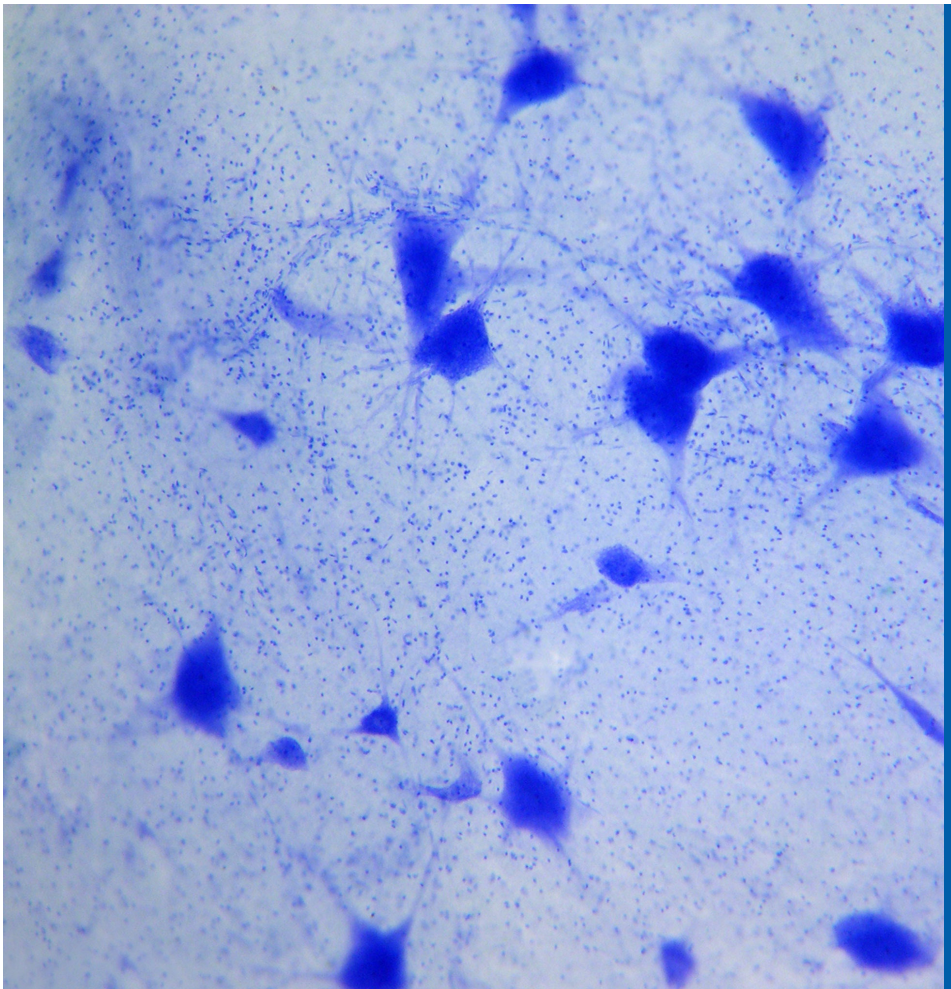

Table of contents

DYSTONIA

TYPE Editorial
PUBLISHED 11 September 2023
DOI 10.3389/dyst.2023.11922

OPEN ACCESS

*CORRESPONDENCE
Roy V. Sillitoe,
sillitoe@bcm.edu

RECEIVED 14 August 2023
ACCEPTED 25 August 2023
PUBLISHED 11 September 2023

CITATION
Gill JS, van der Heijden ME, Shaikh AG and Sillitoe RV (2023), Editorial: Models, mechanisms, and maturation in developmental dystonia.
Dystonia 2:11922.
doi: 10.3389/dyst.2023.11922

Editorial: Models, mechanisms, and maturation in developmental dystonia

Jason S. Gill[1,2,3], Meike E. van der Heijden[1,2], Aasef G. Shaikh[4] and Roy V. Sillitoe[1,2,5,6,7]*

[1]Department of Pathology and Immunology, Baylor College of Medicine, Houston, TX, United States, [2]Jan and Dan Duncan Neurological Research Institute at Texas Children's Hospital, Houston, TX, United States, [3]Division of Pediatric Neurology and Developmental Neuroscience, Baylor College of Medicine, Houston, TX, United States, [4]Department of Neurology, University Hospitals Cleveland Medical Center, Case Western Reserve University, Cleveland, OH, United States, [5]Department of Neuroscience, Baylor College of Medicine, Houston, TX, United States, [6]Department of Pediatrics, Baylor College of Medicine, Houston, TX, United States, [7]Development, Disease Models & Therapeutics Graduate Program, Baylor College of Medicine, Houston, TX, United States

KEYWORDS

dystonia, development, maturation, models, mechanism

Editorial on the Special Issue
Models, mechanisms, and maturation in developmental dystonia

In this Special Issue, a comprehensive examination of dystonia pathogenesis is undertaken through four original research papers. These studies use manipulations at various sites in the cerebello-thalamo-striatal dystonia network using both genetic and functional network analyses. Furthermore, the papers presented here offer a fine-grain dissection of the pathophysiology of one of the most well studied genetic dystonias, DYT1 (and the associated mouse Dyt1), and shed light on possible therapeutic interventions that could be valuable.

The dissection of Dyt1 dystonia pathophysiology includes the work of Xing et al., in which a neurophysiological analysis of a knock-in mouse model of human Dyt1 dystonia reveals alterations in cholinergic tone and dopamine signaling in striatal interneuron populations. This study offers insight into the functional network alterations underlying this genetic dystonia, an important step in understanding this enigmatic disorder. Yellajoshyula et al. delve further into the network effects of Dyt1 dystonia while also taking advantage of the sophisticated manipulations offered by mouse genetics. Using conditional knock-out technology and laser microdissection, Yellajoshyula et al. look at the morphology of striatal cholinergic interneuron-enriched populations and compare them to GABAergic-enriched populations, finding unique differences in dendritic morphology in these neuronal populations that are relevant to dystonia. Furthermore, using high throughput -omics methodologies, they provide a database for understanding downstream gene expression changes that will open up avenues for further exploration, potentially of broader dystonia etiologies. Rounding out the issue's dissection of Dyt1 dystonia, King et al. develop and exploit a translationally-driven approach towards the development of a biomarker platform with validation through application of a candidate therapeutic intervention. Using mouse

embryonic fibroblasts derived from the Dyt1 knock-in mouse model, King et al. isolate and characterize extracellular vesicles (referred to as EVs) from culture, which is a proof of concept for human blood based EVs, and importantly show that application of a candidate therapy, ritonavir, that is known to act on the previously implicated integrated stress response pathway, may correct some of the abnormal changes in the affected Dyt1 EVs.

Finally, Van Der Heijden et al. take a different approach, focusing on functional network manipulations and developmental dystonia. They use targeted and cell-type specific genetic manipulations to functionally silence neurotransmission from inferior olivary neurons onto their target Purkinje cells, a model previously shown to induce severe dystonia in mice, and use a suite of behavioral tools to characterize early onset dystonia in postnatal mice. Given the paucity of studies and tools looking at early onset dystonia, and its importance in clinical pediatric neurology, this is a powerful step towards addressing a gap in the field of dystonia research.

Together, the research perspectives assembled in this Special Issue illuminate both novel technical approaches for better understanding dystonia, covering analytic techniques from laser microdissection to extracellular vesicle analysis, as well as deep analysis of existing models, from the conditional approach used in Yellajoshyula et al. to the novel biomarker platform developed by King et al. Indeed, a key difficulty in understanding dystonia has been the functional component, which manifests both in the incomplete penetrance of genetic dystonias such as Dyt1 but also in the idiopathic dystonias. Van Der Heijden et al. tackle this difficult issue by using an anatomically-driven brain network manipulation and the application of behavioral assays that conveniently characterize motor dysfunction in mouse pups. Through a close reading of the papers in this Special Issue, readers will gain not only an understanding of one of the most important genetic dystonias, Dyt1, but come away with an analytic toolkit to further their own explorations towards untangling the problems in dystonia.

Author contributions

All authors listed have made a substantial, direct, and intellectual contribution to the work and approved it for publication.

Funding

This work was supported by Baylor College of Medicine (BCM), Texas Children's Hospital, The Hamill Foundation, the Dystonia Medical Research Foundation (DMRF) and by the National Institutes of Neurological Disorders and Stroke (NINDS) from R01NS100874, R01NS119301, and R01NS127435 to RS. Research reported in this publication was also supported by the Eunice Kennedy Shriver National Institute of Child Health & Human Development of the National Institutes of Health under Award Number P50HD103555 for work with the Cell and Tissue Pathogenesis Core (the BCM IDDRC). JG was supported by 1K08NS121600. MvdH was supported by a postdoctoral award from the DMRF and by 1K99NS130463. AS was the recipient of a DMRF Clinical Fellowship and is supported by VA CSR&D Merit Review (I01 CX002086-01A2), VA RR&D Merit Review (I01 RX00367-01A2), VA RR&D SPiRE (I21 RX003878-01), Pablove Foundation for Cancer Research, Care-source Ohio Community Partnership Grant, American Parkinson's Disease Association George C. Cotzias fellowship. AS holds philanthropic support in form of Penni and Stephen Weinberg Chair in Brain Health.

Conflict of interest

AS and RS are Editors in Chief of Dystonia.

The remaining authors declare that the research was conducted in the absence of any commercial or financial relationships that could be construed as a potential conflict of interest.

Author disclaimer

The content is solely the responsibility of the authors and does not necessarily represent the official views of the National Institutes of Health.

DYSTONIA

BRIEF RESEARCH REPORT
published: 08 September 2022
doi: 10.3389/dyst.2022.10494

Quantification of Behavioral Deficits in Developing Mice With Dystonic Behaviors

Meike E. Van Der Heijden[1,2], *Jason S. Gill*[2,3], *Alejandro G. Rey Hipolito*[1,2,4], *Luis E. Salazar Leon*[1,2,4] *and Roy V. Sillitoe*[1,2,3,4,5]*

[1]Department of Pathology & Immunology, Baylor College of Medicine, Houston, TX, United States, [2]Jan and Dan Duncan Neurological Research Institute at Texas Children's Hospital, Houston, TX, United States, [3]Department of Pediatrics, Baylor College of Medicine, Houston, TX, United States, [4]Department of Neuroscience, Baylor College of Medicine, Houston, TX, United States, [5]Development, Disease Models & Therapeutics Graduate Program, Baylor College of Medicine, Houston, TX, United States

Converging evidence from structural imaging studies in patients, the function of dystonia-causing genes, and the comorbidity of neuronal and behavioral defects all suggest that pediatric-onset dystonia is a neurodevelopmental disorder. However, to fully appreciate the contribution of altered development to dystonia, a mechanistic understanding of how networks become dysfunctional is required for early-onset dystonia. One current hurdle is that many dystonia animal models are ideally suited for studying adult phenotypes, as the neurodevelopmental features can be subtle or are complicated by broad developmental deficits. Furthermore, most assays that are used to measure dystonia are not suited for developing postnatal mice. Here, we characterize the early-onset dystonia in *Ptf1a*^{Cre};*Vglut2*$^{fl/fl}$ mice, which is caused by the absence of neurotransmission from inferior olive neurons onto cerebellar Purkinje cells. We investigate motor control with two paradigms that examine how altered neural function impacts key neurodevelopmental milestones seen in postnatal pups (postnatal day 7–11). We find that *Ptf1a*^{Cre};*Vglut2*$^{fl/fl}$ mice have poor performance on the negative geotaxis assay and the surface righting reflex. Interestingly, we also find that *Ptf1a*^{Cre};*Vglut2*$^{fl/fl}$ mice make fewer ultrasonic calls when socially isolated from their nests. Ultrasonic calls are often impaired in rodent models of autism spectrum disorders, a condition that can be comorbid with dystonia. Together, we show that these assays can serve as useful quantitative tools for investigating how neural dysfunction during development influences neonatal behaviors in a dystonia mouse model. Our data implicate a shared cerebellar circuit mechanism underlying dystonia-related motor signs and social impairments in mice.

Keywords: dystonia, cerebellum, behavior, development, neurodevelopmental disorders

OPEN ACCESS

Edited by:
Aasef Shaikh,
Case Western Reserve University, United States

Reviewed by:
Mark LeDoux,
University of Memphis, United States
Aasef Shaikh,
Case Western Reserve University, United States

***Correspondence:**
Roy V. Sillitoe
sillitoe@bcm.edu

Received: *09 March 2022*
Accepted: *12 August 2022*
Published: *08 September 2022*

Citation:
Van Der Heijden ME, Gill JS, Rey Hipolito AG, Salazar Leon LE and Sillitoe RV (2022) Quantification of Behavioral Deficits in Developing Mice With Dystonic Behaviors. Dystonia 1:10494. doi: 10.3389/dyst.2022.10494

INTRODUCTION

Dystonia is a complex neurological movement disorder characterized by involuntary muscle contractions that can cause rigid limbs and/or twisting postures (1). These behaviors typically arise because agonist and antagonist muscles either co-contract or contract persistently, causing repetitive and sometimes sustained motions. The affected muscles can be found in a single body part as in focal dystonia or in multiple muscle groups as in generalized dystonia (2). The motor behavioral

features of dystonia are often the predominant signature of the disease and are thought to reflect the underlying neural dysfunctions that cause primary dystonia. However, dystonia can also occur as a secondary symptom in neurodevelopmental conditions, neurodegenerative diseases, or acquired neurologic dysfunction. Mechanistically, this diversity is an important consideration as dystonia onset can occur in patients of all ages. Current evidence indicates that the dystonia-associated motor impairments arise from circuit deficits throughout the brain including the basal ganglia, cerebellum, thalamus, and motor cortex (3–6). Despite the rapidly growing knowledge of the genetic and circuit bases of dystonia pathophysiology, the heterogeneity and complexity of the disease has hindered a full understanding of the etiology and neural deficits that cause the debilitating dystonia-associated symptoms. Specifically, how the altered behaviors arise during development remains unclear.

There is emerging evidence pointing towards impaired neurodevelopment as a key factor in some forms of pediatric dystonia (7). Although certain hereditary childhood-onset dystonias have incomplete penetrance (DYT1 and DYT6), both manifesting and non-manifesting patients have abnormal neural circuit connectivity between multiple nodes within the motor circuit that are associated with dystonia. The main affected brain areas are thought to include the basal ganglia, thalamus, and cerebellum (8,9). Thus, while the appearance of dystonia may rely on additional molecular and circuit modifying factors (7,10,11), aberrant circuit development appears central to the behavioral expression when genetic mutations are associated with the disease. Furthermore, affected patients often display their first motor signs during childhood, whereas carriers who remain asymptomatic through childhood rarely develop symptoms later in life (12,13). This difference in behavioral onset could indicate a neurodevelopmental period during which network dysfunction leads to dystonia, coinciding with a critical developmental window that also appears relevant to other neurodevelopmental disorders including autism spectrum disorders (14). In accordance with this hypothesis, a number of the recently identified dystonia-associated mutations involve genes that are also known for their role in neurodevelopment, including the autism-associated gene, CDH8 (15–20). In addition, dystonia is also a frequent comorbidity in infants with other genetic, neurodevelopmental disorders including Rett syndrome (MECP2 mutations) (21,22), Partington syndrome (ARX mutations) (23), and as mentioned before, in an array of patients with autism spectrum disorders (24,25). Together, these studies suggest that some iterations of pediatric dystonia may emerge from aberrant neurodevelopmental processes. To test this hypothesis *in vivo*, it is crucial to investigate how behavior is shaped during development in the context of dystonia.

Multiple reports now indicate that mouse models harboring loss-of-function mutations in genes that cause the most common hereditary pediatric-onset dystonias (DYT1 and DYT6) do not display the involuntary muscle contractions or abnormal posturing observed in infants with the disorder (26–28). However, mice that have brain-restricted loss of Tor1a or knock-in mutations that mimic the human condition show several limb and body motor abnormalities that are observed in human DYT1 (29). Mouse models with overt dystonia-associated impairments can also be induced by infusing drugs into the brain (30–32) or by downregulating the expression of dystonia-associated genes (33–35) in adult mice. Electrophysiological recordings in the brains of rodent models with overt dystonic postures showed irregular burst-like firing patterns in cerebellar neurons, suggesting abnormal cerebellar function as a critical and likely shared feature of dystonia pathogenesis (30,32–34,36–39). In line with these findings, abnormal cerebellar neuron function has been confirmed in non-manifesting genetic models for DYT1 and DYT6 (40,41). Furthermore, cerebellar dysfunction is also compatible with childhood-onset dystonia of other etiologies; the protracted timeline of cerebellar development (42,43) facilitates the postnatal refinement of motor control (44,45) during a period in which even healthy infants exhibit dystonia-associated features (46–48). Indeed, we have previously found that manipulations during cerebellar development result in early-onset dystonia in mice (36,49). In one of these models, impairing excitatory synaptic transmission from brainstem inferior olive neurons onto cerebellar Purkinje neurons causes dystonia without persistent gross cerebellar malformations ($Ptf1a^{Cre};Vglut2^{fl/fl}$ mice (36,39)), similar to what is found in infants with the disease. As a result, this engineered mouse model offers an excellent platform to investigate how aberrant neural circuit function alters neurodevelopment and subsequently impacts behavior.

However, studying dystonia in the context of neurodevelopment is often challenging. Motor control is refined during postnatal development such that even normally developing infants display high scores on the same dystonia rating scales that are commonly used to examine adults (47,48). Similarly, dystonia rating scales used to quantify dystonic movements in mature mice provide higher scores in developing control mice since the latter's motor control is not yet refined, resulting in the reduced sensitivity of these rating scales. Another approach to quantify dystonia in animal models includes EMG recordings (34,50,51). Unfortunately, these invasive EMG recordings require surgeries and implants that are hard to perform in growing animals with small limbs. Additionally, albeit not specific to dystonia-associated impairments, global measures that are often used to assess motor control in adult mice, including the accelerating rotarod or the open field assay (31,36), cannot be easily performed with reliability and reproducibility in young postnatal developing pups because rodents at this age demonstrate less ambulatory activity and rudimentary motor skills overall.

Importantly, several behavioral assays specifically designed to assess neural function in young rodents do exist (52,53): the negative geotaxis reflex, the righting reflex, and the detection of ultrasonic vocalizations (USVs) after pups are separated from the mother (54,55). Here, using these tests, we quantify the performance of a mouse model with early-onset dystonia, the $Ptf1a^{Cre};Vglut2^{fl/fl}$ mutant (36,39). We have chosen to focus on a key period of neurodevelopment when these motor reflexes

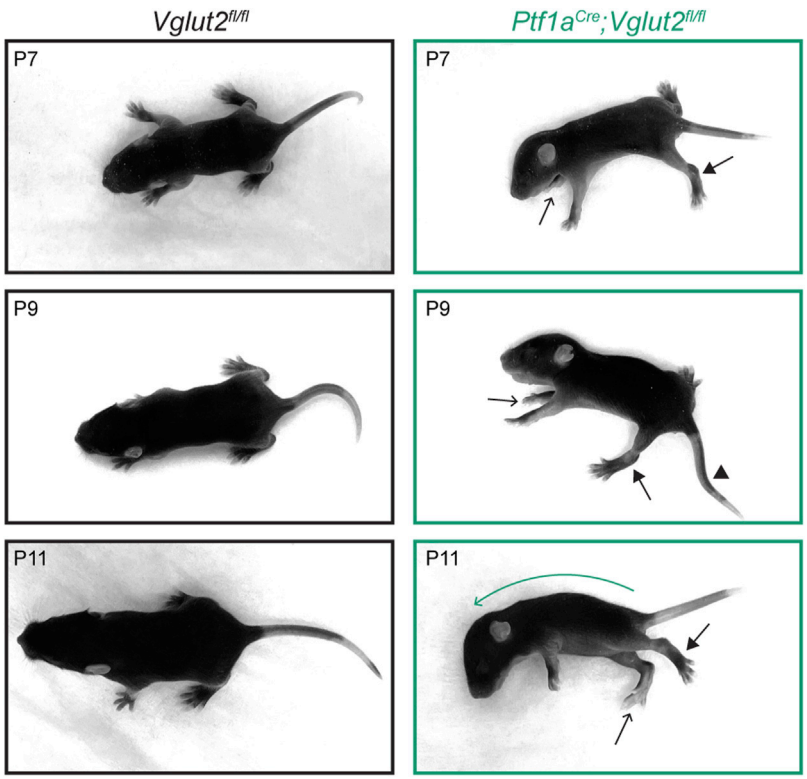

FIGURE 1 | Dystonic postures in *Ptf1a*^{Cre};*Vglut2*$^{fl/fl}$ pups. Pictures of postures in P7–P11 control and *Ptf1a*^{Cre};*Vglut2*$^{fl/fl}$ mice. *Ptf1a*^{Cre};*Vglut2*$^{fl/fl}$ mice have several dystonic postures, including hyper-extended limbs (arrows with closed arrowheads), twisted body posture resulting in asymmetric positioning of the paws (arrows with open arrowheads point to right paws positioned on left side of body), kink in the tail (arrowhead), and curved spine (green curved arrow, P11). These specific dystonic postures were observed in all *Ptf1a*^{Cre};*Vglut2*$^{fl/fl}$ mice (n = 10).

emerge in normally developing mice, from postnatal day (P) 7–11. We found impaired acquisition of these motor behaviors in pups with dystonia, demonstrating that these paradigms may be good quantitative assays for measuring aberrant neurodevelopment in mouse models of pediatric dystonia. Furthermore, we found that the dystonic motor behaviors are accompanied by alterations in USVs. Crucially, the co-expression of motor and non-motor defects mirrors the multi-domain deficits seen in some pediatric neurodevelopmental syndromes.

METHODS

Animals

Mice used in this study were housed in a Level 3, AALAS-certified vivarium. Experiments and studies were reviewed and approved by the Institutional Animal Care and Use Committee (IACUC) of Baylor College of Medicine (BCM). Mice were ear-tagged on the first day of behavioral investigation (P7) and their genotypes determined using allele-specific PCR amplification after the conclusion of experiments so that experimenters were blinded to the genotypes of the mice. The day a copulation plug was detected was considered embryonic day (E) 0.5. We defined P0 as the date of birth. For the experiments in this study, we crossed male mice that were heterozygous for *Ptf1a*^{Cre} (JAX #023329) (56) and homozygous for the *LoxP*-flanked glutamatergic vesicular transporter 2 gene, *Vglut2*^{fl} (JAX #012898) (57), to female mice that were homozygous for *Vglut2*^{fl}. The resulting *Ptf1a*^{Cre};*Vglut2*$^{fl/fl}$ offspring had a conditional deletion of the *Vglut2* allele in the *Ptf1a* lineage, which prevents the loading of glutamate into presynaptic vesicles during fast neurotransmission and therefore eliminates neurotransmission at chemical synapses of glutamatergic, *Ptf1a* lineage neurons (58). Most *Ptf1a* lineage neurons are inhibitory neurons and therefore are not affected by the deletion of *Vglut2*, although inferior olive neurons that send climbing fiber projections to cerebellar Purkinje cells in the molecular layer of the cerebellar cortex are excitatory and do express *Vglut2*. Preventing communication between climbing fibers and Purkinje cells results in severe, early-onset dystonia-associated impairments (36,39). In our study, we used all the pups from 4 litters, which provided us with 21 *Vglut*$^{fl/fl}$ control mice (7 female, 14 male) and 10 *Ptf1a*^{Cre};*Vglut2*$^{fl/fl}$ dystonic mice (5 female, 5 male). When comparing mice from each sex and genotype with each other, we did not observe any sex differences. For this assessment, we performed a two-way ANOVA (genotype, sex) and did not find interactions between genotype and sex (p > 0.05 for all tests) at any of the developmental time-points for any

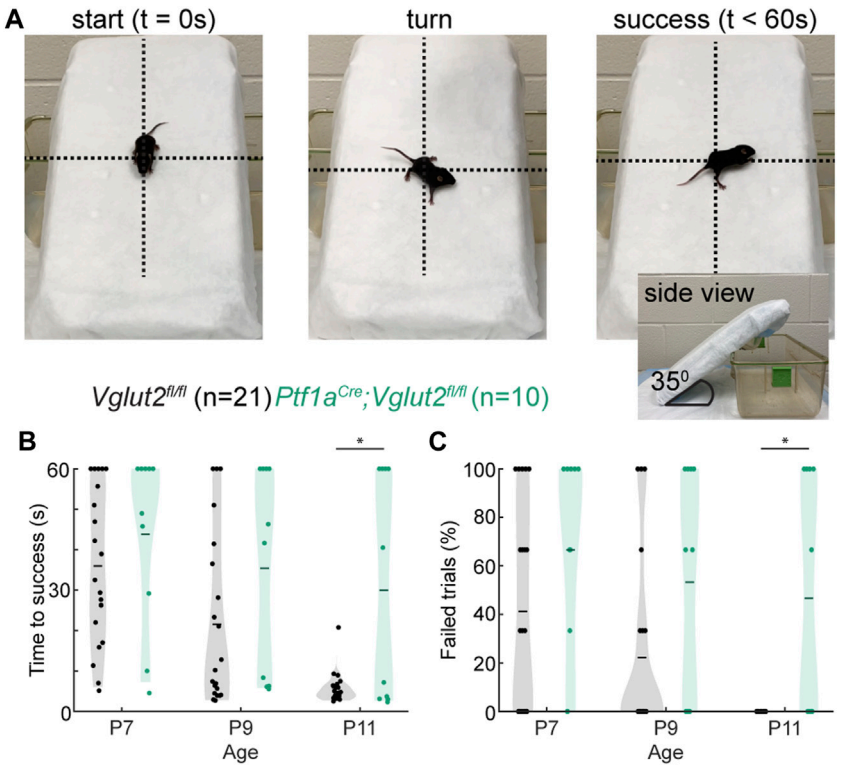

FIGURE 2 | Abnormal negative geotaxis reflex in *Ptf1a*^{Cre};*Vglut2*$^{fl/fl}$ pups. **(A)** Visualization of negative geotaxis reflex paradigm. The time to successful completion of the reflex is measured. **(B)** Average time to reflex was longer in P11 ($p < 0.0001$) *Ptf1a*^{Cre};*Vglut2*$^{fl/fl}$ mice compared to control mice. **(C)** The number of failed trails was higher in P11 ($p < 0.0001$) *Ptf1a*^{Cre};*Vglut2*$^{fl/fl}$ mice compared to control mice. Statistical significance was assessed using a repeated measures ANOVA followed by Tukey Kramer post-hoc analysis.

of the behavioral tests. Therefore, we combined the data collected from male and female mice when performing the statistical analyses reported in this study.

Negative Geotaxis Reflex

Mice were tested in the negative geotaxis assay at P7, P9 and P11 (54,59). A cage top wrapped with a sterile Poly-Lined drape was used to create a ramp with a 35° slope. Mice were placed on this ramp one at a time, oriented to face down the slope. Upon placement and release of the mouse, a 60-s timer was started. A successful trial was considered as one in which the mouse turned >90° on the ramp (crossing the plane perpendicular to the original placement in either direction). The time it took for the mouse to perform this movement was recorded. A failed trial was considered one in which mice were unable to change their orientation within 60-s or in which mice lost their footing on the ramp and fell. After a completed trial (either success or failure), each mouse was returned to their home cage. For each mouse, this process was repeated for a total of three trials per mouse, per behavioral timepoint.

Surface Righting Reflex

The righting reflex was measured at P7, P9, and P11 (49,54). In this assay, each mouse was placed on its back on a clean cage without bedding, and then this position was gently held by one finger until timing started. Upon removal of the finger, the time required for the mouse to right itself onto its four paws was recorded. All mice were tested three times at each age. A "failed" trial was defined as one in which the mouse did not right itself within 60 s.

Ultrasonic Vocalizations

Pup vocalizations were recorded at P7, P9, and P11 as described previously (49,60). Pups were placed in an anechoic, sound-attenuating chamber (Med Associates Inc.) within a round plastic tub that was positioned under a CM16 microphone (Avisoft Bioacoustics) in the center of the chamber. Sound was amplified and digitized using UltraSoundGate 416H at a 250 kHz sampling rate and a bit depth of 16 while Avisoft RECORDER software was used to collect the recordings. The USVs of each pup were monitored for 2 min.

Statistical Analyses

Analyses for this study were performed using MATLAB (Mathworks, United States). We plotted and then quantified statistically significant differences using a repeated-measures ANOVA and quantified the differences between genotypes and time-points using a Tukey Kramer post-hoc analysis. We used an alpha of 0.05 to accept statistical significance.

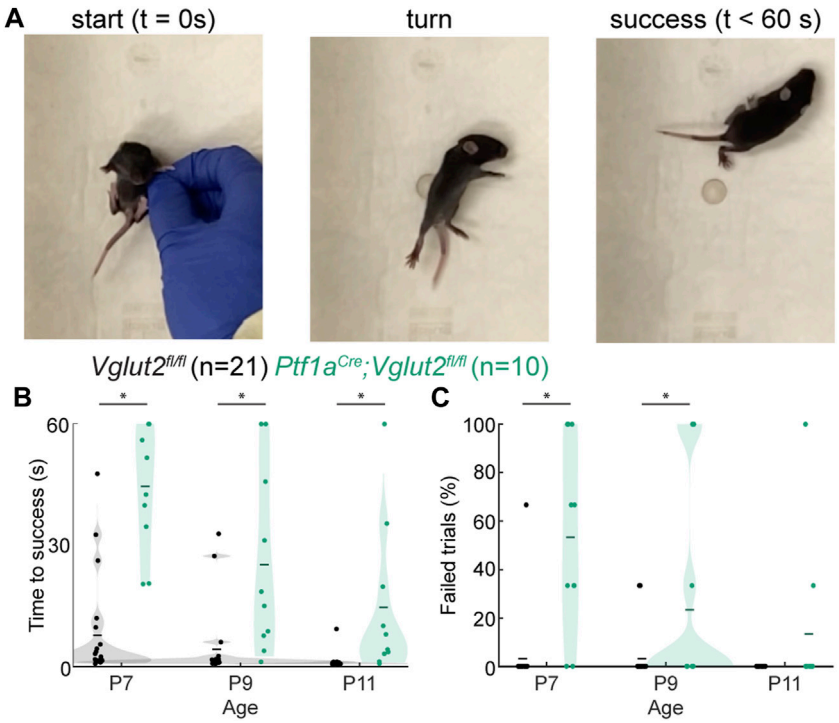

FIGURE 3 | Abnormal righting reflex in *Ptf1a*^{Cre};*Vglut2*$^{fl/fl}$ pups. **(A)** Visualization of righting reflex paradigm. The time to successful completion of the reflex is measured. **(B)** Average time to reflex was longer in P7 ($p < 0.0001$), P9 ($p < 0.0008$), and P11 ($p = 0.0030$) *Ptf1a*^{Cre};*Vglut2*$^{fl/fl}$ mice compared to control mice. **(C)** The number of failed trails was higher in P7 ($p < 0.001$) and P9 ($p = 0.0422$) *Ptf1a*^{Cre};*Vglut2*$^{fl/fl}$ mice compared to control mice. Statistical significance was assessed using a repeated measures ANOVA followed by Tukey Kramer post-hoc analysis.

RESULTS

Dystonic Postures

We started by confirming the presence of dystonic postures in mice during the second postnatal week (P7-P11). At this age, both healthy control and dystonic *Ptf1a*^{Cre};*Vglut2*$^{fl/fl}$ mice show very few coordinated, ambulatory movements, and therefore the ability to accurately distinguish spontaneous dystonic movements is difficult. Nevertheless, when positioned on a flat surface, we observed that the *Ptf1a*^{Cre};*Vglut2*$^{fl/fl}$ pups often remained in fixed dystonic postures without initiating specific dedicated movements. To distinguish the postures seen in *Ptf1a*^{Cre};*Vglut2*$^{fl/fl}$ mutants compared to control mice, we acquired a series of images to help visualize the different body postures displayed from P7 to P11 (**Figure 1**). In addition, we also relied on video recordings to examine the full extent and dynamics of the dystonia-associated behaviors (**Supplementary Video S1**). In the *Ptf1a*^{Cre};*Vglut2*$^{fl/fl}$ mice, we frequently observed dystonic postures including: hyper-extension of the hindlimbs, twisted body posturing that resulted in the front- or hind-paws extending on either side of the body, strongly curved spines and lateral positioning, rigid or kinked tail positioning, and splayed digits on the fore- and hind-paws (39). Combinations of these dystonic postures were evident in all *Ptf1a*^{Cre};*Vglut2*$^{fl/fl}$ mice ($n = 10$) included in our study (**Figure 1**). These data confirm that the *Ptf1a*^{Cre};*Vglut2*$^{fl/fl}$ mutant mice have early-onset dystonia-associated motor impairments that are robust and reproducible from animal to animal.

Negative Geotaxis Reflex

Next, we investigated whether these dystonia-associated impairments prevented *Ptf1a*^{Cre};*Vglut2*$^{fl/fl}$ mice from properly executing the negative geotaxis reflex (**Figure 2A**; **Supplementary Video S2**). This behavioral reflex naturally arises in mice around P7 (61) and when mice mature, their time to complete the negative geotaxis reflex decreases due to their increasing motor control. We found that at the youngest ages tested (P7 and P9), control *Vglut2*$^{fl/fl}$ mice and dystonic *Ptf1a*^{Cre};*Vglut2*$^{fl/fl}$ mice took equally long to complete geotaxis reflexes (**Figure 2B**). However, while control *Vglut2*$^{fl/fl}$ mice showed a rapid decrease in the time needed to successfully turn by P11, the time taken to turn remained prolonged in P11 dystonic *Ptf1a*^{Cre};*Vglut2*$^{fl/fl}$ mice (**Figure 2B**). Similarly, we found that the number of failed trials (trials in which the pup lost grip of the padding and rolled down the slope or did not turn within 60 s) was similar between control and *Ptf1a*^{Cre};*Vglut2*$^{fl/fl}$ mice at P7 and P9, but was higher at P11 in *Ptf1a*^{Cre};*Vglut2*$^{fl/fl}$ mice. Together, these results indicate that, compared to controls, *Ptf1a*^{Cre};*Vglut2*$^{fl/fl}$ mice have delays in the development of the negative geotaxis reflex, which assays the early development of motor control.

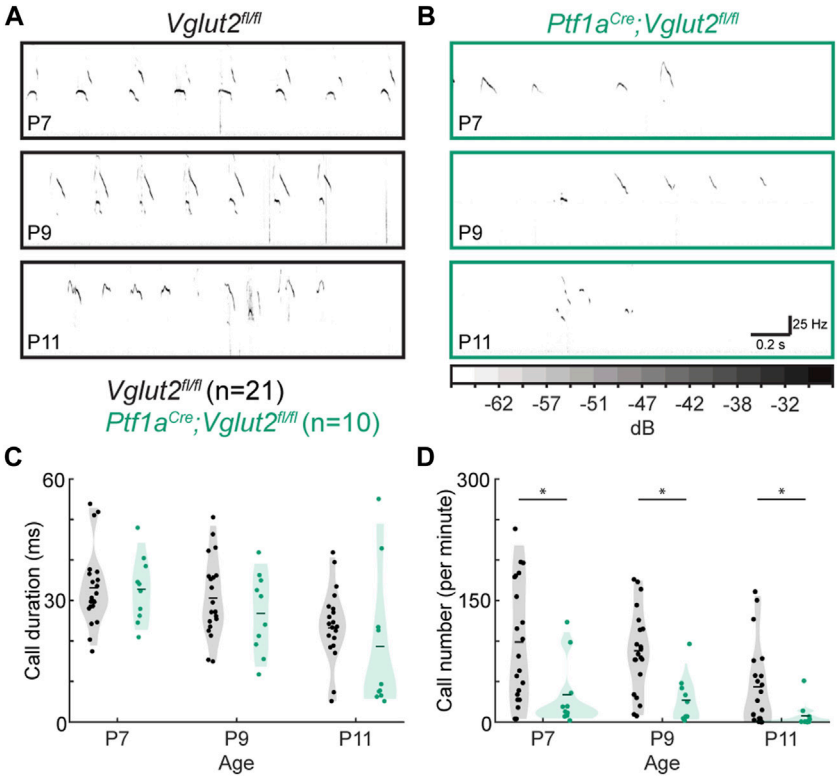

FIGURE 4 | Abnormal vocalizations after separation from the dam in *Ptf1a^{Cre};Vglut2$^{fl/fl}$* pups. **(A)** Representative ultrasonic vocalizations in control pups. **(B)** Representative vocalizations in *Ptf1a^{Cre};Vglut2$^{fl/fl}$* pups. In **(A)** and **(B)**, darker coloring represents louder vocalizations, scaling is the same across all figure panels. **(C)** No difference was found in the durations of calls at any time point. **(D)** The number of calls was lower in P7, P9, and P11 *Ptf1a^{Cre};Vglut2$^{fl/fl}$* mice compared to control mice. Statistical significance was assessed using a repeated measures ANOVA followed by Tukey Kramer post-hoc analysis.

Surface Righting Reflex

We further investigated early motor control in dystonic *Ptf1a^{Cre};Vglut2$^{fl/fl}$* mice by examining their performance of the surface righting reflex (**Figure 3A**; **Supplementary Video S3**). Mice usually acquire this reflex around P5 (62), although some variability in reflex onset and reflex time may be observed. We previously studied *En1^{Cre};Atoh1$^{fl/-}$* mice that have impaired neurogenesis of excitatory neurons, which lead to dystonic motor impairments (49). These mice also exhibit impairments in the surface righting reflex, which was likely due to abnormal motor control. We therefore tested whether the surface righting was also impaired in dystonic *Ptf1a^{Cre};Vglut2$^{fl/fl}$* mice (**Figure 3A**). We found that the *Ptf1a^{Cre};Vglut2$^{fl/fl}$* mutant mice required more time to right themselves from a supine position to all four paws at P7, P9, and P11 (**Figure 3B**) relative to controls, although we did note that the time they took to right decreased with age. Furthermore, we observed that the number of trials in which the *Ptf1a^{Cre};Vglut2$^{fl/fl}$* mice failed to right themselves within 60 s was higher than in control mice at P7 and P9, but not at P11 (**Figure 3C**). Together, these results show that the *Ptf1a^{Cre};Vglut2$^{fl/fl}$* mutant mice, which express striking dystonic behaviors including bouts of twisting of the limbs and torso, also have delayed development of the surface righting reflex, likely reflecting impairments in the development of normal motor control.

Ultrasonic Vocalizations

To test whether the circuit disruptions in *Ptf1a^{Cre};Vglut2$^{fl/fl}$* mice lead to aberrant function in behavioral domains outside of motor control, we tested whether the *Ptf1a^{Cre};Vglut2$^{fl/fl}$* mutant mice had abnormal vocalizations when socially isolated. In the first few postnatal weeks, pups make USVs when separated from the nest and their dam (55) (**Figures 4A,B**). These vocalizations are thought to be a measure of early social behavior in mice and are often changed in number, duration, and/or frequency in models of neurodevelopmental disability and autism spectrum disorders (63–65). Interestingly, pup vocalizations are also abnormal in mouse models with other cerebellar alterations (49,66,67) as well as in dystonic rats (60). We found that while call duration was not statistically different between control *Vglut2$^{fl/fl}$* mice and the dystonic *Ptf1a^{Cre};Vglut2$^{fl/fl}$* mutant mice at P7, P9, or P11 (**Figure 4C**), the number of calls was significantly lower in *Ptf1a^{Cre};Vglut2$^{fl/fl}$* mutants compared to control *Vglut2$^{fl/fl}$* mice at P7, P9, and P11 (**Figure 4D**). These results show that *Ptf1a^{Cre};Vglut2$^{fl/fl}$* mice that express dystonic motor behaviors also produce fewer vocalizations of normal duration compared to littermate controls, reflecting possible deficits in socialization in addition to the observed deficits in motor control (36).

DISCUSSION

In this study, we investigated the expression of early postnatal reflexive behaviors in the *Ptf1a*^{Cre};*Vglut2*$^{fl/fl}$ mouse model of early-onset dystonia (36). We found that these mice have delayed acquisition of the negative geotaxis and surface righting reflexes compared to their control littermates. We further observed that the dystonic *Ptf1a*^{Cre};*Vglut2*$^{fl/fl}$ mice make fewer USVs when separated from their dams, a behavioral impairment that is frequently seen in mouse models of neurodevelopmental disability and autism spectrum disorders. Together, we show that these simple assays can serve as a practical toolkit for investigating delays in the achievement of neurodevelopmental milestones using a circuit-based mouse model of early-onset dystonia.

The behavioral assays described in this study are particularly advantageous as they provide straightforward methods to study the impact of functional neural defects during a postnatal period that is often considered experimentally difficult to assess. The quantification of reflexive behaviors is unbiased, the assays are non-invasive, and the motor assays do not require special equipment. Furthermore, the impairments in these reflexive motor behaviors, as reported here, are not unique to rodent models of dystonia (68). For example, impairments in surface righting, but not the geotaxis reflex, have also been observed in ataxic and tremoring shaker rats (69) and ataxic lurcher mice (70). However, these reflexive behaviors are uniquely impaired in models with impaired development. For example, the neurodegeneration that occurs later in life in a mouse model for spinocerebellar ataxia 6 (SCA6) is not accompanied by impairments in either reflexive behavior (71). Due to their non-invasive nature, these postnatal reflex assays can provide quantitative and reliable measures of the relative motor impairments caused by dystonia or other developmental disorders. Such measures could be used to assess the onset of developmental motor disorders and evaluate improvements of motor behavior after providing treatment.

Regarding the behavior of *Ptf1a*^{Cre};*Vglut2*$^{fl/fl}$ mice, we confirmed that they exhibit dystonic motor behaviors at early postnatal ages (**Figure 1**), making this genetic mouse model a powerful tool to study neurological deficits and circuit dysfunction in pediatric-onset dystonia. Furthermore, a recent study has shown that homozygous loss of *TSPOAP1* causes pediatric-onset dystonia through synaptic abnormalities in the cerebellum, underscoring that aberrant synaptic function in the cerebellum can also cause dystonia in humans (72). Adult *Ptf1a*^{Cre};*Vglut2*$^{fl/fl}$ mice respond to cerebellar deep brain stimulation targeted to the cerebellar nuclei (36), making this mouse a seminal pre-clinical model to predict the efficacy of cerebellar deep brain stimulation in alleviating symptoms in patients with dystonia (73,74). Furthermore, gross cerebellar hemispheric dysfunction is a frequent finding in children born early preterm (75) of whom many suffer from dystonia (76). We therefore propose that even though the specific cerebellar network perturbation in dystonic *Ptf1a*^{Cre};*Vglut2*$^{fl/fl}$ mice differs from those induced in other hereditary or acquired pediatric dystonias, the perturbations that impact the "dystonia network" and cause tractable dystonic motor behaviors that can be easily quantified ultimately may be relevant to and potentially predictive of the neural dysfunction(s) that are exhibited in many forms of dystonia.

Of special interest is our finding that dystonic *Ptf1a*^{Cre};*Vglut2*$^{fl/fl}$ mice exhibit social deficits in the social isolation/USV assay. The comorbidity of social deficits, dystonia, and delayed early behavioral reflexes supports the hypothesis of a possible shared ontogeny in the domains of social interaction and motor control (43,77,78). Intriguingly, in our *Ptf1a*^{Cre};*Vglut2*$^{fl/fl}$ mice, the resulting behaviors can be attributed to initial cerebellar dysfunction due to the precision of the genetic manipulation performed in these mice (36). The observed USV changes further suggest that neurodevelopmental disorders exhibiting deficits across developmental domains, as seen in dystonia, may converge on a shared mechanism of cerebellar dysfunction. Previous work has highlighted the importance of evaluating motor control in mouse models of autism spectrum disorders and cerebellar dysfunction in patients with autism spectrum disorders to uncover the full range of neural dysfunction in these neurodevelopmental disorders (63,79,80). Here, we propose the reverse; in pediatric dystonias and other early-onset movement disorders, social deficits should be taken into consideration and fully evaluated. In conclusion, we postulate that neurodevelopmental disorders that display a spectrum of social and motor deficits may converge at the level of cerebellar dysfunction (42,43,77,81). It would be interesting if future studies were to investigate whether the manifestation of motor and social impairments in dystonia is dependent on region-specific dysfunctions (80), how the resulting dysfunction is related to the underlying genetic mechanisms, and whether the ultimate behavioral abnormalities rely on the timing of genetic or physical insults to the developing cerebellum and its associated brain networks.

DATA AVAILABILITY STATEMENT

The raw data supporting the conclusion of this article will be made available by the authors, without undue reservation.

ETHICS STATEMENT

The animal study was reviewed and approved by the Institutional Animal Care and Use Committee (IACUC) of Baylor College of Medicine (BCM).

AUTHOR CONTRIBUTIONS

MH, JG, and RS conceived the project. MH, AH, and LL collected the data. MH analyzed the data and wrote the first version of the manuscript. MH, JG, AH, LL, and RS interpreted results and edited the manuscript.

FUNDING

This work was supported by Baylor College of Medicine (BCM), Texas Children's Hospital, and the National Institutes of Neurological Disorders and Stroke (NINDS) R01NS100874, R01NS119301, and R01NS127435 to RS. Dystonia Medical Research Foundation (DMRF) and Cure Dystonia Now provided a postdoctoral award to MH. NINDS provided funding to JG (K08NS121600). Further support was provided by the Baylor College of Medicine Intellectual and Developmental Disabilities Research Center (BCM-IDDRC) (US National Institutes of Health (NIH) grant 5P50HD103555).

CONFLICT OF INTEREST

The authors declare that the research was conducted in the absence of any commercial or financial relationships that could be construed as a potential conflict of interest.

ACKNOWLEDGMENTS

We thank Dr. Elizabeth P. Lackey for help with video recordings of control and mutant dystonic behavior.

SUPPLEMENTARY MATERIAL

The Supplementary Material for this article can be found online at: https://www.frontierspartnerships.org/articles/10.3389/dyst.2022.10494/full#supplementary-material.

Supplementary Video S1 | Ambulatory activity in control and dystonic P9 mice. Dystonic motor signs are evident in the *Ptf1a^{Cre};Vglut2$^{fl/fl}$* pups, but note that movements are also relatively uncoordinated in control *Vglut2$^{fl/fl}$* pups.

Supplementary Video S2 | Negative geotaxis reflex in P11 mice. The *Vglut2$^{fl/fl}$* pup immediately turns to face upwards, whereas the *Ptf1a^{Cre};Vglut2$^{fl/fl}$* pup takes longer to turn towards the upward direction.

Supplementary Video S3 | Surface righting reflex. The *Vglut2$^{fl/fl}$* pup immediately turns from the supine position onto its four paws, whereas the *Ptf1a^{Cre};Vglut2$^{fl/fl}$* pup takes longer to right itself.

REFERENCES

1. Pana A, Saggu BM. *Dystonia. StatPearls. Treasure Island (FL)*. Tampa, Florida, USA: StatPearls Publishing (2020).
2. Grütz K, Klein C. Dystonia Updates: Definition, Nomenclature, Clinical Classification, and Etiology. *J Neural Transm* (2021) 128(4):395–404. doi:10.1007/s00702-021-02314-2
3. Neychev VK, Fan X, Mitev VI, Hess EJ, Jinnah HA. The Basal Ganglia and Cerebellum Interact in the Expression of Dystonic Movement. *Brain* (2008) 131(9):2499–509. doi:10.1093/brain/awn168
4. Jinnah HA, Neychev V, Hess EJ. The Anatomical Basis for Dystonia: the Motor Network Model. *Tremor Other Hyperkinet Mov (N Y)* (2017) 7:506. doi:10.7916/D8V69X3S
5. Shakkottai VG, Batla A, Bhatia K, Dauer WT, Dresel C, Niethammer M, et al. Current Opinions and Areas of Consensus on the Role of the Cerebellum in Dystonia. *Cerebellum* (2017) 16(2):577–94. doi:10.1007/s12311-016-0825-6
6. Neychev VK, Gross RE, Lehéricy S, Hess EJ, Jinnah HA. The Functional Neuroanatomy of Dystonia. *Neurobiol Dis* (2011) 42(2):185–201. doi:10.1016/j.nbd.2011.01.026
7. Niethammer M, Carbon M, Argyelan M, Eidelberg D. Hereditary Dystonia as a Neurodevelopmental Circuit Disorder: Evidence from Neuroimaging. *Neurobiol Dis* (2011) 42(2):202–9. doi:10.1016/j.nbd.2010.10.010
8. Argyelan M, Carbon M, Niethammer M, Ulug AM, Voss HU, Bressman SB, et al. Cerebellothalamocortical Connectivity Regulates Penetrance in Dystonia. *J Neurosci* (2009) 29(31):9740–7. doi:10.1523/JNEUROSCI.2300-09.2009
9. Lerner RP, Niethammer M, Eidelberg D. Understanding the Anatomy of Dystonia: Determinants of Penetrance and Phenotype. *Curr Neurol Neurosci Rep* (2013) 13(11):401. doi:10.1007/s11910-013-0401-0
10. Hu CF, Luxton GWG, Lee FC, Hsu CS, Huang SM, Hong JS, et al. *Whole Exome Sequencing Identifies Novel DYT1 Dystonia-Associated Genome Variants as Potential Disease Modifiers* (2020).
11. Walter M, Bonin M, Pullman RS, Valente EM, Loi M, Gambarin M, et al. Expression Profiling in Peripheral Blood Reveals Signature for Penetrance in DYT1 Dystonia. *Neurobiol Dis* (2010) 38(2):192–200. doi:10.1016/j.nbd.2009.12.019
12. Bressman SB, Raymond D, Fuchs T, Heiman GA, Ozelius LJ, Saunders-Pullman R. Mutations in THAP1 (DYT6) in Early-Onset Dystonia: a Genetic Screening Study. *Lancet Neurol* (2009) 8(5):441–6. doi:10.1016/S1474-4422(09)70081-X
13. Bressman SB, Sabatti C, Raymond D, de Leon D, Klein C, Kramer PL, et al. The DYT1 Phenotype and Guidelines for Diagnostic Testing. *Neurology* (2000) 54(9):1746–52. doi:10.1212/wnl.54.9.1746
14. Li J, Kim S, Pappas SS, Dauer WT. CNS Critical Periods: Implications for Dystonia and Other Neurodevelopmental Disorders. *JCI Insight* (2021) 2021(4):142483. doi:10.1172/jci.insight.142483
15. Zech M, Jech R, Boesch S, Škorvánek M, Weber S, Wagner M, et al. Monogenic Variants in Dystonia: an Exome-wide Sequencing Study. *Lancet Neurol* (2020) 19(11):908–18. doi:10.1016/S1474-4422(20)30312-4
16. Carecchio M, Invernizzi F, Gonzàlez-Latapi P, Panteghini C, Zorzi G, Romito L, et al. Frequency and Phenotypic Spectrum of KMT2B Dystonia in Childhood: A Single-center Cohort Study. *Mov Disord* (2019) 34(10):1516–27. doi:10.1002/mds.27771
17. Fernández-Marmiesse A, Kusumoto H, Rekarte S, Roca I, Zhang J, Myers SJ, et al. A Novel Missense Mutation in GRIN2A Causes a Nonepileptic Neurodevelopmental Disorder. *Mov Disord* (2018) 33(6):992–9. doi:10.1002/mds.27315
18. Doummar D, Treven M, Qebibo L, Devos D, Ghoumid J, Ravelli C, et al. Childhood-onset Progressive Dystonia Associated with Pathogenic Truncating Variants in CHD8. *Ann Clin Transl Neurol* (2021) 8(10):1986–90. doi:10.1002/acn3.51444
19. Steel D, Zech M, Zhao C, Barwick KE, Burke D, Demailly D, et al. Loss-of-function Variants in HOPS Complex Genes VPS16 and VPS41 Cause Early-Onset Dystonia Associated with Lysosomal Abnormalities. *Ann Neurol* (2020) 88:867–77. doi:10.1002/ana.25879
20. Steel D, Kurian MA. Recent Genetic Advances in Early-Onset Dystonia. *Curr Opin Neurol* (2020) 33(4):500–7. doi:10.1097/WCO.0000000000000831
21. Brunetti S, Lumsden DE. Rett Syndrome as a Movement and Motor Disorder - A Narrative Review. *Eur J Paediatr Neurol* (2020) 28:29–37. doi:10.1016/j.ejpn.2020.06.020
22. Bell L, Wittkowski A, Hare DJ. Movement Disorders and Syndromic Autism: A Systematic Review. *J Autism Dev Disord* (2019) 49(1):54–67. doi:10.1007/s10803-018-3658-y
23. Strømme P, Mangelsdorf ME, Scheffer IE, Gécz J. Infantile Spasms, Dystonia, and Other X-Linked Phenotypes Caused by Mutations in Aristaless Related Homeobox Gene, ARX *Brain Dev* (2002) 24(5):266–8. doi:10.1016/s0387-7604(02)00079-7
24. Ming X. Evaluation of Dystonia and Dystonic Posturing in a Cohort of Patients with Autism Spectrum Disorder (ASD) (P5.6-039). *Neurology* (2019) 92(15).
25. Damasio AR, Maurer RG. A Neurological Model for Childhood Autism. *Arch Neurol* (1978) 35(12):777–86. doi:10.1001/archneur.1978.00500360001001
26. Ruiz M, Perez-Garcia G, Ortiz-Virumbrales M, Méneret A, Morant A, Kottwitz J, et al. Abnormalities of Motor Function, Transcription and Cerebellar Structure in Mouse Models of THAP1 Dystonia. *Hum Mol Genet* (2015) 24(25):7159–70. doi:10.1093/hmg/ddv384

27. Goodchild RE, Kim CE, Dauer WT. Loss of the Dystonia-Associated Protein torsinA Selectively Disrupts the Neuronal Nuclear Envelope. *Neuron* (2005) 48(6):923–32. doi:10.1016/j.neuron.2005.11.010
28. Dauer W, Goodchild R. Mouse Models of torsinA Dysfunction. *Adv Neurol* (2004) 94:67–72.
29. Liang CC, Tanabe LM, Jou S, Chi F, Dauer WT. TorsinA Hypofunction Causes Abnormal Twisting Movements and Sensorimotor Circuit Neurodegeneration. *J Clin Invest* (2014) 124:3080–92. doi:10.1172/JCI72830
30. Pizoli CE, Jinnah HA, Billingsley ML, Hess EJ. Abnormal Cerebellar Signaling Induces Dystonia in Mice. *J Neurosci* (2002) 22(17):7825–33. doi:10.1523/jneurosci.22-17-07825.2002
31. Calderon DP, Fremont R, Kraenzlin F, Khodakhah K. The Neural Substrates of Rapid-Onset Dystonia-Parkinsonism. *Nat Neurosci* (2011) 14(3):357–65. doi:10.1038/nn.2753
32. Fremont R, Calderon DP, Maleki S, Khodakhah K. Abnormal High-Frequency Burst Firing of Cerebellar Neurons in Rapid-Onset Dystonia-Parkinsonism. *J Neurosci* (2014) 34(35):11723–32. doi:10.1523/JNEUROSCI.1409-14.2014
33. Fremont R, Tewari A, Khodakhah K. Aberrant Purkinje Cell Activity Is the Cause of Dystonia in a shRNA-Based Mouse Model of Rapid Onset Dystonia-Parkinsonism. *Neurobiol Dis* (2015) 82:200–12. doi:10.1016/j.nbd.2015.06.004
34. Fremont R, Tewari A, Angueyra C, Khodakhah K. A Role for Cerebellum in the Hereditary Dystonia DYT1. *Elife* (2017) 2017:e22775. doi:10.7554/eLife.22775
35. Washburn S, Fremont R, Moreno-Escobar MC, Angueyra C, Khodakhah K. Acute Cerebellar Knockdown of Sgce Reproduces Salient Features of Myoclonus-Dystonia (DYT11) in Mice. *Elife* (2019) 2019:e52101. doi:10.7554/eLife.52101
36. White JJ, Sillitoe RV. Genetic Silencing of Olivocerebellar Synapses Causes Dystonia-like Behaviour in Mice. *Nat Commun* (2017) 8:14912. doi:10.1038/ncomms14912
37. LeDoux MS, Hurst DC, Lorden JF. Single-unit Activity of Cerebellar Nuclear Cells in the Awake Genetically Dystonic Rat. *Neuroscience* (1998) 86(2):533–45. doi:10.1016/s0306-4522(98)00007-4
38. LeDoux MS, Lorden JF. Abnormal Spontaneous and Harmaline-Stimulated Purkinje Cell Activity in the Awake Genetically Dystonic Rat. *Exp Brain Res* (2002) 145(4):457–67. doi:10.1007/s00221-002-1127-4
39. Brown AM, van der Heijden ME, Jinnah HA, Sillitoe RV. Cerebellar Dysfunction as a Source of Dystonic Phenotypes in Mice. *Cerebellum* (2022). doi:10.1007/s12311-022-01441-0
40. van der Heijden ME, Kizek DJ, Perez R, Ruff EK, Ehrlich ME, Sillitoe RV. Abnormal Cerebellar Function and Tremor in a Mouse Model for Non-manifesting Partially Penetrant Dystonia Type 6. *J Physiol* (2020) 599(7):2037–54. doi:10.1113/jp280978
41. Liu Y, Xing H, Wilkes BJ, Yokoi F, Chen H, Vaillancourt DE, et al. The Abnormal Firing of Purkinje Cells in the Knockin Mouse Model of DYT1 Dystonia. *Brain Res Bull* (2020) 165:14–22. doi:10.1016/j.brainresbull.2020.09.011
42. van der Heijden ME, Sillitoe RV. Interactions between Purkinje Cells and Granule Cells Coordinate the Development of Functional Cerebellar Circuits. *Neuroscience* (2021) 462:4–21. doi:10.1016/j.neuroscience.2020.06.010
43. Gill JS, Sillitoe RV. Functional Outcomes of Cerebellar Malformations. *Front Cel Neurosci* (2019) 13:441. doi:10.3389/fncel.2019.00441
44. Dooley JC, Sokoloff G, Blumberg MS. Movements during Sleep Reveal the Developmental Emergence of a Cerebellar-dependent Internal Model in Motor Thalamus. *Curr Biol* (2021) 31:5501–11.e5. doi:10.1016/j.cub.2021.10.014
45. van der Heijden ME, Brown AM, Sillitoe RV. Motor Control: Internalizing Your Place in the World. *Curr Biol* (2021) 31(24):R1576–8. doi:10.1016/j.cub.2021.10.056
46. Lin JP, Nardocci N. Recognizing the Common Origins of Dystonia and the Development of Human Movement: A Manifesto of Unmet Needs in Isolated Childhood Dystonias. *Front Neurol* (2016) 7:226. doi:10.3389/fneur.2016.00226
47. Kuiper MJ, Brandsma R, Vrijenhoek L, Tijssen MAJ, Burger H, Dan B, et al. Physiological Movement Disorder-like Features during Typical Motor Development. *Eur J Paediatr Neurol* (2018) 22(4):595–601. doi:10.1016/j.ejpn.2018.03.010
48. Kuiper MJ, Vrijenhoek L, Brandsma R, Lunsing RJ, Burger H, Eggink H, et al. The Burke-Fahn-Marsden Dystonia Rating Scale Is Age-dependent in Healthy Children. *Mov Disord Clin Pract (Hoboken)* (2016) 3(6):580–6. doi:10.1002/mdc3.12339
49. van der Heijden ME, Lackey EP, Perez R, Işleyen FS, Brown AM, Donofrio SG, et al. Maturation of Purkinje Cell Firing Properties Relies on Neurogenesis of Excitatory Neurons. *Elife* (2021) 2021:e68045. doi:10.7554/eLife.68045
50. DeAndrade MP, Trongnetrpunya A, Yokoi F, Cheetham CC, Peng N, Wyss JM, et al. Electromyographic Evidence in Support of a Knock-In Mouse Model of DYT1 Dystonia. *Mov Disord* (2016) 31(11):1633–9. doi:10.1002/mds.26677
51. Scholle HC, Jinnah HA, Arnold D, Biedermann FHW, Faenger B, Grassme R, et al. Kinematic and Electromyographic Tools for Characterizing Movement Disorders in Mice. *Mov Disord* (2010) 25(3):265–74. doi:10.1002/mds.22933
52. Fox WM. Reflex-ontogeny and Behavioural Development of the Mouse. *Anim Behav* (1965) 13(2):234–41. doi:10.1016/0003-3472(65)90041-2
53. Rogers DC, Fisher EM, Brown SD, Peters J, Hunter AJ, Martin JE. Behavioral and Functional Analysis of Mouse Phenotype: SHIRPA, a Proposed Protocol for Comprehensive Phenotype Assessment. *Mamm Genome* (1997) 8(10):711–3. doi:10.1007/s003359900551
54. Feather-Schussler DN, Ferguson TS. A Battery of Motor Tests in a Neonatal Mouse Model of Cerebral Palsy. *J Vis Exp* (2016) 2016(117):53569. doi:10.3791/53569
55. Wiaderkiewicz J, Głowacka M, Grabowska M, Jarosław-Jerzy B. Ultrasonic Vocalizations (USV) in the Three Standard Laboratory Mouse Strains: Developmental Analysis. *Acta Neurobiol Exp (Wars)* (2013) 73(4):557–63.
56. Hoshino M, Nakamura S, Mori K, Kawauchi T, Terao M, Nishimura YV, et al. Ptf1a, a bHLH Transcriptional Gene, Defines GABAergic Neuronal Fates in Cerebellum. *Neuron* (2005) 47(2):201–13. doi:10.1016/j.neuron.2005.06.007
57. Tong Q, Ye C, McCrimmon RJ, Dhillon H, Choi B, Kramer MD, et al. Synaptic Glutamate Release by Ventromedial Hypothalamic Neurons Is Part of the Neurocircuitry that Prevents Hypoglycemia. *Cell Metab* (2007) 5(5):383–93. doi:10.1016/j.cmet.2007.04.001
58. van der Heijden ME, Brown AM, Sillitoe RV. Silencing the Output of Cerebellar Neurons Using Cell Type-specific Genetic Deletion of Vesicular and Transporters. In: Sillitoe RV, editor. *Measuring Cerebellar Function*. New York, NY: Springer US (2022). p. 47–67.
59. Ruhela RK, Soni S, Sarma P, Prakash A, Medhi B. Negative Geotaxis: An Early Age Behavioral Hallmark to VPA Rat Model of Autism. *Ann Neurosci* (2019) 26(1):25–31. doi:10.5214/ans.0972.7531.260106
60. Riede T, Zhao Y, LeDoux MS. Vocal Development in Dystonic Rats. *Physiol Rep* (2015) 3(4):e12350. doi:10.14814/phy2.12350
61. Heyser CJ, Wilson MC, Gold LH. Coloboma Hyperactive Mutant Exhibits Delayed Neurobehavioral Developmental Milestones. *Brain Res Dev Brain Res* (1995) 89(2):264–9. doi:10.1016/0165-3806(95)00130-6
62. Heyser CJ. Assessment of Developmental Milestones in Rodents. *Curr Protoc Neurosci* (2004) 8:8.18. doi:10.1002/0471142301.ns0818s25
63. Simmons DH, Titley HK, Hansel C, Mason P. Behavioral Tests for Mouse Models of Autism: An Argument for the Inclusion of Cerebellum-Controlled Motor Behaviors. *Neuroscience* (2021) 462:303–19. doi:10.1016/j.neuroscience.2020.05.010
64. Scattoni ML, Crawley J, Ricceri L. Ultrasonic Vocalizations: a Tool for Behavioural Phenotyping of Mouse Models of Neurodevelopmental Disorders. *Neurosci Biobehav Rev* (2009) 33(4):508–15. doi:10.1016/j.neubiorev.2008.08.003
65. Kazdoba TM, Leach PT, Crawley JN. Behavioral Phenotypes of Genetic Mouse Models of Autism. *Genes Brain Behav* (2016) 15(1):7–26. doi:10.1111/gbb.12256
66. Tsai PT, Hull C, Chu Y, Greene-Colozzi E, Sadowski AR, Leech JM, et al. Autistic-like Behaviour and Cerebellar Dysfunction in Purkinje Cell Tsc1 Mutant Mice. *Nature* (2012) 488(7413):647–51. doi:10.1038/nature11310
67. Al-Afif S, Staden M, Krauss JK, Schwabe K, Hermann EJ. Splitting of the Cerebellar Vermis in Juvenile Rats-Eeffects on Social Behavior, Vocalization

and Motor Activity. *Behav Brain Res* (2013) 250:293–8. doi:10.1016/j.bbr.2013.05.013
68. Lalonde R, Strazielle C. Behavioral Effects of Neonatal Lesions on the Cerebellar System. *Int J Dev Neurosci* (2015) 43:58–65. doi:10.1016/j.ijdevneu.2015.04.007
69. Wolf LW, LaRegina MC, Tolbert DL. A Behavioral Study of the Development of Hereditary Cerebellar Ataxia in the Shaker Rat Mutant. *Behav Brain Res* (1996) 75(1–2):67–81. doi:10.1016/0166-4328(96)00159-3
70. Thullier F, Lalonde R, Cousin X, Lestienne F. Neurobehavioral Evaluation of Lurcher Mutant Mice during Ontogeny. *Brain Res Dev Brain Res* (1997) 100(1):22–8. doi:10.1016/s0165-3806(97)00010-2
71. Jayabal S, Ljungberg L, Watt AJ. Transient Cerebellar Alterations during Development Prior to Obvious Motor Phenotype in a Mouse Model of Spinocerebellar Ataxia Type 6. *J Physiol (Lond)* (2017) 595(3):949–66. doi:10.1113/JP273184
72. Mencacci NE, Brockmann MM, Dai J, Pajusalu S, Atasu B, Campos J, et al. Bi-allelic Variants in *TSPOAP1*, Encoding the Active Zone Protein RIMBP1, Cause Autosomal Recessive Dystonia. *J Clin Invest* (2021) 131:e140625. doi:10.1172/JCI140625
73. Horisawa S, Kohara K, Nonaka T, Mochizuki T, Kawamata T, Taira T. Case Report: Deep Cerebellar Stimulation for Tremor and Dystonia. *Front Neurol* (2021) 12:642904. doi:10.3389/fneur.2021.642904
74. Brown EG, Bledsoe IO, Luthra NS, Miocinovic S, Starr PA, Ostrem JL. Cerebellar Deep Brain Stimulation for Acquired Hemidystonia. *Mov Disord Clin Pract* (2020) 7(2):188–93. doi:10.1002/mdc3.12876
75. Volpe JJ. *Neurology of the Newborn E-Book*. 5th ed. New York, NY: Elsevier Health Sciences (2008).
76. Bracewell M, Marlow N. Patterns of Motor Disability in Very Preterm Children. *Ment Retard Dev Disabil Res Rev* (2002) 8(4):241–8. doi:10.1002/mrdd.10049
77. van der Heijden ME, Gill JS, Sillitoe RV. Abnormal Cerebellar Development in Autism Spectrum Disorders. *Dev Neurosci* (2021) 43(3–4):181–90. doi:10.1159/000515189
78. Wang SS-H, Kloth AD, Badura A. The Cerebellum, Sensitive Periods, and Autism. *Neuron* (2014) 83(3):518–32. doi:10.1016/j.neuron.2014.07.016
79. Kelly E, Escamilla CO, Tsai PT. Cerebellar Dysfunction in Autism Spectrum Disorders: Deriving Mechanistic Insights from an Internal Model Framework. *Neuroscience* (2020) 462:274–87. doi:10.1016/j.neuroscience.2020.11.012
80. Kelly E, Meng F, Fujita H, Morgado F, Kazemi Y, Rice LC, et al. Regulation of Autism-Relevant Behaviors by Cerebellar-Prefrontal Cortical Circuits. *Nat Neurosci* (2020) 23(9):1102–10. doi:10.1038/s41593-020-0665-z
81. Stoodley CJ, Limperopoulos C. Structure-function Relationships in the Developing Cerebellum: Evidence from Early-Life Cerebellar Injury and Neurodevelopmental Disorders. *Semin Fetal Neonatal Med* (2016) 21(5):356–64. doi:10.1016/j.siny.2016.04.010

DYSTONIA

ORIGINAL RESEARCH
published: 21 July 2022
doi: 10.3389/dyst.2022.10557

Electrophysiological Characterization of the Striatal Cholinergic Interneurons in *Dyt1 ΔGAG* Knock-In Mice

Hong Xing, Fumiaki Yokoi, Ariel Luz Walker†, Rosemarie Torres-Medina, Yuning Liu and Yuqing Li**

Department of Neurology, Norman Fixel Institute of Neurological Diseases, College of Medicine, University of Florida, Gainesville, FL, United States

DYT1 dystonia is an inherited early-onset movement disorder characterized by sustained muscle contractions causing twisting, repetitive movements, and abnormal postures. Most DYT1 patients have a heterozygous trinucleotide GAG deletion mutation (*ΔGAG*) in *DYT1/TOR1A,* coding for torsinA. *Dyt1* heterozygous ΔGAG knock-in (KI) mice show motor deficits and reduced striatal dopamine receptor 2 (D2R). Striatal cholinergic interneurons (ChIs) are essential in regulating striatal motor circuits. Multiple dystonia rodent models, including KI mice, show altered ChI firing and modulation. However, due to the errors in assigning KI mice, it is essential to replicate these findings in genetically confirmed KI mice. Here, we found irregular and decreased spontaneous firing frequency in the acute brain slices from *Dyt1* KI mice. Quinpirole, a D2R agonist, showed less inhibitory effect on the spontaneous ChI firing in *Dyt1* KI mice, suggesting decreased D2R function on the striatal ChIs. On the other hand, a muscarinic receptor agonist, muscarine, inhibited the ChI firing in both wild-type (WT) and *Dyt1* KI mice. Trihexyphenidyl, a muscarinic acetylcholine receptor M1 antagonist, had no significant effect on the firing. Moreover, the resting membrane property and functions of hyperpolarization-activated cyclic nucleotide-gated (HCN) channels, μ-opioid receptors, and large-conductance calcium-activated potassium (BK) channels were unaffected in *Dyt1* KI mice. The results suggest that the irregular and low-frequency firing and decreased D2R function are the main alterations of striatal ChIs in *Dyt1* KI mice. These results appear consistent with the reduced dopamine release and high striatal acetylcholine tone in the previous reports.

Keywords: dystonia, cholinergic interneuron, dopamine receptor, muscarine, μ-opioid receptor, quinpirole, trihexyphenidyl, torsinA

OPEN ACCESS

Edited by:
Meike E. van der Heijden, Baylor College of Medicine, United States

Reviewed by:
Karen Jaunarajs, University of Alabama at Birmingham, United States
Heather Snell, Albert Einstein College of Medicine, United States

****Correspondence:***
Fumiaki Yokoi
fumiaki.yokoi@neurology.ufl.edu
Yuqing Li
yuqingli@ufl.edu

†Present address:
Ariel Luz Walker, Department of Neuroscience, Center for Translational Research in Neurodegenerative Disease, McKnight Brain Institute, University of Florida, Gainesville, FL, United States

Received: *08 April 2022*
Accepted: *29 June 2022*
Published: *21 July 2022*

Citation:
Xing H, Yokoi F, Walker AL, Torres-Medina R, Liu Y and Li Y (2022) Electrophysiological Characterization of the Striatal Cholinergic Interneurons in Dyt1 ΔGAG Knock-In Mice. Dystonia 1:10557. doi: 10.3389/dyst.2022.10557

Abbreviations: ACh, acetylcholine; AChE, acetylcholinesterase; ACSF, artificial cerebrospinal fluid; BK channel, large-conductance calcium-activated potassium channel; BSA, bovine serum albumin; ChAT, choline acetyltransferase; ChKO mice, cholinergic neuron-specific *Dyt1* conditional knockout mice; ChI, cholinergic interneuron; CV, coefficient of variation; dMSNs, direct pathway medium spiny neurons; D1R, dopamine receptor 1; D2R, dopamine receptor 2; DF, degrees of freedom; Dlx-CKO mice, forebrain-specific conditional knockout of torsinA mice; *Dyt1* KI mice, *Dyt1 ΔGAG* heterozygous knock-in mice; HCN channels, hyperpolarization-activated cyclic nucleotide-gated channels; iMSNs, indirect pathway medium spiny neurons; I_H, hyperpolarization and cyclic nucleotide activated cation current; IR, input resistance; ISI, interspike intervals; KO, knockout; LTD, long-term depression; MSN, medium spiny neuron; PB, phosphate buffer; PBS, phosphate-buffered saline; RMP, resting membrane potential; SD, standard deviations; THP, trihexyphenidyl; TTX, tetrodotoxin; WT, wild-type

INTRODUCTION

Dystonia is a movement disorder with abnormal postures, twisting, and repetitive movements caused by sustained muscle contractions (1, 2). Dystonia can be caused by multiple etiologies, such as stroke, brain injury, sporadic, and gene alterations. DYT1 dystonia is an inherited movement disorder characterized by early-onset, generalized torsion, twisting, repetitive movements, or abnormal postures [DYT-TOR1A; Online Mendelian Inheritance in Man (OMIM) identifier #128100]. Most patients have a heterozygous in-frame trinucleotide deletion (ΔGAG) in *DYT1*/*TOR1A*, coding for torsinA (3). The penetrance is about 30%–40%, and non-symptomatic carriers of the *DYT1* gene mutation have an impairment in sequence learning (4, 5). Trihexyphenidyl (THP), an antagonist mainly to muscarinic acetylcholine receptor M1, ameliorates dystonic symptoms in DYT1 patients, suggesting a functional alteration in cholinergic or its related system (6, 7).

Two independent mutant mouse lines with the corresponding trinucleotide deletion in the endogenous *Dyt1*/*Tor1a* have been reported, i.e., the *Dyt1* ΔGAG heterozygous knock-in (KI) mice (www.informatics.jax.org; Allele Symbol: Tor1a^{tm1Yql}) (8) and *Tor1a*$^{+/\Delta gag}$ KI mice (Tor1a^{tm2Wtd}) (9). Although both lines do not show overt dystonic symptoms, motor deficits of the hind limbs in the beam-walking test were reproduced in distinct batches of one line (8, 10, 11) and another line (12, 13). The same motor deficits in the beam-walking test were observed in other genetic dystonia mouse models, such as DYT11 myoclonus-dystonia and DYT12 rapid-onset dystonia with parkinsonism (14, 15), suggesting beam-walking deficits as a typical motor phenotype in these genetic dystonia mouse models. Motor deficits using other behavioral tests were also reported in other genetic animal models (16–19), such as rat (20), nematode (11), and fruit fly (21, 22). *Dyt1* KI mice exhibit the corticostriatal long-term depression (LTD) deficits (23), sustained contraction and co-contraction of agonist and antagonist muscles of hind limbs (24), motor deficits in the beam-walking test (8), and impaired motor-skill transfer (25). These phenotypes are ameliorated by trihexyphenidyl (THP) (23, 24, 26), suggesting that these phenotypes are caused by the same mechanism as DYT1 dystonia patients.

The fibroblasts from DYT1 patients show a reduction of torsinA (9). The mutant torsinA is quickly degraded in transfected cells, suggesting that the GAG deletion causes partial loss of torsinA function (27, 28). Both *Dyt1* knockdown mice (29) and *Dyt1* heterozygous KO mice (30) show motor deficits in the beam-walking test, suggesting that partial loss of torsinA contributes to the motor deficits. Both cerebral cortex-specific *Dyt1* conditional knockout (KO) mice (31), which were produced by crossing *Dyt1 loxP* mice and *Emx1-Cre mice* (32), and striatum-specific *Dyt1* conditional KO mice (33), which were produced by crossing *Dyt1 loxP* mice and *Rgs9-Cre* mice (34), also show beam-walking deficits (31). Therefore, the loss of torsinA function in the corticostriatal pathway contributes to motor deficits. Moreover, both cholinergic neuron-specific torsinA knockout (ChKO) mice with *Neo* cassette (35) and those without *Neo* cassette (Ch2KO) mice show motor deficits (36). Dopamine receptor 2 (D2R)-expressing-cell-specific *Dyt1* conditional KO (d2KO) mice also show beam-walking deficits (37). On the other hand, the cerebellar Purkinje cell-specific *Dyt1* conditional KO and dopamine receptor 1 (D1R)-expressing-cell-specific *Dyt1* conditional KO (d1KO) mice show better performance in beam-walking (38). On the other hand, acute suppression of torsinA expression *via* AAV-TorsinA shRNA-GFP induces a dystonia-like phenotype (39), highlighting the contribution of the cerebellum to the pathogenesis of DYT1 dystonia (40). *Dyt1* KI mice show striatal D1R (25) and D2R reductions (23). *Dyt1* sKO and *Dyt1* d2KO mice show striatal D2R reduction and *Dyt1* d1KO mice show striatal D1R maturation deficits, suggesting that the D1R and D2R reductions are intrinsic cellular properties caused by the loss of torsinA in the corresponding neurons. *Dyt1* ΔGAG homozygous KI and *Dyt1* homozygous KO mice show neonatal lethality (8, 9, 31). On the other hand, the mutant mice with a combination of neuron- and glia-cell-specific *Dyt1* conditional KO and heterozygous KO show growth retardation and infant lethality, which can be rescued by enhanced care (41, 42).

Both *Dyt1* KI and heterozygous KO mice show similar hippocampal neurotransmitter releasing deficits (30, 43). *Tor1a*$^{+/\Delta gag}$ KI mice show abnormal synaptic vesicle recycling, glutamate release, and calcium dynamics (44–46). Moreover, Dlx-CKO mice, which have a combination of forebrain-specific conditional KO of torsinA in one allele and heterozygous KO in the other allele, show neurodegeneration of the striatal ChIs, and the surviving ChIs showed a trend of reduced spontaneous firing (47). Transgenic hMT mice (48), transgenic ΔETorA rats (20), and "*Tor1a*$^{+/\Delta gag}$ KI mice" (49) show abnormal ChI firing properties. However, it should be noted that "*Tor1a*$^{+/\Delta gag}$ KI mice" in the paper were purchased from Jackson Lab (Stock No. 006251), which is *Tor1a*$^{+/-}$ heterozygous KO mice lacking exons 2–4. Another recent report showed enhanced functions of μ-opioid receptors and large-conductance calcium-activated potassium (BK) channels of the striatal ChIs in *Tor1a* heterozygous KO mice (50).

Striatal ChIs show autonomous firing rather than reflections from the various synaptic input (51). The spontaneous firing patterns are affected by intrinsic membrane properties and the selective coupling of calcium currents to calcium-activated potassium currents and calcium dynamics (52–54). However, recent studies suggest that the striatal ChIs receive inputs from multiple neurons, including the cortical and the thalamic neurons (55) and the striatal medium spiny neurons (MSNs) (56–59). The striatal ChIs have an autofeedback mechanism through the inhibitory muscarinic acetylcholine receptors M2/M4 and RGS4 pathway (60, 61). Muscarine, a muscarinic acetylcholine receptor agonist, inhibits the striatal ChI firing in the rat brain slices by reducing N-, P- and L-type Ca^{2+} currents (62). Striatal ChIs affect the corticostriatal plasticity of the striatal MSNs (63). M1 and M4 muscarinic acetylcholine receptor mRNAs are expressed at high levels by the striatal MSNs (64) and have subtle changes in *Tor1a*$^{+/\Delta gag}$ KI mice (65). The released ACh binds M1-type receptors and depolarizes the MSNs. ACh also

binds to M4 receptors on the direct pathway MSNs and modulates their activity (66). Moreover, striatal ACh binds to nicotinic acetylcholine receptors on the axons of dopaminergic neurons projecting from the substantia nigra pars compacta and synchronously stimulates local dopamine release (67). The released dopamine stimulates the surrounding D1R and D2R on the MSNs and D2R on the ChIs (57, 68).

Here, the striatal ChIs in the *Dyt1* KI mice were characterized by electrophysiological recording of acute brain slices and a cellular morphological approach. The spontaneous firing of striatal ChIs and its modulation by muscarine (muscarinic acetylcholine receptor agonist), quinpirole (D2R agonist), and THP (M1 receptor antagonist) were examined. Furthermore, the effect of DAMGO (μ-opioid receptor agonist) and PAX (BK channel blocker) on the membrane currents was investigated (50). Moreover, the resting membrane property, the intrinsic excitability and hyperpolarization-activated cyclic nucleotide-gated (HCN) channels of the striatal ChIs were measured. Finally, the dendritic structure and soma size of the recorded ChIs were quantified.

MATERIALS AND METHODS

Animals

All experiments were carried out in compliance with the USPHS Guide for Care and Use of Laboratory Animals and approved by the Institutional Animal Care and Use Committees of the University of Florida. *Dyt1* KI mice ($Tor1a^{tm1Yql}$) and their littermate WT mice were prepared and genotyped by PCR (8, 69). Since male *Dyt1* KI mice exhibited significant motor deficits in the previous study (8), only males were used for the present experiments. Mice were housed under a 12 h light and 12 h dark cycle with *ad libitum* access to food and water. All experiments were performed by investigators blind to the genotypes. This study followed the recommended heterogenization of study samples of various ages, and the data were analyzed with age as a covariate (70).

Brain Slices

Electrophysiological recordings for spontaneous firing and evoked firing of the striatal ChIs were obtained from 25 WT and 25 KI littermate male mice (6–11 weeks old), as described previously (71, 72).

Mice were anesthetized by the inhalation of isoflurane and decapitated. The brains were rapidly removed and briefly chilled in the ice-cold cutting solution containing (in mM) 190 Sucrose, 2.5 KCl, 1.25 NaH_2PO_4, 25 $NaHCO_3$, 1 $CaCl_2$, 10 $MgCl_2$, and 10 D-glucose and was oxygenated with 95% O_2–5% CO_2 (pH 7.35–7.45). In the same ice-cold cutting solution, coronal brain slices (300 μm-thick) were obtained with a Vibratome (LEICA VT 1000S, Leica Microsystems, Wetzlar, Germany). Slices were first incubated on a brain slice keeper (AutoMate Scientific, Inc. Berkeley, CA) with a thin layer of artificial cerebrospinal fluid (ACSF) containing (in mM) 127 NaCl, 2.5 KCl, 1.25 NaH_2PO_4, 25 $NaHCO_3$, 2 $CaCl_2$, 5 $MgCl_2$, and 10 D-glucose, saturated with 95% O_2 and 5% CO_2 (pH 7.35–7.45) at 35°C for 60 min, followed by incubation at room temperature. After a minimum of 60-min incubation, each slice was transferred to a submerged recording chamber with the continuous flow (2 ml/min) of ACSF containing (in mM) 127 NaCl, 2.5 KCl, 1.25 NaH_2PO_4, 25 $NaHCO_3$, 2 $CaCl_2$, 1 $MgCl_2$, and 10 D-glucose and was constantly oxygenated with 95% O_2 and 5% CO_2 (pH 7.35–7.45). All experiments were carried out at 32 ± 0.5°C by a dual automatic temperature controller (TC-344B, Harvard Apparatus) under visual guidance using an inverted microscope equipped with infrared differential interference contrast (IR-DIC) videomicroscopy (Axioskop-FS; Carl Zeiss, Jena, Germany) and a 40× water-immersion lens.

Cell-Attached Recordings

The large neurons with ellipsoid-like soma were selected in the dorsal striatum under the microscope for the electrophysiological recordings. ChIs are further identified by whole-cell recording with step-current injection (73) and, in some cases, by a post hoc immunohistochemistry with an anti-ChAT antibody (71). Patch electrodes had a resistance of 5–10 MΩ when filled with a K-gluconate-based solution containing the following intracellular solution containing (in mM): 112.5 K-gluconate, 4 NaCl, 17.5 KCl, 0.5 $CaCl_2$, 1 $MgCl_2$, 5 K_2ATP, 1 NaGTP, 5 EGTA, 10 HEPES, pH 7.2 (270–280 mOsm/l). Biocytin (0.1%) was added to the recording electrode solution to allow post hoc immunohistochemical identification of the recorded cells. While approaching the cell, positive pressure was applied to the patch electrode. The seal (>5 GΩ) between the recording pipette and the cell membrane was obtained by suctioning the electrode. Action potential currents were recorded in the voltage-clamp mode, maintaining an average of 0 pA holding current. After baseline recording, some ChIs were investigated further with bath applications of muscarine [(+)-Muscarine chloride (Sigma Aldrich, M6532-5MG), 10 μM, 90 s (s)] or, THP [DL-Trihexyphenidyl hydrochloride (Sigma Aldrich, T1516-5G), 5 μM, 90 s)] for testing the effect of agonist and antagonist to the muscarinic acetylcholine receptors on the ChIs, respectively. Moreover, some other ChIs were investigated with bath applications of quinpirole [Quinpirole hydrochloride (Sigma Aldrich, Q102-25MG), 10 μM, 2 min] for testing the effect of the agonist to D2R on the ChIs. The effect of quinpirole on spontaneous firing was also examined in a different condition., the spontaneous firing was recorded for 30 s just before adding the drug into the recording bath. The drug was added for 90 s, and recording data in the last 30 s during the drug treatment period were used as "after treatment". In another condition, the firing was recorded for 3 min at around 10 min after starting the cell-attached recording. Ten μM quinpirole was then applied into the recording chamber for 3 min, followed by a 2 min wash out with ACSF and 3 min recording.

Whole-Cell Recording of the Striatal ChIs

Whole-cell recordings were made by breaking through the membrane. The electrophysiological intrinsic membrane properties (capacitance, input resistance, and time constant) were measured while holding the membrane potential at −60 mV. The liquid junction potential was compensated.

Electrode access resistances during all whole-cell recordings were maintained at <25 MΩ. The current steps were injected in multiple 200 pA from −0.8 to 0.6 nA, and the evoked-action-potentials were recorded in the whole-cell recording mode with the current clamp.

To further characterize the electrophysiological properties of μ-opioid receptors and BK channels of the striatal ChIs in *Dyt1* KI (n = 5) and control WT littermate male mice (n = 4) at 13–21 weeks-old, the current-voltage relationship of the striatal ChIs was measured by whole-cell recording mode during the voltage ramp (50) with the glass recording electrode filled with a K-gluconate solution containing the following (in mM): 125 K-gluconate, 0.5 EGTA, 19 HEPES, 0.3 GTP, 1 Mg-ATP, 10 NaCl, 2 $MgCl_2$, 1 $CaCl_2$. The brain slices were prepared as described above and incubated until recording. Each slice was transferred to a submerged recording chamber with the continuous flow (2 ml/min) of ACSF. The dorsal striatal ChIs were identified from their shape, and the spontaneous firing was confirmed in cell-attached mode, and then the membrane current was recorded in whole-cell recording mode. The membrane potential was held at −70 mV with a voltage clamp. The voltage ramp was applied from −60 to −140 mV in 500 ms, and the membrane current was recorded during the ramp. After multiple recordings, voltage ramp protocols were repeated when the recorded neurons were exposed to 1 μM tetrodotoxin (TTX), 1 μM TTX + 1 μM D-Ala2-MePhe4-Gly[ol]5enkephaline (DAMGO; AdipoGen; AG-CP3-0005V-M005), 1 μM TTX + 1 μM DAMGO + 1 μM Paxilline (PAX; Alomone labs; P-450) sequentially.

Recording Data Analysis

The recording data were acquired using pClamp 10 software and further analyzed by Mini Analysis Program (Synaptosoft). Signals were filtered at 5 kHz, and digitized at 10 kHz with a DigiData 1440 (Molecular Devices). Investigators who were blind to the genotypes performed the electrophysiological recordings and analysis. The 30 s (s) before drug treatment and the last 30 s during the drug treatment were used to analyze the drug effect on the spontaneous firing. For the 10-min quinpirole recording analysis, the 3 min before quinpirole treatment and the 3 min after 2 min of quinpirole washout were quantified.

Double-Staining of the Recorded Striatal ChIs and Tracing of the Dendrites

Since the neurons were recorded with the internal solution containing 0.1% biocytin, the recorded neurons were stained with fluorescent-conjugated streptavidin through biocytin-streptavidin binding. After the recordings, the brain slices were fixed overnight with 4% paraformaldehyde in 0.1M phosphate buffer (PB; pH 7.3) and stored in 0.1M PB. The slices were rinsed twice with 0.5% Triton X-100 in 0.02M PB for 10 min and then incubated for 2 hours protected from light in 0.5% (v/v) Triton X-100, 1% (w/v) bovine serum albumin (BSA), 0.02M PB, 0.2% (v/v) streptavidin Alexa Fluor 594 conjugate (Life technologies, S11227). The slices were rinsed with 0.5% Triton X-100 in 0.02M PB twice for 5 min each and then 0.02M PB once. The slices were washed in 10 mM glycine/PBS three times 5 min each and blocked in 2% gelatin/PBS for 15 min, 10 mM glycine/PBS for 5 min, and 0.1% BSA/PBS for 5 min. The blocked slices were incubated in goat anti-ChAT antibody (EMD Millipore, AB144P; 1:100 dilution) in 1% BSA/PBS for 2 h and washed in 0.1% BSA/PBS six times 5 min each. The slices were then incubated with Alexa Fluor 488 donkey anti-goat IgG (H+L) (Invitrogen, A11055; 1:200 dilution) in 1% BSA/PBS for 2 h and washed in 0.1% BSA/PBS six times 5 min each. The slices were mounted on glass slides with Vectashield Hard Set mounting medium for fluorescence (Vector Lab Inc., H-1400) and stored at 4°C overnight. The double-positive cells were confirmed using a ZEISS Axiophot RZGF-1 microscope with 2.5× or ×20 Plan-NEOFLUAR objective lens and FITC filter for Alexa Fluor 488 and Texas Red filter for Alexa Fluor 594, respectively. The dendrites were stained with streptavidin Alexa Fluor 594 conjugate and digitized at ×40 magnification using MBF Bioscience Neurolucida 7 and NeuroExplorer software (MicroBrightFields Bioscience). Sholl analysis (74) was performed using ImageJ software (NIH). Representative images were also taken by Olympus IX81-DSU Spinning Disk Confocal Microscope with ×60 Water immersion objective lens, FITC filter for Alexa Fluor 488, and Texas Red filter for Alexa Fluor 594, respectively.

Statistics

The spontaneous firing frequency and the drug effects were analyzed by a linear mixed model (lme), generalized linear mixed model (glmmTMB), and emmeans program in R version 4.1.2 (R Foundation for Statistical Computing, Vienna, Austria) for the animal-based nested data, or SAS GENMOD Procedure GEE model. The distribution of the data was checked by R shapiro.test. The coefficient of variation (CV), which is defined by standard deviations (SD) of the interspike intervals (ISI) per mean ISI (73), was analyzed by a generalized linear mixed model (R glmer) for the animal-based nested SD of ISI in gamma distribution concerning the offset log mean ISI. The number of paradoxically-excited ChIs was analyzed by R fisher.test. Wilcoxon rank-sum exact test was performed by R wilcox.test.

Median and confidence interval was analyzed by R MedianCI. The resting membrane property and I_H current were analyzed by R lme with the animal-based nested data. The recording order per ChI was also used as a variable for I_H. The current-step-evoked firing was analyzed by the SAS GENMOD Procedure GEE model with a negative binomial distribution. The membrane currents produced by voltage ramps were analyzed by the SAS GENMOD with gamma distribution concerning age. The number of intersections in Sholl analysis and the soma size of the ChIs were analyzed by Student's t-test (75). The length of the longest traced dendrites was analyzed by glmmTMB. Significance was assigned at $p < 0.05$.

RESULTS

Decreased Spontaneous Firing Frequency and Increased CV of the Striatal ChIs in *Dyt1* KI Mice

The striatal ChIs play a vital role in the pathogenesis of dystonia (76). The striatal ChIs in the *Dyt1* KI mice were

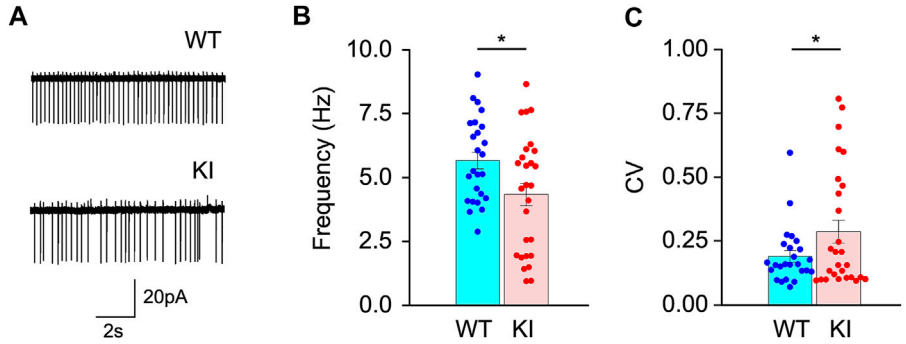

FIGURE 1 | Spontaneous firing of the striatal ChIs in the acute brain slices. **(A)** The representative traces of the striatal ChIs. Spontaneous firing frequency **(B)** significantly decreased, and CV **(C)** significantly increased in *Dyt1* KI mice. The bars represent means ± standard errors. The dots represent each data point. *$p < 0.05$.

characterized by the electrophysiological recording of acute brain slices. The spontaneous firing of the striatal ChIs was recorded by cell-attached recording mode with a voltage clamp (WT, 25 cells/14 mice; KI, 27 cells/15 mice). As shown in the representative traces of the striatal ChIs (**Figure 1A**), the firing frequency was significantly decreased in *Dyt1* KI mice compared to WT mice [mean ± standard errors Hz; WT, 5.7 ± 0.3; KI, 4.3 ± 0.4; t(DF: 27) = −2.17, p = 0.039; **Figure 1B**]. *Dyt1* KI mice also showed significantly increased CV [WT, 0.19 ± 0.02; KI, 0.29 ± 0.04; t(27) = 2.02, p = 0.044; **Figure 1C**]. Increased CV suggests a high irregularity of firing.

Less Inhibitory Effect of Quinpirole on the Firing of the Striatal ChIs in *Dyt1* KI Mice

D2R is reduced in the striatum of KI mice (23), but it is not known whether it is specifically reduced in striatal ChIs or not. The effect of quinpirole, a D2R agonist, on the spontaneous firing of striatal ChIs was further analyzed (WT, 10 cells/6 mice; KI, 12 cells/6 mice). A representative trace is shown in **Figure 2A**. The firing frequencies were decreased by quinpirole in both WT [Hz; before, 4.4 ± 0.8; after, 2.6 ± 0.8; t(13) = −2.9, p = 0.014; **Figure 2B**] and *Dyt1* KI mice [Hz; before, 3.2 ± 0.4; after, 2.2 ± 0.4; t(17) = −3.0, p = 0.0087; **Figure 2C**]. After the quinpirole application, the recording chamber solution was changed to ACSF for more than 2 minutes. Most ChIs showed recovery of the spontaneous action potentials in both WT and *Dyt1* KI mice. To compare the quinpirole inhibitory effect, we divided the frequency after the treatment by that before. Quinpirole showed less inhibitory effect in *Dyt1* KI mice compared to WT mice [WT, 54 ± 6%; KI, 80 ± 5%; Chi-Square (1) = 4.47, p = 0.034; **Figure 2D**]. Since the inhibitory D2R is expressed on the striatal ChIs, the results suggest that the inhibition through D2R may be less effective in *Dyt1* KI mice. As shown in **Figures 2B,C**, none of the ten ChIs in WT mice and two out of twelve ChIs in *Dyt1* KI mice showed paradoxical excitation, which is a reversed excitatory response to quinpirole. Although paradoxically-excited ChIs were observed only in *Dyt1* KI mice, Fisher's exact test showed no statistically significant difference in the number of paradoxically-excited ChIs between WT and *Dyt1* KI mice (p = 0.48). On the other hand, there was no significant difference in the CV after the quinpirole treatment in WT (before, 0.30 ± 0.07; after, 0.34 ± 0.08; z = 0.70, p = 0.49) and *Dyt1* KI mice (before, 0.33 ± 0.07; after, 0.42 ± 0.09; z = 0.88, p = 0.38). Moreover, there was no significant difference between WT and *Dyt1* KI mice in the effect of quinpirole on the CV (WT, 125 ± 20%; KI, 146 ± 34%; z = 0.60, p = 0.55).

No Significant Difference in the Paradoxical Excitation of Striatal ChIs Between WT and *Dyt1* KI Mice After Quinpirole Treatment

Paradoxical activation of D2R by quinpirole was reported in several mouse and rat models of DYT1 dystonia (77–79). However, the paradoxical activation was not reproduced as detailed above. These published studies examined the quinpirole effect after extended baseline recording. Therefore we repeated the quinpirole experiment to mimic their recording condition. The firing frequency was compared before and after quinpirole treatment (WT, 14 cells/7 mice; KI, 14 cells/8 mice). The representative traces are shown in **Figure 2E**. There was no significant long-term effect of quinpirole on the firing frequencies in both WT [Hz; before, 2.6 ± 0.4; after, 2.4 ± 0.4; t(20) = −0.37 p = 0.72; **Figure 2F**] and *Dyt1* KI mice [Hz; before, 2.6 ± 0.4; after, 2.8 ± 0.4; t(20) = 0.31, p = 0.76; **Figure 2G**]. As shown in **Figures 2F,G**, five out of fourteen ChIs in WT mice and seven out of fourteen ChIs in *Dyt1* KI mice showed increased frequency compared to those before quinpirole treatment, which would qualify as paradoxical excitation. Fisher's exact test showed no significant difference in the number of paradoxically-excited ChIs between WT and *Dyt1* KI mice (p = 0.70). These results suggest no significant difference in the appearance of paradoxical excitation cells between the genotypes. The frequency after the treatment was divided by that before the treatment. Shapiro test showed that the ratio data were not normally distributed (WT, p = 0.030; KI, $p = 1.7 \times 10^{-6}$; all, $p = 5.6 \times 10^{-10}$). Wilcoxon rank-sum exact test showed that there was no significant difference in the long-term effect of quinpirole between WT and *Dyt1* KI mice [median, (lower,

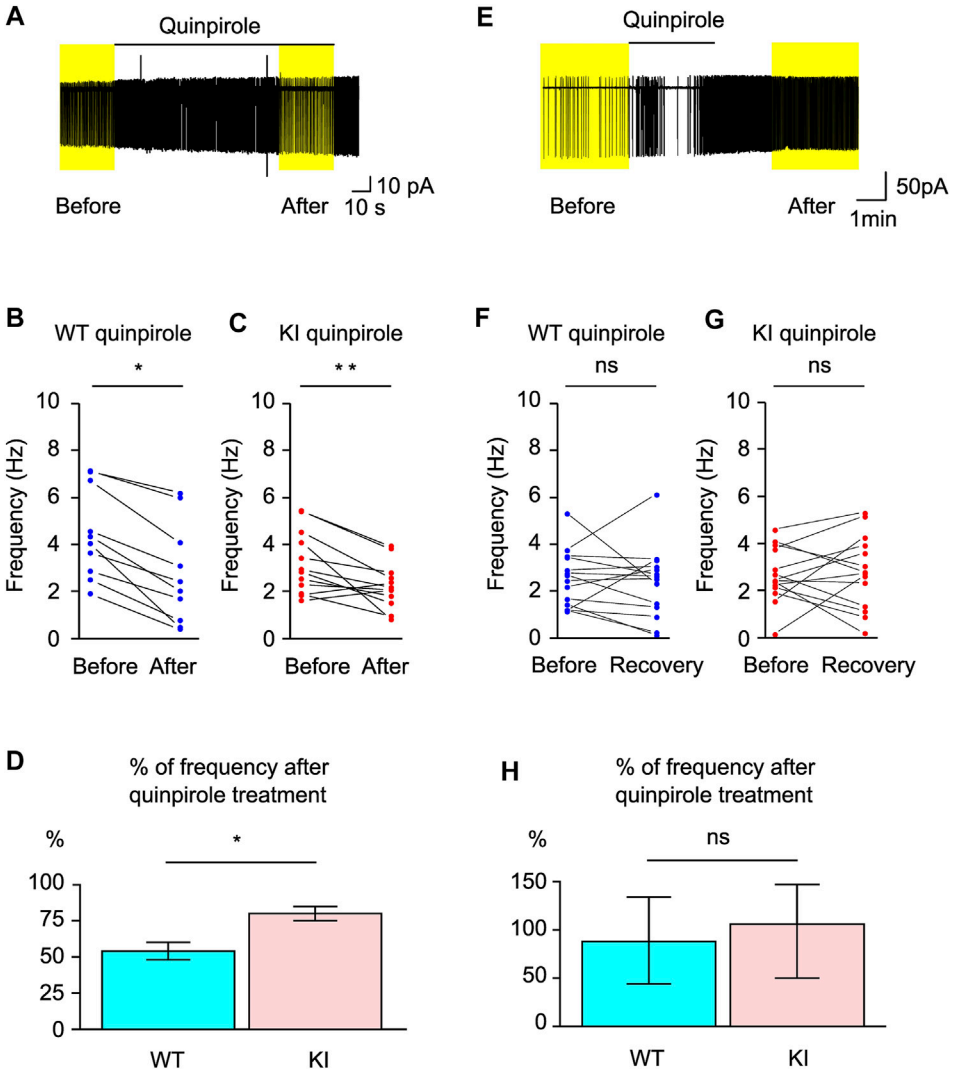

FIGURE 2 | Responses of the striatal ChIs in the acute brain slices to quinpirole. Representative trace of the spontaneous firing and the inhibitory response to quinpirole **(A)**. The spontaneous firings were inhibited by quinpirole in both WT **(B)** and *Dyt1* KI mice **(C)**. The percentage of frequency (Hz) after quinpirole **(D)** treatment was compared to those before treatment. The 30 s before drug application and the last 30 s during the drug application (yellow boxes) were used to analyze drug effects. There was significantly less quinpirole inhibition in the KI mice. **(E)** An extreme case of the paradoxical excitation of a KI ChI after quinpirole treatment was applied 13 min after the cell-attached recording. The lines under Quinpirole show the duration of drug application [**(E)**, 120 s]. Overall, the spontaneous firings were not significantly inhibited by quinpirole in both WT **(F)** and *Dyt1* KI mice **(G)**. The frequency after quinpirole treatments was compared to before treatment **(H)**. The bar graph show median of the percentage. The error bars show upper and lower 95% confidence intervals. The 3 min before drug application and the 3 min after 2 min washout (yellow boxes) were used to analyze the quinpirole effect. ns: not significant, $^{*}p < 0.05$, $^{**}p < 0.01$.

upper 95% confidence interval); WT, 88, (44, 134); KI, 106, (50, 147); W = 111, $p = 0.57$; **Figure 2H**].

Equivalent Inhibitory Effect of Muscarine on the Firing of the Striatal ChIs Between WT and *Dyt*1 KI Mice

Muscarine, a muscarinic acetylcholine receptor agonist, inhibits the striatal ChI firing, and this effect was found to be absent in ChKO mice (35) but was found to be normal Ch2KO mice (36). The effect of muscarine on the spontaneous firing of striatal ChIs in KI mice has not been examined and is explored here. We compared the firing before and after muscarine application (WT, 11 cells/6 mice; KI, 13 cells/6 mice). The firing frequencies were significantly decreased by muscarine in both WT [Hz; before, 4.9 ± 0.5; after, 2.6 ± 0.5; t(15) = −3.15, $p = 0.0066$; **Figure 3A**] and *Dyt1* KI mice [Hz; before, 4.6 ± 0.7; after, 2.2 ± 0.5; z = −3.2, $p = 0.0012$; **Figure 3B**]. To compare the inhibitory effect, we divided the frequency after the treatment by before the treatment. There was no significant difference in the inhibitory effect of muscarine between WT and *Dyt1* KI mice [WT, 53 ± 3%; KI, 54 ± 5%; Chi-Square (1) = 0.02, $p = 0.90$; **Figure 2C**]. Since inhibitory muscarinic acetylcholine receptors, M2/M4, are

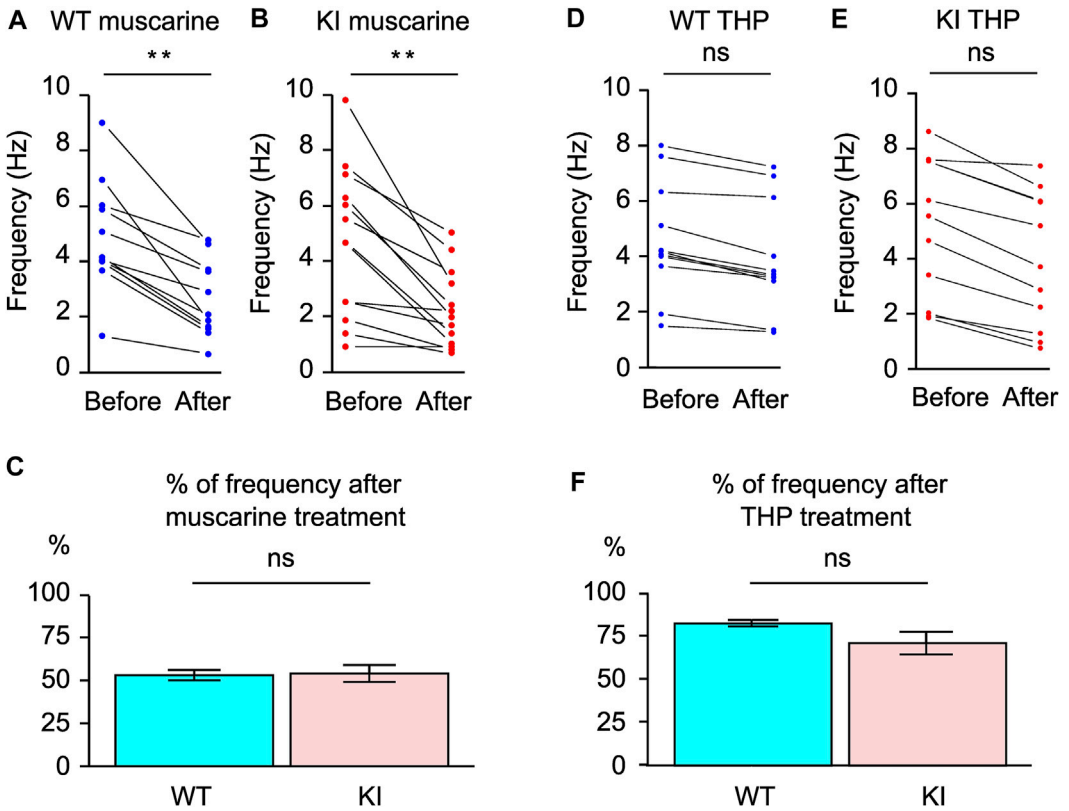

FIGURE 3 | Responses of the striatal ChIs in the acute brain slices to muscarine and THP. The spontaneous firings were inhibited by muscarine in both WT **(A)** and *Dyt1* KI mice **(B)**. The percentage of frequency (Hz) after muscarine **(C)** was analyzed by comparing it to those before treatment. There was no significant alteration in the spontaneous firing frequencies after THP application in WT **(D)** and *Dyt1* KI mice **(E)**. The percentage of frequency (Hz) after THP treatment was compared to those before treatment **(F)**. The bars represent means ± standard errors **(C,F)**. ns, not significant, $^{**}p < 0.01$.

expressed on the striatal ChIs, these results suggest that the inhibition through M2/M4 is not altered in *Dyt1* KI mice.

No Significant Effect of Trihexyphenidyl on the Firing of the Striatal ChIs in WT and *Dyt1* KI Mice

THP, a muscarinic acetylcholine receptor M1 antagonist, is effective in treating DYT1 patients and can reverse motor, electrophysiological, and EMG deficits in KI mice (23, 24, 26). The effect of THP on the spontaneous firing of striatal ChIs was examined to explore whether THP reverses the deficits by acting on striatal ChIs. We compared the firing before and after THP application (WT, 11 cells/3 mice; KI, 11 cells/4 mice). There was no significant alteration in the firing frequencies by THP in both WT [Hz; before, 4.6 ± 0.7; after, 3.8 ± 0.7; Chi-Square (1) = 2.76, $p = 0.097$; **Figure 3D**] and *Dyt1* KI mice [Hz; before, 5.5 ± 1.0; after, 4.1 ± 1.0; Chi-Square(1) = 3.74, $p = 0.053$; **Figure 3E**]. To compare the THP effect, we divided the frequency after the treatment by that of before and compared WT and *Dyt1* KI mice. There was no significant difference in the effect of THP between WT and *Dyt1* KI mice [WT, 83 ± 2%; KI, 71 ± 7%; Chi-Square(1) = 1.80, $p = 0.18$; **Figure 3F**]. These results suggest that THP does not affect the spontaneous firing of the ChIs in KI mice.

No Significant Alteration in the Membrane Property and the Intrinsic Excitability of the Striatal ChIs in *Dyt1* KI Mice

This series of experiments is to determine whether the membrane property and intrinsic excitability contribute to the reduced spontaneous firing of striatal ChIs in the KI mice or not. After recording the spontaneous firing by cell-attached mode, the intrinsic membrane properties were measured in whole-cell recording mode. The resting membrane property of the striatal ChIs was characterized in the brain slices from 11 WT (29 cells) and 15 *Dyt1* KI mice (26 cells). There was no significant difference in the resting membrane potential (RMP), the membrane capacitance, the input resistance (IR), or the time constant between WT and *Dyt1* KI mice (**Table 1**).

The intrinsic excitability of the striatal ChIs in the brain slices was measured with current step injections (**Figures 4A–C**). The recorded neurons showed typical electrophysiological properties of the striatal ChIs (51). The hyperpolarization and cyclic nucleotide activated cation current (I_H) was calculated (80). There was no significant alteration in I_H between WT and

TABLE 1 | Electrophysiological characterization of the ChI resting membrane property in the dorsal striatum.

	RMP (mV)	Capacitance (pF)	IR (MΩ)	Time Constant (ms)	I_H
WT	–61.2 ± 1.9	77.7 ± 5.0	150 ± 9.0	0.91 ± 0.08	20.6 ± 4.3
KI	–61.2 ± 1.9	75.1 ± 5.2	148 ± 9.3	0.91 ± 0.08	22.0 ± 4.6
t (DF)	–0.01 (8)	–0.37 (8)	–0.12 (8)	0.04 (8)	0.23 (17)
p	0.99	0.72	0.91	0.97	0.83

The resting membrane property was obtained from 5 WT (12 cells) and 5 Dyt1 *KI, mice (11 cells).* I_H, *was obtained from one or two recordings per cell in 3 WT (14 recordings from10 cells) and 3* Dyt1 *KI mice (10 recordings from 9 cells). The p-value was calculated by R lme program with the animal-based nested data and the recording order per cell as a variable (for* I_H*). There was no significant difference between the first and the second recordings (p = 0.60 for* I_H*). The mean ± standard error was calculated by R emmeans program. RMP, resting membrane potential; IR, input resistance;* I_H, *hyperpolarization and cyclic nucleotide activated cation current; DF, degree of freedom.*

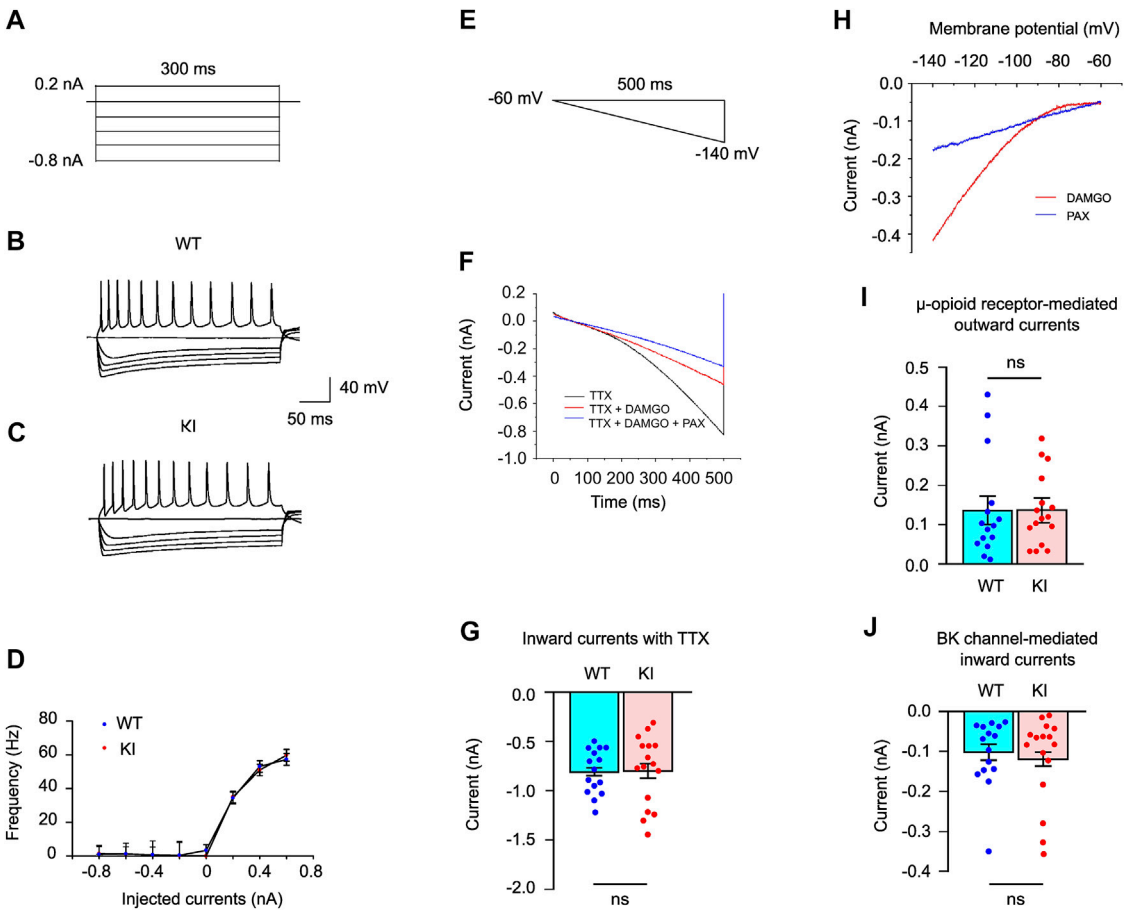

FIGURE 4 | Whole-cell recording of the striatal ChIs. Representative current steps [–0.8–0.2 nA, **(A)**] and traces **(B,C)**. There was no significant difference in the frequency-current relationship generated by the current steps (–0.8–0.6 nA) between WT and *Dyt1* KI mice **(D)**. Voltage ramp used for whole-cell voltage-clamp recording of ChIs **(E)**. Representative traces of the electrophysiological responses of the striatal ChIs with 1 μM TTX, 1 μM TTX + 1 μM DAMGO, and 1 μM TTX + 1 μM DAMGO + 1 μM PAX **(F)**. Measured inward currents at −140 mV of the hyperpolarized ChI membranes in WT and *Dyt1* KI mice are plotted **(G)**. The digitally subtracted currents with DAMGO and PAX treatments **(H)**. There is no difference in the μ-opioid receptor-induced outward currents between WT and *Dyt1* KI mice **(I)**. There is no difference in the BK channel-mediated inward currents in WT and *Dyt1* KI mice **(J)**. The bar graphs in G, I, and J show means ± standard errors. ns, not significant.

Dyt1 KI mice (**Table 1**), suggesting that HCN channels were normal in *Dyt1* KI mice.

Moreover, the frequency-current relationship showed that there was no significant alteration in the firing frequencies between WT and *Dyt1* KI mice (0.2 nA injection; WT, 34.4 ± 3.5 Hz; KI, 35.0 ± 3.4 Hz; z = 0.32, $p = 0.75$; 0.4 nA injection; WT, 53.1 ± 3.4 Hz; KI, 51.0 ± 3.4 Hz; z = −0.97, $p = 0.33$; 0.6 nA injection; WT, 57.3 ± 3.5 Hz; KI, 59.8 ± 3.5 Hz; z = 0.46, $p = 0.65$; **Figure 4D**). These results suggest that the intrinsic excitability of the striatal ChIs is not altered in *Dyt1* KI mice.

No Significant Alteration in the Inward Currents Induced by Hyperpolarization of the Striatal ChIs in *Dyt1* KI Mice

Hyperpolarization of the membrane potential by voltage ramp induces an influx of cation ions through multiple voltage-gated ion channels and causes inward currents. Changes in opioid receptor signaling and BK channels have been reported in DYT1 mouse models (50). We decided to validate the findings in our KI mice. The membrane potential of the striatal ChIs was hyperpolarized by voltage ramp (−60 to −140 mV in 500 ms; **Figure 4E**) with 1 μM TTX (voltage-dependent Na^+ channel blocker) in the brain slices from 4 WT (15 cells) and 5 *Dyt1* KI mice (16 cells). The inward currents induced by the voltage ramp were recorded in whole-cell recording mode (**Figure 4F**). The recorded currents with TTX at −140 mV are shown in **Figure 4G**. There was no significant alteration in the inward currents with TTX between WT and *Dyt1* KI mice [WT, −0.81 ± 0.04 nA; KI, −0.80 ± 0.07 nA; z = 0.12, p = 0.91; **Figure 4G**], suggesting that the overall hyperpolarization-activated ion channel function is normal in *Dyt1* KI mice.

No Significant Alteration in the Striatal ChI Outward Currents Induced by Stimulation of μ-opioid Receptors in *Dyt1* KI Mice

Stimulation of μ-opioid receptors produces outward currents by inducing the outflux of potassium ions (K^+) and inhibiting the influx of calcium ions (Ca^{2+}) through the G-protein-coupling mechanism (81). DAMGO stimulates μ-opioid receptors and attenuates the inward currents (82). DAMGO (μ-opioid receptor agonist; 1 μM) was used to analyze the property of μ-opioid receptors during the voltage ramp (50). DAMGO attenuated the inward currents of the hyperpolarized ChI membranes in WT and *Dyt1* KI mice (**Figures 4E,F**). The DAMGO-induced outward currents were calculated by digital subtraction of the currents recorded with TTX and DAMGO from those with only TTX (**Figure 4H**). The currents recorded with TTX and DAMGO at −140 mV are shown in **Figure 4I**. There was no significant alteration in the μ-opioid receptor-induced outward currents between WT and *Dyt1* KI mice [WT, 0.14 ± 0.04 nA; KI, 0.14 ± 0.03 nA; z = 0.0, p = 1.0; **Figure 4I**], suggesting normal μ-opioid receptor function in *Dyt1* KI mice.

No Significant Alteration in the Striatal ChI Inward Current Through BK Channels in *Dyt1* KI Mice

The opening of multiple ion channels induces hyperpolarization-activated inward currents in this recording condition. Among the ion channels, the flow of potassium ions through the BK channel is bidirectional, depending on the membrane potential (83, 84). In the depolarized membrane potential, the opening of the BK channel produces an outflux of potassium ions (K^+). It causes outward currents during the falling phase of the action potential (85). When the membrane potential is hyperpolarized artificially by voltage ramp, the opening of the BK channel induces an influx of potassium ions (K^+), which causes inward currents. Therefore, blocking the BK channel attenuates the inward currents of the artificially hyperpolarized membrane potential.

The BK channel activity was characterized by adding 1 μM PAX (BK channel blocker) during the voltage ramp. PAX blocked the BK channel and attenuated the BK-channel-derived inward currents (**Figures 4E,F**). The BK-channel-derived inward currents were calculated by digital subtraction of the currents recorded with TTX, DAMGO, and PAX from those with only TTX and DAMGO (**Figure 4H**). The currents recorded with TTX, DAMGO, and PAX at −140 mV are shown in **Figure 4J**. There was no significant alteration in the inward current through the BK channels between WT and *Dyt1* KI mice [WT, −0.10 ± 0.02 nA; KI, −0.12 ± 0.02 nA; z = −0.65, p = 0.52; **Figure 4J**], suggesting normal ChI BK-channel function in *Dyt1* KI mice.

No Significant Morphological Alteration in the Striatal ChI Dendrites in *Dyt1* KI Mice

The dendrite structures and soma size of the recorded ChIs were examined by Sholl analysis (74). The morphology of the ChI dendrites was analyzed by digital tracing. Dorsal striatal ChIs were filled with biocytin during the whole-cell patch-clamp recording and labeled with streptavidin Alexa Fluor 594 (**Figure 5A**). The brain slices were stained with goat anti-ChAT/anti-goat IgG Alexa Fluor 488 to verify cholinergic identity (**Figure 5B**). The representative dendrites of the striatal ChIs labeled with biocytin/streptavidin Alexa Fluor 594 (**Figures 5C,D**) and their digitized dendrites are shown (**Figures 5E,F**). The dendritic branch numbers in 8 ChIs from 6 WT mice and 17 ChIs from 10 *Dyt1* KI mice were quantified by Sholl analysis (74) and the ImageJ program (NIH). There was no significant alteration in the number of intersections between WT and *Dyt1* KI mice (p > 0.05 at each comparable data point; **Figure 5G**). Moreover, there was no significant alteration in the length of the longest traced dendrites between WT and *Dyt1* KI mice (length ± standard errors; WT: 125 ± 9 μm; KI: 116 ± 6 μm; p = 0.38; **Figure 5G**). There was no significant alteration in the soma size between WT and *Dyt1* KI mice (cell body area ± standard errors; WT: 261 ± 27 μm^2; KI: 281 ± 14 μm^2; p = 0.47; **Figure 5H**). The results suggest no significant morphological alteration in the striatal ChI dendrites between WT and *Dyt1* KI mice.

DISCUSSION

TorsinA has been shown to be involved in multiple cellular processes, including protein quality control and secretion, calcium homeostasis, nuclear envelope integrity, nucleo-cytoplasmic transport, nucleo-cytoskeletal coupling, lipid metabolism, and synaptic transmission and plasticity (86). TorsinA is likely a molecular chaperon that processes various proteins, including the maturation of striatal D2R (37, 77) and D1R (38). Heterozygous *Dyt1* KI mice, which have the corresponding mutation, show motor deficits and less reduced locomotor response to raclopride, a D2R antagonist. *Dyt1* KI

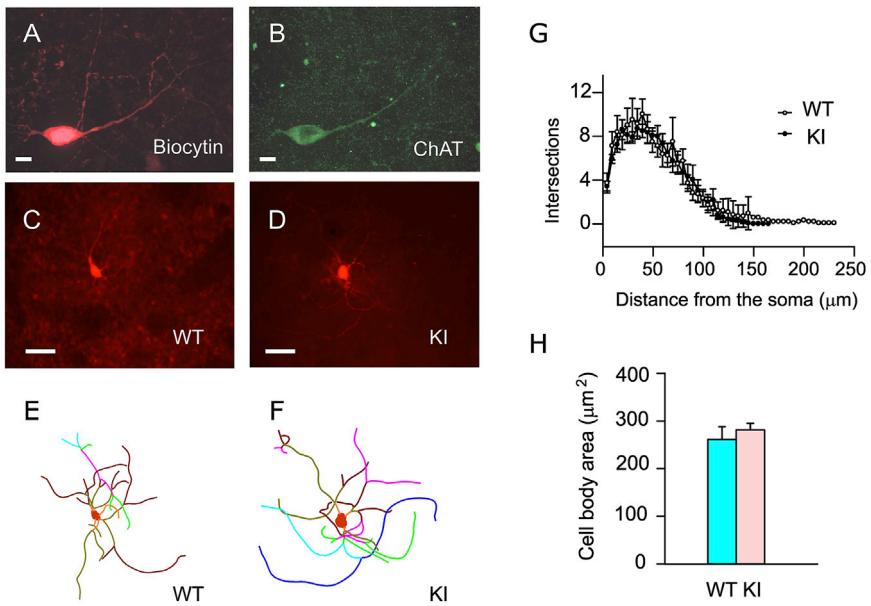

FIGURE 5 | Morphological analysis of the striatal ChIs. Representative confocal microscopic images of the dorsal striatal ChIs stained with biocytin/streptavidin conjugate **(A)** and goat anti-ChAT antibody **(B)**. The representative fluorescence images of the biocytin/streptavidin-stained ChIs **(C,D)** and their dendrites' reconstructed traces **(E,F)** are shown. The intersection numbers at every Sholl ring (5 μm increment) from the center of the soma were plotted (means ± standard errors; **(G)**]. There was no significant alteration in the dendritic branch numbers and soma size **(H)** between WT and *Dyt1* KI mice. The dots and error bars in **(G)** and the bars in **(H)** show means ± standard errors. Scale bars: **(A,B)**, 10 μm; **(C,D)**, 50 μm.

mice also show decreases in striatal D2R, D2R ligand binding, and torsinA levels. Since the striatal D2R reduction in *Dyt1* KI mice was mainly derived from the striatal indirect pathway medium spiny neurons (iMSNs), it was not known whether D2R function on striatal ChIs is reduced as well or not. Here, the striatal ChIs in acute brain slices showed irregular spontaneous firing with decreased frequency in *Dyt1* KI mice, whereas the intrinsic excitability was normal. Quinpirole, a D2R agonist, showed less inhibitory effect on the spontaneous ChI firing in *Dyt1* KI mice, suggesting decreased D2R function on the striatal ChIs. Muscarine, a muscarinic receptor agonist, inhibited the ChI firing in *Dyt1* KI mice, whereas trihexyphenidyl, a muscarinic acetylcholine receptor M1 antagonist, had no significant effect on the firing. Moreover, the resting membrane property, HCN channels, μ-opioid receptors, and BK channels of striatal ChIs were unchanged in *Dyt1* KI mice. These results suggest that the irregular and low-frequency firing and decreased D2R function are the main alterations of striatal ChIs in *Dyt1* KI mice. Consistent with the dystonic symptom caused by the side effect of D2R blockers, the striatal D2R defect on the striatal ChIs and iMSNs may contribute to the symptoms of DYT1 dystonia (13).

Paradoxical excitation to D2R activation was reported in several mouse and rat models of DYT1 dystonia (77-79, 87), *Thap1* $^{C54Y/+}$ knock-in mice (DYT6 dystonia model) and *Gnal* $^{+/-}$ KO mice (DYT25 dystonia model) (87). We did not find such a difference between WT and *Dyt*1 KI mice in two separate quinpirole experiments. We found less inhibitory response during quinpirole treatment, in contrast to the paradoxical excitation reported in the transgenic hMT mice (48), ChKO mice (35), transgenic ΔETorA rats (20), and *Tor1a*$^{+/\Delta gag}$ mice (49, 78, 79, 87). The mutations introduced in ChKO mice differ from the ΔGAG mutation commonly seen in most DYT1 dystonia patients and the *Dyt1* KI mice. Transgenic hMT mice and ΔETorA rats might have non-physiological levels of torsinA and ectopic expression of the exogenous mutant torsinA. Abnormal motor behaviors have been reported in overexpression mouse models of human WT and mutant *DYT1/TOR1A* gene (88), highlighting the importance of using *Dyt1* KI mice to study the pathophysiology of DYT1 dystonia (16). The discrepancy in paradoxical excitation between *Tor1a*$^{+/\Delta gag}$ mice and *Dyt1* KI mice is not known and could be attributed to the difference in KI mouse construction, animal husbandry, recording configuration, sample size, statistical analysis methods, and other unknown contributing factors.

Enhanced functions of μ-opioid receptors and large-conductance calcium-activated potassium (BK) channels of the striatal ChIs were found in *Tor1a* heterozygous KO mice (50). The authors were able to show similarly enhanced μ-opioid receptor function on the firing rate of striatal ChIs in *Tor1a*$^{+/\Delta gag}$ KI mice. We did not find any significant difference in the functions of μ-opioid receptors and BK channels in the *Dyt1* KI mice. Our results are consistent with the normal opioid binding in DYT1 patients (89). Since mutant torsinA still has low ATPase activity (90), which might be sufficient to maintain the normal function of μ-opioid receptors and BK channels in *Dyt1* KI mice.

Mechanisms to produce a low frequency of the ChI firing in *Dyt1* KI mice are not known. Here the intrinsic membrane property was normal in *Dyt1* KI mice. Moreover, the quinpirole showed a less inhibitory effect through D2R on the ChIs in *Dyt1* KI mice. These results suggest that the low frequency may be caused by a network effect rather than the intrinsic characteristic of the ChIs. Although striatal ChIs are pacemaker cells with spontaneous firing, they receive multiple inputs, including GABA from MSNs (56-59, 91). Since striatal D2R is decreased in *Dyt1* KI mice, the D2-expressing MSNs, i.e., iMSNs, may increase the firing probability of releasing GABA and suppress the ChIs. On the other hand, striatal D1R is also decreased in *Dyt1* KI mice. Therefore, the D1R-expressing MSNs, i.e., direct pathway medium spiny neurons (dMSNs), may reduce the release probability of GABA for suppressing the ChIs. Since the average ChI firing frequency is decreased in *Dyt1* KI mice, the increased GABA inputs from iMSNs seem more dominant than reduced GABA inputs from dMSNs. This may be consistent with the electron microscopic observations that 47% of the indirect pathway terminals and 36% of the direct pathway terminals of the GABAergic neurons target striatal ChIs in rhesus monkeys (92). Increased GABA inputs from other neurons may also decrease the ChI firing frequency in *Dyt1* KI mice; further characterization of GABAergic inputs to the ChIs, such as IPSCs, in *Dyt1* KI mice is needed to elucidate the mechanism of the low and irregular frequency of ChIs.

Since acetylcholine released from the ChIs synchronously stimulates striatal dopamine release (67), the low frequency of the ChIs may cause striatal dopamine release deficits in *Dyt1* KI mice. The basal level of striatal extracellular dopamine and amphetamine-stimulated dopamine release are consistently reduced in another KI mouse line of DYT1 dystonia (12). Suppression of the dopaminergic system is known to produce dystonic symptoms in humans. For example, dystonic symptoms are a well-known side effect of D2R antagonists used as antipsychotics (93). Dopamine synthesis deficits cause DYT5 dopa-responsive dystonia (94). The indirectly defected dopaminergic pathway may cause the dystonic symptoms in DYT1 dystonia.

Quinpirole showed a less inhibitory effect on the striatal ChIs in *Dyt1* KI mice, suggesting decreased D2R function on the ChIs. This is consistent with the previous reports of decreased striatal D2R protein level (23), reduced binding of D2R radioligand [^{3}H] YM-09151 to the striatum, and less reduced locomotor response to D2R antagonist raclopride in *Dyt1* KI mice (38). However, the measured striatal D2R protein level and D2R radioligand binding are mainly derived from the striatal iMSNs. TorsinA is a molecular chaperon that contributes to the trafficking of polytopic membrane-bound proteins, including G protein-coupled receptors (95). Moreover, *Dyt1* d2KO mice show striatal D2R maturation deficits (37). Since *Dyt*1 KI mice express decreased striatal torsinA levels (96), these results suggest that the partial loss of torsinA may reduce D2R in the ChIs as well as the iMSNs.

The mechanism of the irregular ChI firing or high CV in *Dyt1* KI mice is unknown. The decreased D2R function in the ChIs itself causes less inhibition by dopamine and contributes to an increased ChI firing frequency. Therefore, the ChIs may receive both the increased GABA release from iMSNs and less inhibitory signal by dopamine. Combining these opposing signals may cause the irregular frequency of the ChIs in the KI mice. Since *Dyt1* KI mice show irregular spontaneous firing in the cerebellar Purkinje cells (97), the heterozygous ΔGAG mutation seems to produce irregular firing in both ChIs and Purkinje cells. We found BK channel activity is increased in the KI Purkinje cells, which could underlie the irregular firing pattern (97). Here, we demonstrated no change of BK channel activity in the KI ChIs. The ionic mechanisms responsible for the altered ChI firing regularity remain to be investigated.

The spontaneous firing was inhibited by muscarine in WT and *Dyt1* KI mice, suggesting normal inhibitory function through M2 on the ChIs in *Dyt1* KI mice. The cholinergic neuron-specific torsinA knockout (Ch2KO) mice consistently show normal inhibitory responses (36). However, the striatal ChIs in cholinergic neuron-specific torsinA knockout (ChKO) mice with Neo cassette show no reaction to muscarine (35). The normal M2 function may also decrease the firing frequency of the ChIs if the striatal cholinergic tone is increased in the *Dyt1* KI mice, as shown in another line of KI mice (79). The mechanism to produce a high cholinergic tone is still not known. It may relate to the irregular firing of ChIs or the partial loss of ChIs in *Dyt1* KI mice (26). The irregular and low-frequency firing of striatal ChIs in *Dyt1* KI mice seems consistent with the high striatal acetylcholine tone in the previous reports (79). Further analysis of the striatal acetylcholine overflow mechanism will elucidate the pathophysiology of DYT1 dystonia.

The ChIs in both WT and *Dyt1* KI mice did not significantly respond to THP, consistent with the lack of expression of M1-type stimulatory muscarinic acetylcholine receptors on the striatal ChIs (98, 99). THP likely affected other neurons, such as MSNs in the corticostriatal pathway. *Dyt1* KI mice exhibit corticostriatal LTD deficits, abnormal muscle contraction, motor deficits, and impaired motor-skill transfer (8, 12, 23, 25, 100). These deficits are ameliorated by THP treatment (23, 24, 26), suggesting functional alteration of cholinergic or its related circuits in *Dyt1* KI mice. As discussed above, the decreased frequency of the ChIs may be caused indirectly by decreased D2R on iMSNs. MSNs project GABAergic axons to ChIs and inhibit the ChI firing. The iMSNs with decreased D2R may increase GABA release to ChIs and suppress the firing of the ChIs in *Dyt1* KI mice. THP may also intervene in this pathway and attenuate the symptoms by recovering the ChI firing. Further analysis of the network effect of these neurons will elucidate the contribution of each pathway to producing the motor deficits.

DYT1 dystonia is known as a circuit disorder rather than a neurodegenerative disorder. There is no overt neurodegeneration in DYT1 dystonia patients (1) and *Dyt1* KI mice (8). Consistently, cerebral cortex-specific *Dyt1* conditional KO mice do not show overt developmental alteration in cerebral cortex neurons (31). However, there is a slight morphological alteration in the cerebellar Purkinje cells in *Dyt1* KI mice and Purkinje cell-specific *Dyt1* conditional KO mice (101). The size of the

central nucleus of the amygdala is significantly reduced in the KI mice (69). Subtle morphological alterations in the cerebellar Purkinje cells were also reported in another line of KI mice (102). Moreover, the KI mice show a reduced ratio of axo-spinous to axo-dendritic synaptic inputs to MSNs from glutamatergic and dopaminergic sources (103). We found no significant alteration in dendritic branch numbers, suggesting that local connection with the striatal ChIs is mostly normal in *Dyt1* KI mice. Since the striatal ChIs show abnormal firing patterns, the electrophysiological alteration may not be caused by overt local neuronal connection changes. However, *Dyt1* KI mice have a slightly decreased number of dorsolateral striatal ChIs (26). The normal dendrite of the examined striatal ChIs does not exclude the possibility that a few ChIs with abnormal structure were already degenerated or eliminated during the development. The relationship between functional alteration and neuronal connections remains to be further examined.

DATA AVAILABILITY STATEMENT

The datasets presented in this article are not readily available because of the lack of a public electrophysiological data depository. Requests to access the datasets should be directed to the corresponding authors.

ETHICS STATEMENT

The animal study was reviewed and approved by the Institutional Animal Care and Use Committees of the University of Florida.

AUTHOR CONTRIBUTIONS

HX, FY, and YLi designed the experiments. HX, FY, AW, RT-M, and YLu performed the experiments. HX, FY, AW, and YLI analyzed the data. FY wrote the manuscript. HX, AW, and YLI edited the manuscript.

FUNDING

This work was supported by Tyler's Hope for a Dystonia Cure, Inc., "Mini-Moonshot" Fixel-MBI Pilot Grant Mechanism for Dystonia and Related Disorders, National Institutes of Health (NS54246, NS72782, NS75012, NS82244, NS111498, and NS118397), startup funds Department of Neurology (UF), Bachmann-Strauss Dystonia and Parkinson Foundation, Inc. and the Department of Defence (W81XWH1810099 and W81XWH2110198). FY, HX, and YL were partially supported by the Office of the Assistant Secretary of Defense for Health Affairs through the Peer-Reviewed Medical Research Program Discovery Award.

AUTHOR DISCLAIMER

Opinions, interpretations, conclusion, and recommendations are those of the author and are not necessarily endorsed by the Department of Defense.

CONFLICT OF INTEREST

The authors declare that the research was conducted in the absence of any commercial or financial relationships that could be construed as a potential conflict of interest.

ACKNOWLEDGMENTS

We thank the animal care staff, Douglas E. Smith, Kelly M. Dexter, Jessica Artille, Jareisha Vickers, Aysha Awal, and other undergraduate students for their technical assistance.

REFERENCES

1. Breakefield XO, Blood AJ, Li Y, Hallett M, Hanson PI, Standaert DG, et al. The Pathophysiological Basis of Dystonias. *Nat Rev Neurosci* (2008) 9: 222–34. doi:10.1038/nrn2337
2. Albanese A, Bhatia K, Bressman SB, Delong MR, Fahn S, Fung VS, et al. Phenomenology and Classification of Dystonia: A Consensus Update. *Mov Disord* (2013) 28:863–73. doi:10.1002/mds.25475
3. Ozelius LJ, Hewett JW, Page CE, Bressman SB, Kramer PL, Shalish C, et al. The Early-Onset Torsion Dystonia Gene (DYT1) Encodes an ATP-Binding Protein. *Nat Genet* (1997) 17:40–8. doi:10.1038/ng0997-40
4. Ghilardi MF, Carbon M, Silvestri G, Dhawan V, Tagliati M, Bressman S, et al. Impaired Sequence Learning in Carriers of the DYT1 Dystonia Mutation. *Ann Neurol* (2003) 54:102–9. doi:10.1002/ana.10610
5. Carbon M, Argyelan M, Ghilardi MF, Mattis P, Dhawan V, Bressman S, et al. Impaired Sequence Learning in Dystonia Mutation Carriers: A Genotypic Effect. *Brain* (2011) 134:1416–27. doi:10.1093/brain/awr060
6. Fahn S. High Dosage Anticholinergic Therapy in Dystonia. *Neurology* (1983) 33:1255–61. doi:10.1212/wnl.33.10.1255
7. Jankovic J. Treatment of Dystonia. *Lancet Neurol* (2006) 5:864–72. doi:10.1016/S1474-4422(06)70574-9
8. Dang MT, Yokoi F, McNaught KS, Jengelley TA, Jackson T, Li J, et al. Generation and Characterization of Dyt1 DeltaGAG Knock-In Mouse as a Model for Early-Onset Dystonia. *Exp Neurol* (2005) 196:452–63. doi:10.1016/j.expneurol.2005.08.025
9. Goodchild RE, Kim CE, Dauer WT. Loss of the Dystonia-Associated Protein torsinA Selectively Disrupts the Neuronal Nuclear Envelope. *Neuron* (2005) 48:923–32. doi:10.1016/j.neuron.2005.11.010
10. Yokoi F, Dang MT, Li Y. Improved Motor Performance in Dyt1 ΔGAG Heterozygous Knock-In Mice by Cerebellar Purkinje-Cell Specific Dyt1 Conditional Knocking-Out. *Behav Brain Res* (2012) 230:389–98. doi:10.1016/j.bbr.2012.02.029
11. Cao S, Hewett JW, Yokoi F, Lu J, Buckley AC, Burdette AJ, et al. Chemical Enhancement of torsinA Function in Cell and Animal Models of Torsion Dystonia. *Dis Model Mech* (2010) 3:386–96. doi:10.1242/dmm.003715
12. Song CH, Fan X, Exeter CJ, Hess EJ, Jinnah HA. Functional Analysis of Dopaminergic Systems in a DYT1 Knock-In Mouse Model of Dystonia. *Neurobiol Dis* (2012) 48:66–78. doi:10.1016/j.nbd.2012.05.009
13. Liu Y, Xing H, Yokoi F, Vaillancourt DE, Li Y. Investigating the Role of Striatal Dopamine Receptor 2 in Motor Coordination and Balance: Insights into the Pathogenesis of DYT1 Dystonia. *Behav Brain Res* (2021) 113137. doi:10.1016/j.bbr.2021.113137

14. Yokoi F, Dang MT, Li J, Li Y. Myoclonus, Motor Deficits, Alterations in Emotional Responses and Monoamine Metabolism in Epsilon-Sarcoglycan Deficient Mice. *J Biochem* (2006) 140:141–6. doi:10.1093/jb/mvj138
15. DeAndrade MP, Yokoi F, van Groen T, Lingrel JB, Li Y. Characterization of Atp1a3 Mutant Mice as a Model of Rapid-Onset Dystonia with Parkinsonism. *Behav Brain Res* (2011) 216:659–65. doi:10.1016/j.bbr.2010.09.009
16. Oleas J, Yokoi F, DeAndrade MP, Pisani A, Li Y. Engineering Animal Models of Dystonia. *Mov Disord* (2013) 28:990–1000. doi:10.1002/mds.25583
17. Oleas J, Yokoi F, DeAndrade MP, Li Y. Rodent Models of Autosomal Dominant Primary Dystonia. In: LeDoux MS, editor. *Movement Disorders: Genetics and Models*. New York: Academic Press Elsevier (2015). p. 483–505.
18. Imbriani P, Ponterio G, Tassone A, Sciamanna G, El Atiallah I, Bonsi P, et al. Models of Dystonia: An Update. *J Neurosci Methods* (2020) 339:108728. doi:10.1016/j.jneumeth.2020.108728
19. Richter F, Richter A. Genetic Animal Models of Dystonia: Common Features and Diversities. *Prog Neurobiol* (2014) 121:91–113. doi:10.1016/j.pneurobio.2014.07.002
20. Grundmann K, Glockle N, Martella G, Sciamanna G, Hauser TK, Yu L, et al. Generation of a Novel Rodent Model for DYT1 Dystonia. *Neurobiol Dis* (2012) 47:61–74. doi:10.1016/j.nbd.2012.03.024
21. Wakabayashi-Ito N, Ajjuri RR, Henderson BW, Doherty OM, Breakefield XO, O'Donnell JM, et al. Mutant Human torsinA, Responsible for Early-Onset Dystonia, Dominantly Suppresses GTPCH Expression, Dopamine Levels and Locomotion in *Drosophila melanogaster*. *Biol Open* (2015) 4:585–95. doi:10.1242/bio.201411080
22. Koh YH, Rehfeld K, Ganetzky B. A Drosophila Model of Early Onset Torsion Dystonia Suggests Impairment in TGF-β Signaling. *Hum Mol Genet* (2004) 13:2019–30. doi:10.1093/hmg/ddh208
23. Dang MT, Yokoi F, Cheetham CC, Lu J, Vo V, Lovinger DM, et al. An Anticholinergic Reverses Motor Control and Corticostriatal LTD Deficits in Dyt1 ΔGAG Knock-In Mice. *Behav Brain Res* (2012) 226:465–72. doi:10.1016/j.bbr.2011.10.002
24. DeAndrade MP, Trongnetrpunya A, Yokoi F, Cheetham CC, Peng N, Wyss JM, et al. Electromyographic Evidence in Support of a Knock-In Mouse Model of DYT1 Dystonia. *Mov Disord* (2016) 31:1633–9. doi:10.1002/mds.26677
25. Yokoi F, Dang MT, Liu J, Gandre JR, Kwon K, Yuen R, et al. Decreased Dopamine Receptor 1 Activity and Impaired Motor-Skill Transfer in Dyt1 ΔGAG Heterozygous Knock-In Mice. *Behav Brain Res* (2015) 279:202–10. doi:10.1016/j.bbr.2014.11.037
26. Yokoi F, Dang MT, Zhang L, Dexter KM, Efimenko I, Krishnaswamy S, et al. Reversal of Motor-Skill Transfer Impairment by Trihexyphenidyl and Reduction of Dorsolateral Striatal Cholinergic Interneurons in Dyt1 ΔGAG Knock-In Mice. *IBRO Neurosci Rep* (2021) 11:1–7. doi:10.1016/j.ibneur.2021.05.003
27. Giles LM, Chen J, Li L, Chin LS. Dystonia-associated Mutations Cause Premature Degradation of torsinA Protein and Cell-type-specific Mislocalization to the Nuclear Envelope. *Hum Mol Genet* (2008) 17:2712–22. doi:10.1093/hmg/ddn173
28. Gordon KL, Gonzalez-Alegre P. Consequences of the DYT1 Mutation on torsinA Oligomerization and Degradation. *Neuroscience* (2008) 157:588–95. doi:10.1016/j.neuroscience.2008.09.028
29. Dang MT, Yokoi F, Pence MA, Li Y. Motor Deficits and Hyperactivity in Dyt1 Knockdown Mice. *Neurosci Res* (2006) 56:470–4. doi:10.1016/j.neures.2006.09.005
30. Yokoi F, Chen HX, Dang MT, Cheetham CC, Campbell SL, Roper SN, et al. Behavioral and Electrophysiological Characterization of Dyt1 Heterozygous Knockout Mice. *PLoS One* (2015) 10:e0120916. doi:10.1371/journal.pone.0120916
31. Yokoi F, Dang MT, Mitsui S, Li J, Li Y. Motor Deficits and Hyperactivity in Cerebral Cortex-specific Dyt1 Conditional Knockout Mice. *J Biochem* (2008) 143:39–47. doi:10.1093/jb/mvm191
32. Jin XL, Guo H, Mao C, Atkins N, Wang H, Avasthi PP, et al. Emx1-specific Expression of Foreign Genes Using "Knock-In" Approach. *Biochem Biophys Res Commun* (2000) 270:978–82. doi:10.1006/bbrc.2000.2532
33. Yokoi F, Dang MT, Li J, Standaert DG, Li Y. Motor Deficits and Decreased Striatal Dopamine Receptor 2 Binding Activity in the Striatum-specific Dyt1 Conditional Knockout Mice. *PLoS One* (2011) 6:e24539. doi:10.1371/journal.pone.0024539
34. Dang MT, Yokoi F, Yin HH, Lovinger DM, Wang Y, Li Y, et al. Disrupted Motor Learning and Long-Term Synaptic Plasticity in Mice Lacking NMDAR1 in the Striatum. *Proc Natl Acad Sci U S A* (2006) 103:15254–9. doi:10.1073/pnas.0601758103
35. Sciamanna G, Hollis R, Ball C, Martella G, Tassone A, Marshall A, et al. Cholinergic Dysregulation Produced by Selective Inactivation of the Dystonia-Associated Protein torsinA. *Neurobiol Dis* (2012) 47:416–27. doi:10.1016/j.nbd.2012.04.015
36. Liu Y, Xing H, Sheng W, Singh KN, Korkmaz AG, Comeau C, et al. Alteration of the Cholinergic System and Motor Deficits in Cholinergic Neuron-specific Dyt1 Knockout Mice. *Neurobiol Dis* (2021) 154:105342. doi:10.1016/j.nbd.2021.105342
37. Yokoi F, Oleas J, Xing H, Liu Y, Dexter KM, Misztal C, et al. Decreased Number of Striatal Cholinergic Interneurons and Motor Deficits in Dopamine Receptor 2-expressing-cell-specific Dyt1 Conditional Knockout Mice. *Neurobiol Dis* (2020) 134:104638. doi:10.1016/j.nbd.2019.104638
38. Yokoi F, Chen HX, Oleas J, Dang MT, Xing H, Dexter KM, et al. Characterization of the Direct Pathway in Dyt1 ΔGAG Heterozygous Knock-In Mice and Dopamine Receptor 1-expressing-cell-specific Dyt1 Conditional Knockout Mice. *Behav Brain Res* (2021) 411:113381. doi:10.1016/j.bbr.2021.113381
39. Fremont R, Tewari A, Angueyra C, Khodakhah K. A Role for Cerebellum in the Hereditary Dystonia DYT1. *Elife* (2017) 6:e22775. doi:10.7554/eLife.22775
40. Shakkottai VG, Batla A, Bhatia K, Dauer WT, Dresel C, Niethammer M, et al. Current Opinions and Areas of Consensus on the Role of the Cerebellum in Dystonia. *Cerebellum* (2017) 16:577–94. doi:10.1007/s12311-016-0825-6
41. Yokoi F, Jiang F, Dexter K, Salvato B, Li Y. Improved Survival and Overt "dystonic" Symptoms in a torsinA Hypofunction Mouse Model. *Behav Brain Res* (2020) 381:112451. doi:10.1016/j.bbr.2019.112451
42. Liang CC, Tanabe LM, Jou S, Chi F, Dauer WT. TorsinA Hypofunction Causes Abnormal Twisting Movements and Sensorimotor Circuit Neurodegeneration. *J Clin Invest* (2014) 124:3080–92. doi:10.1172/JCI72830
43. Yokoi F, Cheetham CC, Campbell SL, Sweatt JD, Li Y. Pre-synaptic Release Deficits in a DYT1 Dystonia Mouse Model. *PLoS One* (2013) 8:e72491. doi:10.1371/journal.pone.0072491
44. Kakazu Y, Koh JY, Ho KW, Gonzalez-Alegre P, Harata NC. Synaptic Vesicle Recycling is Enhanced by torsinA that Harbors the DYT1 Dystonia Mutation. *Synapse* (2012) 66:453–64. doi:10.1002/syn.21534
45. Kakazu Y, Koh JY, Iwabuchi S, Gonzalez-Alegre P, Harata NC. Miniature Release Events of Glutamate from Hippocampal Neurons are Influenced by the Dystonia-Associated Protein torsinA. *Synapse* (2012) 66:807–22. doi:10.1002/syn.21571
46. Iwabuchi S, Kakazu Y, Koh JY, Harata NC. Abnormal Cytoplasmic Calcium Dynamics in central Neurons of a Dystonia Mouse Model. *Neurosci Lett* (2013) 548:61–6. doi:10.1016/j.neulet.2013.05.047
47. Pappas SS, Darr K, Holley SM, Cepeda C, Mabrouk OS, Wong JM, et al. Forebrain Deletion of the Dystonia Protein torsinA Causes Dystonic-like Movements and Loss of Striatal Cholinergic Neurons. *Elife* (2015) 4:e08352. doi:10.7554/eLife.08352
48. Sciamanna G, Tassone A, Martella G, Mandolesi G, Puglisi F, Cuomo D, et al. Developmental Profile of the Aberrant Dopamine D2 Receptor Response in Striatal Cholinergic Interneurons in DYT1 Dystonia. *PLoS One* (2011) 6:e24261. doi:10.1371/journal.pone.0024261
49. Martella G, Maltese M, Nistico R, Schirinzi T, Madeo G, Sciamanna G, et al. Regional Specificity of Synaptic Plasticity Deficits in a Knock-In Mouse Model of DYT1 Dystonia. *Neurobiol Dis* (2014) 65:124–32. doi:10.1016/j.nbd.2014.01.016
50. Ponterio G, Tassone A, Sciamanna G, Vanni V, Meringolo M, Santoro M, et al. Enhanced Mu Opioid Receptor-dependent Opioidergic Modulation of Striatal Cholinergic Transmission in DYT1 Dystonia. *Mov Disord* (2018) 33:310–20. doi:10.1002/mds.27212

51. Wilson CJ. The Mechanism of Intrinsic Amplification of Hyperpolarizations and Spontaneous Bursting in Striatal Cholinergic Interneurons. *Neuron* (2005) 45:575–85. doi:10.1016/j.neuron.2004.12.053
52. Bennett BD, Callaway JC, Wilson CJ. Intrinsic Membrane Properties Underlying Spontaneous Tonic Firing in Neostriatal Cholinergic Interneurons. *J Neurosci* (2000) 20:8493–503. doi:10.1523/jneurosci.20-22-08493.2000
53. Goldberg JA, Wilson CJ. Control of Spontaneous Firing Patterns by the Selective Coupling of Calcium Currents to Calcium-Activated Potassium Currents in Striatal Cholinergic Interneurons. *J Neurosci* (2005) 25:10230–8. doi:10.1523/JNEUROSCI.2734-05.2005
54. Goldberg JA, Teagarden MA, Foehring RC, Wilson CJ. Nonequilibrium Calcium Dynamics Regulate the Autonomous Firing Pattern of Rat Striatal Cholinergic Interneurons. *J Neurosci* (2009) 29:8396–407. doi:10.1523/JNEUROSCI.5582-08.2009
55. Mamaligas AA, Barcomb K, Ford CP. Cholinergic Transmission at Muscarinic Synapses in the Striatum Is Driven Equally by Cortical and Thalamic Inputs. *Cell Rep* (2019) 28:1003–14. doi:10.1016/j.celrep.2019.06.077
56. Straub C, Tritsch NX, Hagan NA, Gu C, Sabatini BL. Multiphasic Modulation of Cholinergic Interneurons by Nigrostriatal Afferents. *J Neurosci* (2014) 34:8557–69. doi:10.1523/JNEUROSCI.0589-14.2014
57. Chuhma N, Mingote S, Moore H, Rayport S. Dopamine Neurons Control Striatal Cholinergic Neurons via Regionally Heterogeneous Dopamine and Glutamate Signaling. *Neuron* (2014) 81:901–12. doi:10.1016/j.neuron.2013.12.027
58. Lim SA, Kang UJ, McGehee DS. Striatal Cholinergic Interneuron Regulation and Circuit Effects. *Front Synaptic Neurosci* (2014) 6:22. doi:10.3389/fnsyn.2014.00022
59. Suzuki E, Momiyama T. M1 Muscarinic Acetylcholine Receptor-Mediated Inhibition of GABA Release from Striatal Medium Spiny Neurons onto Cholinergic Interneurons. *Eur J Neurosci* (2021) 53:796–813. doi:10.1111/ejn.15074
60. Yan Z, Surmeier DJ. Muscarinic (M2/m4) Receptors Reduce N- and P-type Ca2+ Currents in Rat Neostriatal Cholinergic Interneurons through a Fast, Membrane-Delimited, G-Protein Pathway. *J Neurosci* (1996) 16:2592–604. doi:10.1523/jneurosci.16-08-02592.1996
61. Ding J, Guzman JN, Tkatch T, Chen S, Goldberg JA, Ebert PJ, et al. RGS4-dependent Attenuation of M4 Autoreceptor Function in Striatal Cholinergic Interneurons Following Dopamine Depletion. *Nat Neurosci* (2006) 9:832–42. doi:10.1038/nn1700
62. Howe AR, Surmeier DJ. Muscarinic Receptors Modulate N-P-And L-type Ca2+ Currents in Rat Striatal Neurons through Parallel Pathways. *J Neurosci* (1995) 15:458–69. doi:10.1523/jneurosci.15-01-00458.1995
63. Wang Z, Kai L, Day M, Ronesi J, Yin HH, Ding J, et al. Dopaminergic Control of Corticostriatal Long-Term Synaptic Depression in Medium Spiny Neurons is Mediated by Cholinergic Interneurons. *Neuron* (2006) 50:443–52. doi:10.1016/j.neuron.2006.04.010
64. Yan Z, Flores-Hernandez J, Surmeier DJ. Coordinated Expression of Muscarinic Receptor Messenger RNAs in Striatal Medium Spiny Neurons. *Neuroscience* (2001) 103:1017–24. doi:10.1016/s0306-4522(01)00039-2
65. Richter F, Klein L, Helmschrodt C, Richter A. Subtle Changes in Striatal Muscarinic M1 and M4 Receptor Expression in the DYT1 Knock-In Mouse Model of Dystonia. *PLoS One* (2019) 14:e0226080. doi:10.1371/journal.pone.0226080
66. Mamaligas AA, Ford CP. Spontaneous Synaptic Activation of Muscarinic Receptors by Striatal Cholinergic Neuron Firing. *Neuron* (2016) 91:574–86. doi:10.1016/j.neuron.2016.06.021
67. Threlfell S, Lalic T, Platt NJ, Jennings KA, Deisseroth K, Cragg SJ, et al. Striatal Dopamine Release is Triggered by Synchronized Activity in Cholinergic Interneurons. *Neuron* (2012) 75:58–64. doi:10.1016/j.neuron.2012.04.038
68. Maurice N, Mercer J, Chan CS, Hernandez-Lopez S, Held J, Tkatch T, et al. D2 Dopamine Receptor-Mediated Modulation of Voltage-dependent Na+ Channels Reduces Autonomous Activity in Striatal Cholinergic Interneurons. *J Neurosci* (2004) 24:10289–301. doi:10.1523/JNEUROSCI.2155-04.2004
69. Yokoi F, Dang MT, Miller CA, Marshall AG, Campbell SL, Sweatt JD, et al. Increased C-Fos Expression in the central Nucleus of the Amygdala and Enhancement of Cued Fear Memory in Dyt1 DeltaGAG Knock-In Mice. *Neurosci Res* (2009) 65:228–35. doi:10.1016/j.neures.2009.07.004
70. Voelkl B, Altman NS, Forsman A, Forstmeier W, Gurevitch J, Jaric I, et al. Reproducibility of Animal Research in Light of Biological Variation. *Nat Rev Neurosci* (2020) 21:384–93. doi:10.1038/s41583-020-0313-3
71. Lyu S, Xing H, DeAndrade MP, Liu Y, Perez PD, Yokoi F, et al. The Role of BTBD9 in Striatum and Restless Legs Syndrome. *eNeuro* (2019) 6:ENEURO.0277-19.2019. doi:10.1523/ENEURO.0277-19.2019
72. Lyu S, Xing H, Liu Y, Girdhar P, Zhang K, Yokoi F, et al. Deficiency of Meis1, a Transcriptional Regulator, in Mice and Worms: Neurochemical and Behavioral Characterizations with Implications in the Restless Legs Syndrome. *J Neurochem* (2020) 155:522–37. doi:10.1111/jnc.15177
73. Bennett BD, Wilson CJ. Spontaneous Activity of Neostriatal Cholinergic Interneurons *In Vitro*. *J Neurosci* (1999) 19:5586–96. doi:10.1523/jneurosci.19-13-05586.1999
74. Sholl DA. Dendritic Organization in the Neurons of the Visual and Motor Cortices of the Cat. *J Anat* (1953) 87:387–406.
75. Student. The Probable Error of a Mean. *Biometrika* (1908) 6:1. doi:10.2307/2331554
76. Eskow Jaunarajs KL, Bonsi P, Chesselet MF, Standaert DG, Pisani A. Striatal Cholinergic Dysfunction as a Unifying Theme in the Pathophysiology of Dystonia. *Prog Neurobiol* (2015) 127-128:91–107. doi:10.1016/j.pneurobio.2015.02.002
77. Bonsi P, Ponterio G, Vanni V, Tassone A, Sciamanna G, Migliarini S, et al. RGS9-2 Rescues Dopamine D2 Receptor Levels and Signaling in DYT1 Dystonia Mouse Models. *EMBO Mol Med* (2019) 11:e9283. doi:10.15252/emmm.201809283
78. Caffall ZF, Wilkes BJ, Hernández-Martinez R, Rittiner JE, Fox JT, Wan KK, et al. The HIV Protease Inhibitor, Ritonavir, Corrects Diverse Brain Phenotypes across Development in Mouse Model of DYT-TOR1A Dystonia. *Sci Transl Med* (2021) 13:eabd3904. doi:10.1126/scitranslmed.abd3904
79. Scarduzio M, Zimmerman CN, Jaunarajs KL, Wang Q, Standaert DG, McMahon LL, et al. Strength of Cholinergic Tone Dictates the Polarity of Dopamine D2 Receptor Modulation of Striatal Cholinergic Interneuron Excitability in DYT1 Dystonia. *Exp Neurol* (2017) 295:162–75. doi:10.1016/j.expneurol.2017.06.005
80. Oswald MJ, Oorschot DE, Schulz JM, Lipski J, Reynolds JN. IH Current Generates the Afterhyperpolarisation Following Activation of Subthreshold Cortical Synaptic Inputs to Striatal Cholinergic Interneurons. *J Physiol* (2009) 587:5879–97. doi:10.1113/jphysiol.2009.177600
81. Zhang L, Zhang JT, Hang L, Liu T. Mu Opioid Receptor Heterodimers Emerge as Novel Therapeutic Targets: Recent Progress and Future Perspective. *Front Pharmacol* (2020) 11:1078. doi:10.3389/fphar.2020.01078
82. Ponterio G, Tassone A, Sciamanna G, Riahi E, Vanni V, Bonsi P, et al. Powerful Inhibitory Action of Mu Opioid Receptors (MOR) on Cholinergic Interneuron Excitability in the Dorsal Striatum. *Neuropharmacology* (2013) 75:78–85. doi:10.1016/j.neuropharm.2013.07.006
83. Brelidze TI, Niu X, Magleby KL. A Ring of Eight Conserved Negatively Charged Amino Acids Doubles the Conductance of BK Channels and Prevents Inward Rectification. *Proc Natl Acad Sci U S A* (2003) 100:9017–22. doi:10.1073/pnas.1532257100
84. Carvacho I, Gonzalez W, Torres YP, Brauchi S, Alvarez O, Gonzalez-Nilo FD, et al. Intrinsic Electrostatic Potential in the BK Channel Pore: Role in Determining Single Channel Conductance and Block. *J Gen Physiol* (2008) 131:147–61. doi:10.1085/jgp.200709862
85. Tsantoulas C, McMahon SB. Opening Paths to Novel Analgesics: The Role of Potassium Channels in Chronic Pain. *Trends Neurosci* (2014) 37:146–58. doi:10.1016/j.tins.2013.12.002
86. Gonzalez-Alegre P. Advances in Molecular and Cell Biology of Dystonia: Focus on torsinA. *Neurobiol Dis* (2019) 127:233–41. doi:10.1016/j.nbd.2019.03.007
87. Eskow Jaunarajs KL, Scarduzio M, Ehrlich ME, McMahon LL, Standaert DG. Diverse Mechanisms Lead to Common Dysfunction of Striatal Cholinergic Interneurons in Distinct Genetic Mouse Models of Dystonia. *J Neurosci* (2019) 39:7195–205. doi:10.1523/JNEUROSCI.0407-19.2019
88. Grundmann K, Reischmann B, Vanhoutte G, Hubener J, Teismann P, Hauser TK, et al. Overexpression of Human Wildtype torsinA and Human

DeltaGAG torsinA in a Transgenic Mouse Model Causes Phenotypic Abnormalities. *Neurobiol Dis* (2007) 27:190–206. doi:10.1016/j.nbd.2007.04.015

89. Whone AL, Von Spiczak S, Edwards M, Valente EM, Hammers A, Bhatia KP, et al. Opioid Binding in DYT1 Primary Torsion Dystonia: An 11C-Diprenorphine PET Study. *Mov Disord* (2004) 19:1498–503. doi:10.1002/mds.20238
90. Pham P, Frei KP, Woo W, Truong DD. Molecular Defects of the Dystonia-Causing torsinA Mutation. *Neuroreport* (2006) 17:1725–8. doi:10.1097/WNR.0b013e3280101220
91. Gonzales KK, Smith Y. Cholinergic Interneurons in the Dorsal and Ventral Striatum: Anatomical and Functional Considerations in normal and Diseased Conditions. *Ann N Y Acad Sci* (2015) 1349:1–45. doi:10.1111/nyas.12762
92. Gonzales KK, Pare JF, Wichmann T, Smith Y. GABAergic Inputs from Direct and Indirect Striatal Projection Neurons onto Cholinergic Interneurons in the Primate Putamen. *J Comp Neurol* (2013) 521:2502–22. doi:10.1002/cne.23295
93. van Harten PN, Hoek HW, Kahn RS. Acute Dystonia Induced by Drug Treatment. *BMJ* (1999) 319:623–6. doi:10.1136/bmj.319.7210.623
94. Ichinose H, Ohye T, Takahashi E, Seki N, Hori T, Segawa M, et al. Hereditary Progressive Dystonia with Marked Diurnal Fluctuation Caused by Mutations in the GTP Cyclohydrolase I Gene. *Nat Genet* (1994) 8:236–42. doi:10.1038/ng1194-236
95. Torres GE, Sweeney AL, Beaulieu JM, Shashidharan P, Caron MG. Effect of torsinA on Membrane Proteins Reveals a Loss of Function and a Dominant-Negative Phenotype of the Dystonia-Associated DeltaE-torsinA Mutant. *Proc Natl Acad Sci U S A* (2004) 101:15650–5. doi:10.1073/pnas.0308088101
96. Yokoi F, Yang G, Li J, DeAndrade MP, Zhou T, Li Y, et al. Earlier Onset of Motor Deficits in Mice with Double Mutations in Dyt1 and Sgce. *J Biochem* (2010) 148:459–66. doi:10.1093/jb/mvq078
97. Liu Y, Xing H, Wilkes BJ, Yokoi F, Chen H, Vaillancourt DE, et al. The Abnormal Firing of Purkinje Cells in the Knockin Mouse Model of DYT1 Dystonia. *Brain Res Bull* (2020) 165:14–22. doi:10.1016/j.brainresbull.2020.09.011
98. Dawson VL, Dawson TM, Wamsley JK. Muscarinic and Dopaminergic Receptor Subtypes on Striatal Cholinergic Interneurons. *Brain Res Bull* (1990) 25:903–12. doi:10.1016/0361-9230(90)90186-4
99. Alcantara AA, Mrzljak L, Jakab RL, Levey AI, Hersch SM, Goldman-Rakic PS, et al. Muscarinic M1 and M2 Receptor Proteins in Local Circuit and Projection Neurons of the Primate Striatum: Anatomical Evidence for Cholinergic Modulation of Glutamatergic Prefronto-Striatal Pathways. *J Comp Neurol* (2001) 434:445–60. doi:10.1002/cne.1186
100. Rittiner JE, Caffall ZF, Hernández-Martinez R, Sanderson SM, Pearson JL, Tsukayama KK, et al. Functional Genomic Analyses of Mendelian and Sporadic Disease Identify Impaired eIF2α Signaling as a Generalizable Mechanism for Dystonia. *Neuron* (2016) 92:1238–51. doi:10.1016/j.neuron.2016.11.012
101. Zhang L, Yokoi F, Jin YH, Deandrade MP, Hashimoto K, Standaert DG, et al. Altered Dendritic Morphology of Purkinje Cells in Dyt1 ΔGAG Knock-In and Purkinje Cell-specific Dyt1 Conditional Knockout Mice. *PLoS One* (2011) 6:e18357. doi:10.1371/journal.pone.0018357
102. Song CH, Bernhard D, Hess EJ, Jinnah HA. Subtle Microstructural Changes of the Cerebellum in a Knock-In Mouse Model of DYT1 Dystonia. *Neurobiol Dis* (2014) 62:372–80. doi:10.1016/j.nbd.2013.10.003
103. Song CH, Bernhard D, Bolarinwa C, Hess EJ, Smith Y, Jinnah HA, et al. Subtle Microstructural Changes of the Striatum in a DYT1 Knock-In Mouse Model of Dystonia. *Neurobiol Dis* (2013) 54:362–71. doi:10.1016/j.nbd.2013.01.008

DYSTONIA

TYPE Original Research
PUBLISHED 14 December 2022
DOI 10.3389/dyst.2022.10892

OPEN ACCESS

EDITED BY
Roy Sillitoe,
Baylor College of Medicine,
United States

*CORRESPONDENCE
Samuel S. Pappas,
Samuel.Pappas@UTSouthwestern.edu

RECEIVED 09 September 2022
ACCEPTED 25 November 2022
PUBLISHED 14 December 2022

CITATION
Yellajoshyula D, Opeyemi S, Dauer WT and Pappas SS (2022), Genetic evidence of aberrant striatal synaptic maturation and secretory pathway alteration in a dystonia mouse model.
Dystonia 1:10892.
doi: 10.3389/dyst.2022.10892

Genetic evidence of aberrant striatal synaptic maturation and secretory pathway alteration in a dystonia mouse model

Dhananjay Yellajoshyula[1], Sunday Opeyemi[2], William T. Dauer[2,3,4] and Samuel S. Pappas[2,3]*

[1]Department of Neurosciences, Case Western Reserve University, Cleveland, OH, United States, [2]Peter O'Donnell Jr. Brain Institute, University of Texas Southwestern Medical Center, Dallas, TX, United States, [3]Department of Neurology, University of Texas Southwestern Medical Center, Dallas, TX, United States, [4]Department of Neuroscience, University of Texas Southwestern Medical Center, Dallas, TX, United States

Animal models of DYT-TOR1A dystonia consistently demonstrate abnormalities of striatal cholinergic function, but the molecular pathways underlying this pathophysiology are unclear. To probe these molecular pathways in a genetic model of DYT-TOR1A, we performed laser microdissection in juvenile mice to isolate striatal cholinergic interneurons and non-cholinergic striatal tissue largely comprising spiny projection neurons during maturation. Both cholinergic and GABAergic enriched samples demonstrated a defined set of gene expression changes consistent with a role of torsinA in the secretory pathway. GABAergic enriched striatum samples also showed alteration to genes regulating synaptic transmission and an upregulation of activity dependent immediate early genes. Reconstruction of Golgi-Cox stained striatal spiny projection neurons from adult mice demonstrated significantly increased spiny density, suggesting that torsinA null striatal neurons have increased excitability during striatal maturation and long lasting increases in afferent input. These findings are consistent with a developmental role for torsinA in the secretory pathway and link torsinA loss of function with functional and structural changes of striatal cholinergic and GABAergic neurons. These transcriptomic datasets are freely available as a resource for future studies of torsinA loss of function-mediated striatal dysfunction.

KEYWORDS

dystonia, torsinA, TOR1A, DYT1, striatum, cholinergic, synaptic, maturation

Introduction

DYT-TOR1A (DYT1) is a dominantly inherited dystonia characterized by early onset involuntary abnormal movements and postures (1, 2). TorsinA resides in the endoplasmic reticulum and nuclear envelope lumen, where interaction with cofactors LAP1 and LULL1 promote its ATPase activity (3-9). The DYT-TOR1A disease mutation deletes a single glutamic acid (ΔE) (2), impairing torsinA function (5,8,10-12). The natural history

of DYT-TOR1A suggests that processes occurring during development are particularly important for disease pathogenesis (reviewed in (13)) and findings in mouse models suggest that the functions of the *Tor1a* encoded protein torsinA are essential during a developmental critical period but dispensable in adult animals (14). Several CNS developmental processes are altered by torsinA loss of function. In animal models, *Tor1a* deletion or *Tor1a*$^{\Delta E}$ knock-in disrupts nuclear envelope structure (15, 16) and alters nuclear pore distribution and function (17, 18) during a postnatal CNS developmental period in which neuronal nuclear pore complex biogenesis and insertion is upregulated (19). TorsinA dysfunction causes deficits in secretory processing, protein quality control, and translational control (20-26) and alters synapse formation (27-30), all of which potentially contribute to the altered synaptic plasticity identified in dystonia (31-34). The mechanisms underlying synaptic changes in torsinA deficient neurons are not defined.

Multiple animal models of torsinA dysfunction display aberrant corticostriatal plasticity, including enhanced long term potentiation and decreased synaptic inhibition (24,35-37). Abnormal cholinergic signaling contributes to disrupted plasticity in some DYT-TOR1A models (36) and antimuscarinic compounds improve disease features in some people with DYT-TOR1A (38). Altered striatal plasticity is an early pathophysiological feature. Knock-in mice expressing the *Tor1a*$^{\Delta E/+}$ disease mutation exhibit premature long term potentiation, impaired long term depression, and increased AMPA receptor abundance in corticostriatal synapses during early striatal development (29). This converging evidence suggests that diminished inhibitory synaptic function (39) and dysfunction of striatal cholinergic interneurons (ChI) (40) are drivers of dystonia and suggest that processes occurring during development or maturation are critical for dystonia pathogenesis.

To mechanistically explore the relationship between torsinA loss-of-function and synaptic and behavioral change, we modeled DYT-TOR1A dystonia by conditionally deleting torsinA in forebrain inhibitory and cholinergic neurons using Dlx5/6-Cre (41) ("Dlx-CKO mice"). TorsinA is thus deleted from all neurons in the striatum, globus pallidus, reticular thalamic nucleus, and basal forebrain, and from inhibitory interneurons in the cortex and hippocampus in Dlx-CKO mice. Like the natural history of DYT-TOR1A, Dlx-CKO mice exhibit motor dysfunction beginning as juveniles, which worsens with increased handling and is responsive to antimuscarinic treatment (41). During the same juvenile period, a subpopulation of ChI in the dorsolateral striatum selectively degenerate. These findings suggest that Dlx-CKO mice model a link between cholinergic and motor dysfunction (42) believed important in human DYT-TOR1A dystonia (43).

To probe the mechanisms by which torsinA loss alters ChI and surrounding cell types during striatal maturation, we conducted RNAseq analyses on maturing Dlx-CKO striatal ChI somas or surrounding striatum tissue (mainly comprised of spiny projection neuron somas, with a small proportion of GABAergic interneuron somas, glia, and neural processes) isolated using laser microdissection. Striatal cholinergic and non-cholinergic enriched samples from control vs. Dlx-CKO identified a core set of genes enriched in secretory pathway and synaptic function. We further demonstrate abnormal synaptic structure in Dlx-CKO striatum with Golgi-Cox staining of spiny projection neurons. This study identifies a role for torsinA within the secretory pathway and implicates abnormal synaptic structure in the torsinA deficient striatum.

Materials and methods

Animals

Animal work described in this manuscript has been approved and conducted under the oversight of the UT Southwestern Institutional Animal Care and Use Committee. Male and female control (Tor1a$^{Flx/+}$) and Dlx-CKO (Dlx5/6-Cre^{+}; Tor1a$^{Flx/-}$) mice expressing ChAT(BAC)-eGFP (JAX strain 007902) were generated as previously described (41).

Laser microdissection and RNA isolation

Brains were harvested at postnatal day 14 (P14) and snap frozen in dry ice-chilled isopentane. 16 μm fresh frozen brain sections were generated with a cryostat, mounted on PET membrane slides, and dehydrated in ethanol and xylenes. Laser microdissection was performed using the ×20 objective of a Leica LMD7 microscope. ChAT-eGFP+ cell bodies (341–524 GFP+ somas per brain) or GFP-negative striatal tissue (1–1.5 million μm^2 tissue area collected per brain) was laser microdissected and lysed in buffer RLT with 1% β-mercaptoethanol (Qiagen). Total RNA was isolated using a RNeasy-micro kit (Qiagen) and eluted in RNase-free water. RNA quantity and integrity was assessed using an Agilent Bioanalyzer and samples with RIN between 7.6–9.3 were used for RNA sequencing. Samples were derived from the following number of animals: ChI soma $n = 6$ control and $n = 6$ Dlx-CKO; Striatum: $n = 4$ control and $n = 5$ Dlx-CKO.

RNA sequencing and analysis

RNA-seq was performed using the HiSeq2500 (Illumina) platform in the University of Michigan Sequencing Core. RNA-seq libraries were generated using SmartSeq4 (Clontech). Libraries were quantified and normalized using an Agilent Bioanalyzer and sequenced using the HiSeq2500 High-Output SBS V4 single-end 50 cycle kit. The quality of the raw reads data was checked using FastQC (version 0.11.3). Low quality bases

TABLE 1 Differentially Expressed genes from striatal cholinergic interneuron soma samples.

Gene	Gene ID	Description	Control FPKM	Dlx-CKO FPKM	Fold change	q_value
Pdlim3	53318	PDZ and LIM domain 3	6.324	12.967	2.05	.01740
Rbm45	241490	RNA binding motif protein 45	7.387	14.970	2.03	.01740
Hmox1	15368	heme oxygenase 1	3.711	7.056	1.90	.03139
Cd59a	12509	CD59a antigen	14.549	26.403	1.81	.01740
Pdyn	18610	Prodynorphin	22.559	39.175	1.74	.01740
Prr5l	72446	proline rich 5 like	1.567	2.589	1.65	.04447
Fos	14281	FBJ osteosarcoma oncogene	7.107	11.580	1.63	.01740
Sdf2l1	64136	stromal cell-derived factor 2-like 1	31.479	49.964	1.59	.01740
Itga9	104099	integrin alpha 9	2.025	3.135	1.55	.04447
Grtp1	66790	GH regulated TBC protein 1	30.451	20.193	.66	.01740
Npy	109648	neuropeptide Y	609.880	401.328	.66	.01740
Sv2c	75209	synaptic vesicle glycoprotein 2c	11.522	7.481	.65	.01740
Cartpt	27220	CART prepropeptide	69.853	43.915	.63	.01740
Sst	20604	Somatostatin	1,044.770	646.451	.62	.01740
Beta-s	100503605	hemoglobin, beta adult s chain	351.612	213.052	.61	.01740
Col1a2	12843	collagen, type I, alpha 2	3.317	1.927	.58	.01740
F2r	14062	coagulation factor II (thrombin) receptor	2.813	1.626	.58	.04447
Hba-a2	110257	hemoglobin alpha, adult chain 2	185.868	107.032	.58	.01740
Igfbp2	16008	insulin-like growth factor binding protein 2	30.841	17.678	.57	.01740
Hddc3	68695	HD domain containing 3	47.292	26.738	.57	.01740
Insrr	23920	insulin receptor-related receptor	3.712	2.047	.55	.01740
Gfap	14580	glial fibrillary acidic protein	36.399	17.785	.49	.01740
Serping1	12258	serine (or cysteine) peptidase inhibitor, clade G, member 1	5.829	2.531	.43	.01740
Igf2	16002	insulin-like growth factor 2	6.092	2.557	.42	.01740
Gjb2	14619	gap junction protein, beta 2	2.135	.887	.42	.01740
Col1a1	12842	collagen, type I, alpha 1	1.983	.690	.35	.01740
Nov	18133	nephroblastoma overexpressed gene	4.641	1.409	.30	.01740
Spp1	20750	secreted phosphoprotein 1	3.096	.907	.29	.01740
Dcn	13179	Decorin	5.817	1.624	.28	.01740
Slc6a13	14412	solute carrier family 6 (neurotransmitter transporter, GABA), member 13	2.547	.686	.27	.01740
Fam180a	208164	family with sequence similarity 180, member A	2.217	.384	.17	.01740
Vip	22353	vasoactive intestinal polypeptide	2.470	.374	.15	.01740
Fmod	14264	Fibromodulin	2.703	.293	.11	.01740
Aldh1a2	19378	aldehyde dehydrogenase family 1, subfamily A2	2.253	.205	.09	.01740
Slc13a4	243755	solute carrier family 13 (sodium/sulfate symporters), member 4	2.153	.170	.08	.01740
Ptgds	19215	prostaglandin D2 synthase (brain)	609.567	43.543	.07	.01740
Tuba1c	22146	tubulin, alpha 1C	14.184	.407	.03	.01740
Tor1a	30931	torsin family 1, member A (torsin A)	47.518	10.149	.21	.01740

from individual reads were trimmed using CutAdapt. Tuxedo Suite software package was used for alignment, differential expression analysis, and post-analysis diagnostics (44-46). We aligned reads (genome build UCSC mm10) using TopHat (version 2.0.14) and Bowtie (version 2.2.1). We used FastQC for a second round of post-alignment quality control to ensure that only high quality data would be input to expression quantitation and differential expression analysis. We used Cufflinks/CuffDiff (Version 2.2.1) for expression quantitation, normalization, and differential expression analysis. Diagnostic plots were generated with CummeRbund package. We used locally developed scripts to format and annotate the differential expression data output from CuffDiff. Genes were designated as DE if they passed quality control (Cuffdiff/Cufflinks QC test status = "ok"), had Benjamini-Hochberg FDR q-values <0.05, and fold change >1.5 (Tables 1, 2). The

TABLE 2 Differentially Expressed genes from non-cholinergic striatum samples.

Gene	Gene ID	Description	Control FPKM	Dlx-CKO FPKM	Fold change	q_value
Eln	13717	Elastin	1.577	13.526	8.58	.01960
Tuba1c	22146	tubulin, alpha 1C	.624	4.356	6.98	.01960
Ptgds	19215	prostaglandin D2 synthase (brain)	2.139	14.035	6.56	.01960
Serpina3n	20716	serine (or cysteine) peptidase inhibitor, clade A, member 3N	1.554	5.061	3.26	.01960
Crhbp	12919	corticotropin releasing hormone binding protein	1.592	4.775	3.00	.03323
Pdlim3	53318	PDZ and LIM domain 3	6.686	19.440	2.91	.01960
Npas4	225872	neuronal PAS domain protein 4	1.169	2.943	2.52	.04679
Gadd45g	23882	growth arrest and DNA-damage-inducible 45 gamma	24.837	62.021	2.50	.01960
Doc2g	60425	double C2, gamma	3.626	8.125	2.24	.03323
Igf1	16000	insulin-like growth factor 1	.655	1.438	2.20	.01960
Npas2	18143	neuronal PAS domain protein 2	4.878	10.687	2.19	.01960
Crip1	12925	cysteine-rich protein 1 (intestinal)	27.202	58.769	2.16	.01960
Dcdc2a	195208	doublecortin domain containing 2a	.946	1.942	2.05	.01960
Arc	11838	activity regulated cytoskeletal-associated protein	44.295	89.269	2.02	.01960
Hspb1	15507	heat shock protein 1	13.250	25.970	1.96	.03323
Ctgf	14219	connective tissue growth factor	3.671	6.825	1.86	.03323
Nr4a1	15370	nuclear receptor subfamily 4, group A, member 1	51.004	93.507	1.83	.01960
Pdyn	18610	Prodynorphin	21.950	39.961	1.82	.03323
Fos	14281	FBJ osteosarcoma oncogene	7.206	12.946	1.80	.04679
Rbp4	19662	retinol binding protein 4, plasma	19.486	34.677	1.78	.01960
Egr4	13656	early growth response 4	97.187	172.884	1.78	.01960
Gfap	14580	glial fibrillary acidic protein	19.204	32.604	1.70	.01960
Mgp	17313	matrix Gla protein	55.013	92.441	1.68	.03323
Rps21	66481	ribosomal protein S21	899.763	1,416.980	1.57	.01960
Sec61b	66212	Sec61 beta subunit	197.548	309.101	1.56	.04679
Etl4	208618	enhancer trap locus 4	5.189	3.150	.61	.03323
Cdr1	631990	cerebellar degeneration related antigen 1	103.307	62.310	.60	.01960
Gpx6	75512	glutathione peroxidase 6	27.586	15.782	.57	.01960
Cnih3	72978	cornichon family AMPA receptor auxiliary protein 3	23.884	12.954	.54	.01960
Xist	213742	inactive X specific transcripts	5.991	2.035	.34	.01960
Pla2g4e	329502	phospholipase A2, group IVE	2.525	.854	.34	.01960
Tor1a	30931	torsin family 1, member A (torsin A)	34.565	6.742	.20	.01960

raw count data for all replicates are provided in Supplementary Tables S7, S8 and the alignment rates are provided in Supplementary Table S9.

Gene ontology analyses

Differentially expressed genes identified from RNAseq were further analyzed for the identification of biologically enriched pathways by gene ontology (GO) enrichment analyses using the following web based applications: GENEONTOLOGY http://geneontology.org/docs/go-enrichment-analysis/ and DAVID https://david.ncifcrf.gov/home.jsp.

Golgi-cox staining

Brains from 10 to 14 week old female control ($Tor1a^{Flx/+}$) and Dlx-CKO (Dlx5/6-Cre^{+}; $Tor1a^{Flx/-}$) mice were harvested fresh and immediately processed using the FD Rapid Golgi stain kit (FD Neurotechnologies) as per manufacturer's instructions and as described previously (41). Slides were observed under brightfield microscopy and striatal spiny projection neurons with dense Golgi-cox impregnation without dendritic breaks or obstructions were imaged with a ×63 objective lens and reconstructed using Neurolucida (MBF Bioscience). Spines were assessed on 3rd order or higher dendrites at ≥ 80 μm from the soma. A total of 31 neurons from 6 control animals and 25 neurons from 5 Dlx-CKO animals were assessed.

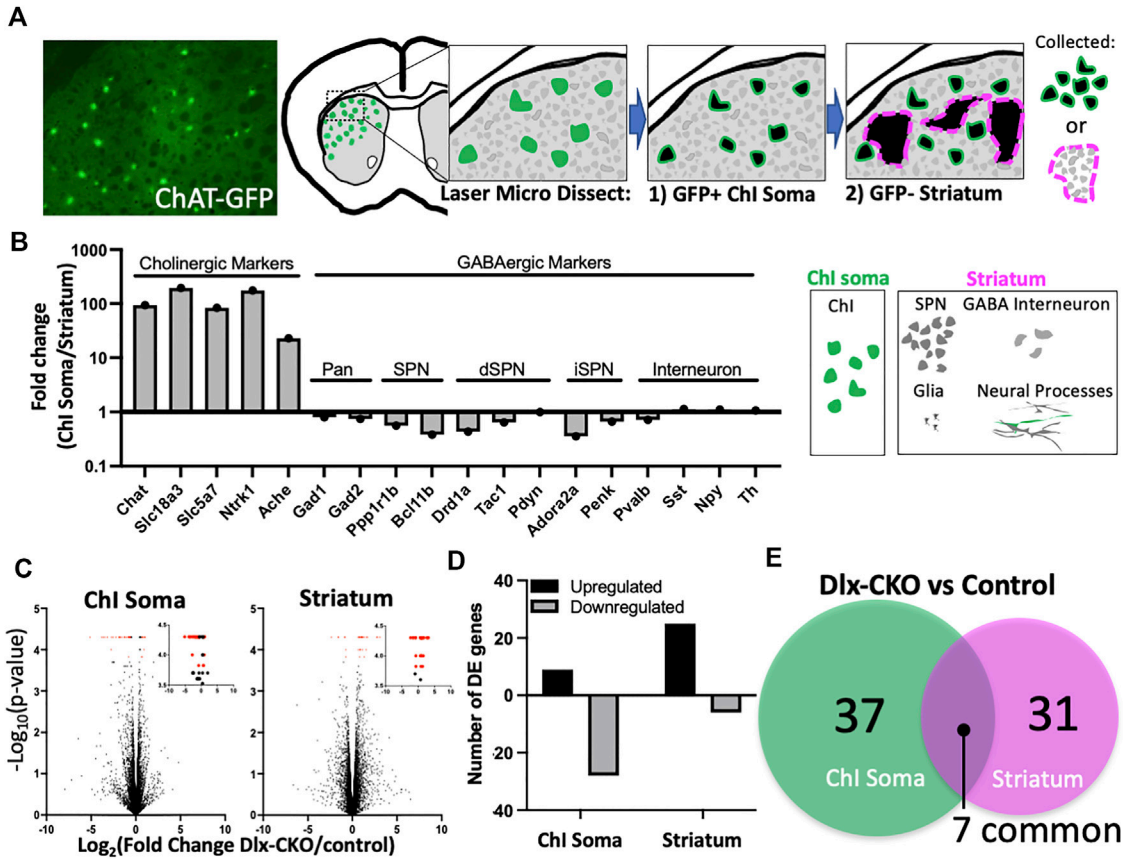

FIGURE 1
Laser microdissection of cholinergic interneuron somas and non-cholinergic striatum samples identifies differentially expressed genes in Dlx-CKO vs. control genotypes. **(A)** Laser microdissection workflow. ChI somas were dissected from ChAT-GFP+ cells followed by dissection of surrounding GFP-negative striatum comprised mainly of SPN somas, as well as GABA interneuron somas, glia, and neural processes. **(B)** Fold change of cholinergic and GABAergic markers (derived from FPKM) demonstrates enrichment of laser microdissected samples. **(C)** Control vs. Dlx-CKO differentially expressed genes (highlighted in red) identified from RNA-seq analyses (ChI soma samples derived from n = 6 control and n = 6 Dlx-CKO mice; Striatum samples derived from n = 4 controls and n = 5 Dlx-CKO mice). Insets show the same data from 3.5–4.5 on the y-axis. All differentially expressed genes are listed in Tables 1, 2. **(D)** Upregulated and downregulated genes from ChI soma and striatum. **(E)** Overlap between ChI soma and striatum differentially expressed genes.

Statistics

All data are reported as mean ± SEM unless otherwise indicated. All statistical tests reported (Student's t-tests, One-way or two-way ANOVAs) were performed using Graphpad Prism (Version 9.3.1).

Results

RNA-seq of cholinergic somas and striatal non-cholinergic tissue in maturing striatum

To explore the effects of torsinA loss of function on striatal cholinergic interneurons (ChI) and non-cholinergic cells during development, we performed laser microdissection of dorsolateral striatal ChI somas or surrounding non-cholinergic striatum containing spiny projection neuron cell bodies, interneurons, glia, and neural processes (Figure 1A). We purified total RNA from control (*Tor1a*$^{Flx/+}$) and Dlx-CKO (Dlx5/6-Cre^{+}; *Tor1a*$^{Flx/-}$) ChI soma (n = 6 control and n = 6 Dlx-CKO) and non-cholinergic striatum (n = 4 control and n = 5 Dlx-CKO) samples and performed RNA-seq analyses (Methods). ChI soma samples demonstrated up to 193.7-fold higher expression of cholinergic-selective markers compared to striatum samples. Non-cholinergic striatum samples were enriched up to 2.8-fold for GABAergic markers (Figure 1B). Within each sample type, there were not significant differences in the expression of cholinergic or GABAergic markers between control and Dlx-CKO genotypes except for *Pdyn* (Supplementary Table S1). We identified control vs. Dlx-CKO differentially expressed (DE) genes in both ChI soma and striatum samples (Figure 1C, DE genes in red; Methods) after filtering out genes with FPKM values less than 1 in both

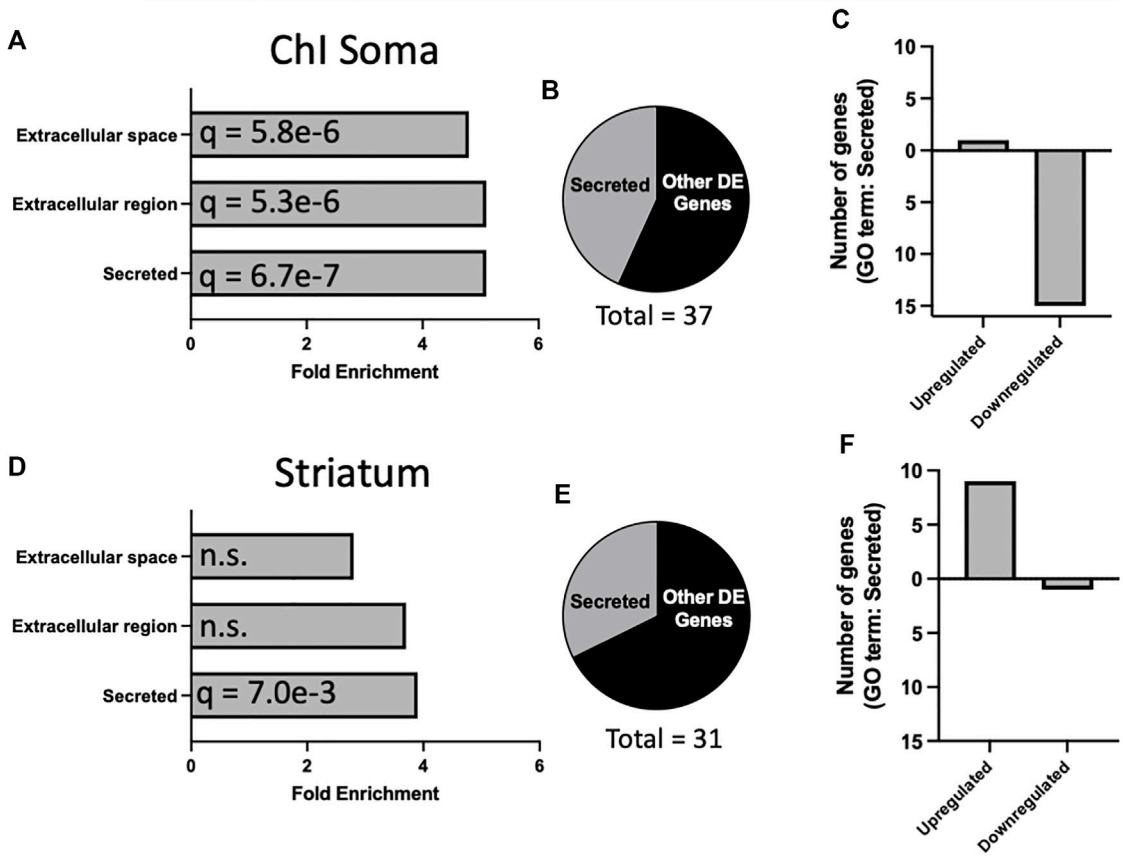

FIGURE 2
Gene ontology analysis demonstrates over-representation of genes encoding secreted proteins in Dlx-CKO mice. **(A)** A cellular component annotation cluster of secreted, extracellular region, and extracellular space related genes was significantly over-represented in ChI soma samples. **(B)** Percent of all ChI soma differentially expressed genes annotated as secreted. **(C)** Number of upregulated vs. downregulated genes in ChI soma analyses. **(D)** A cellular component annotation cluster of genes encoding secreted proteins was significantly over-represented in non-cholinergic striatum samples. **(E)** Percent of all non-cholinergic striatum differentially expressed genes annotated as secreted. **(F)** Number of upregulated vs. downregulated genes in non-cholinergic striatum samples.

genotypes (Supplementary Table S2). DE genes were cross referenced with the brainrnaseq.org database of purified cell types (47), which confirmed expected expression levels (FPKM) in the brain. Over 75% of DE genes in ChI somas were downregulated (28/37 genes downregulated), and 80% of DE genes in striatum samples were upregulated (25/31 genes upregulated) (Figure 1D). From these comparisons we identified a core set of 7 genes differentially regulated in both ChI soma and striatum samples (Figure 1E).

Overrepresentation of differentially expressed genes encoding secreted and extracellular components in ChI soma and non-cholinergic striatum

To assess the functional significance of control vs. Dlx-CKO DE genes, we first determined their subcellular localization by cross referencing with the COMPARTMENTS database (48). Consistent with the role of torsinA in the secretory pathway, 62% of DE genes in ChI soma (23/37 genes) and 42% of DE genes in striatum (13/31 genes) were categorized as secreted, extracellular, extracellular matrix, or plasma membrane localized in mouse (Supplementary Table S3). Similarly, 48% of DE genes in ChI soma (18/37 genes) and 29% of DE in striatum (9/31 genes) are present in the human secretome (49) (Supplementary Table S4).

Gene ontology (GO) analysis of *Tor1a* CKO DE genes using DAVID (50) identified a significant over-representation of genes encoding secreted factors in both ChI soma and striatum samples (Supplementary Table S5). An annotation cluster comprising secreted, extracellular region, and extracellular space was significantly over-represented in ChI samples (16/37 genes; cellular component; enrichment score 6.52; Figures 2A, B). Most of these DE genes in ChI were downregulated (Figure 2C). Striatum samples were also over-represented for

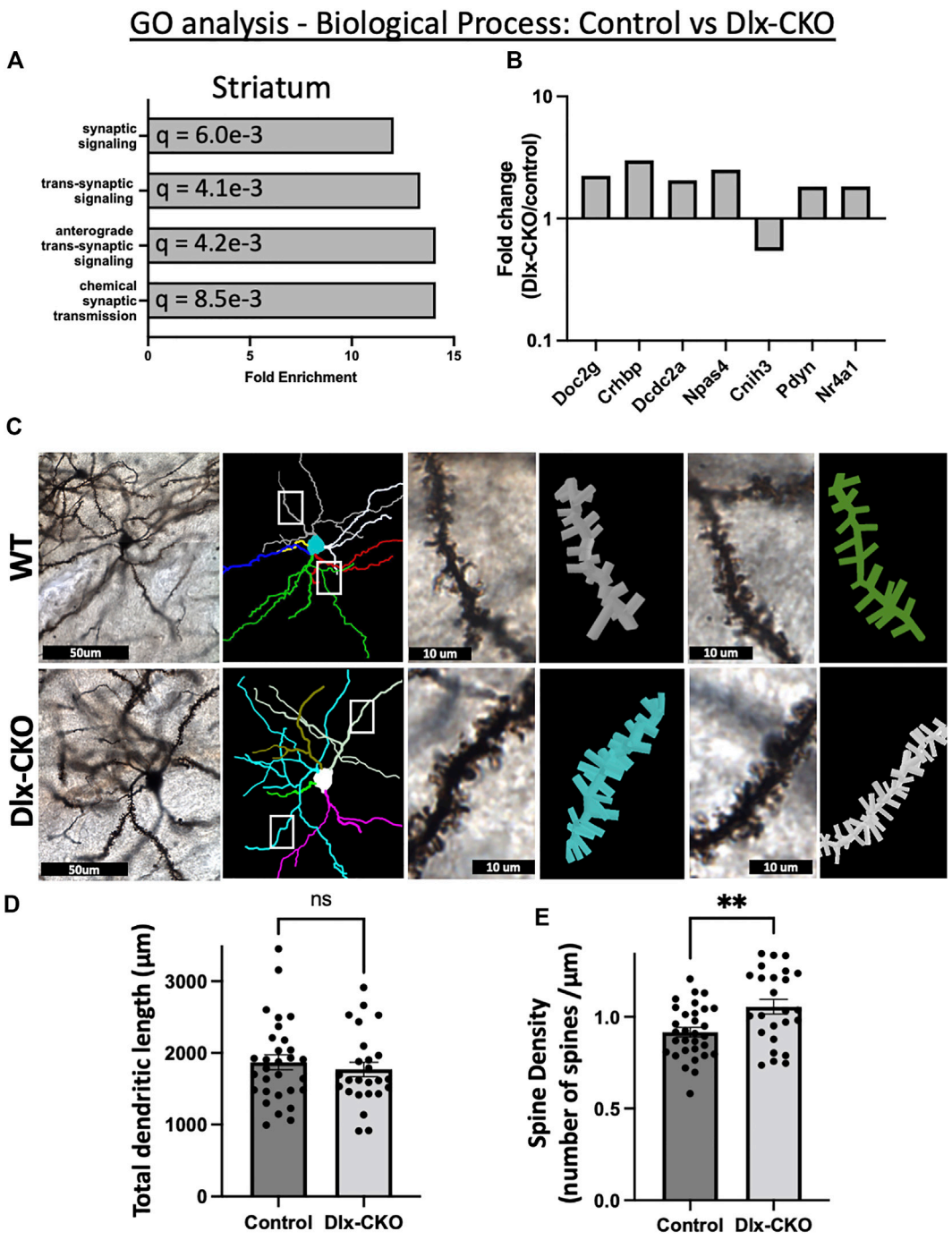

FIGURE 3
Alterations to synaptic structure and function in Dlx-CKO striatal GABAergic neurons. **(A)** A biological process annotation cluster of synaptic signaling related genes was significantly over-represented in non-cholinergic striatum samples. **(B)** Fold change of the annotated synaptic signaling genes (derived from FPKM). **(C)** Golgi-Cox impregnated striatal spiny projection neurons and associated dendritic arbor reconstructions from control and Dlx-CKO adult mouse brains. **(D)** Total dendritic length of spiny projection neurons (control: n = 30 neurons from 6 mice, Dlx-CKO: n = 25 neurons from 5 mice. t_{53} = .6718, p = .5046). **(E)** Spine density of third order dendrites on spiny projection neurons (control: n = 31 neurons from 6 mice, Dlx-CKO: n = 25 neurons from 5 mice, t_{54} = 3.008, p = .004).

genes encoding secreted factors (13/31 genes; cellular component; enrichment score 2.07; Figures 2D, E), and most of these DE genes were upregulated (Figure 2F).

Overrepresentation of synaptic genes in non-cholinergic striatum and dendritic spine alterations in striatal spiny projection neurons

GO analyses (geneontology.org) (51, 52) identified broad changes to synaptic function in non-cholinergic striatum from Dlx-CKO samples as compared to control (Supplementary Table S6). An annotation cluster comprising synaptic signaling, anterograde trans-synaptic signaling, and chemical synaptic transmission was significantly over-represented in striatum samples (Figure 3A). Of the annotated synaptic genes, *Doc2g*, *Crhbp*, *Dcdc2a*, *Npas4*, *Pdyn*, and *Nr4a1* were upregulated, and *Cnih3* was downregulated (Figure 3B). This cluster of gene expression changes suggests that striatal synaptic structure may be altered in Dlx-CKO mice.

To assess this possibility, we examined dendritic structure in Dlx-CKO and control mice by performing Golgi-Cox impregnation and assessing striatal spiny projection neuron morphology using light microscopy (Figure 3C). Spiny projection neurons are morphologically immature at P14 and their inputs onto dendritic spines continue to mature into adulthood (53-55), so we assessed morphology and spine density in adult brains. Consistent with our previous findings (41), the length of the dendritic arbors of striatal spiny projection neurons were not significantly different between control and Dlx-CKO mice ($t_{53} = 0.6718$, $p = 0.5046$; Figure 3D). However, the spine density of 3rd order dendritic branches was significantly increased in Dlx-CKO brains compared to control ($t_{54} = 3.008$, $p = 0.004$; Figure 3D).

Increased spine density reflects increased excitatory input to spiny projection neurons. Consistent with the potential for increased excitability, activity-dependent immediate early genes were significantly upregulated in Dlx-CKO non-cholinergic striatum samples. At least 7 immediate early genes were upregulated in striatum, including *Fos* (1.8 fold), *Arc* (2 fold), *Egr4* (1.8 fold), *Nr4a1* (1.8 fold), *Npas4* (2.5 fold), *Npas2* (2.2 fold), and *Ctgf* (1.85 fold). In ChI samples, *Fos* was significantly upregulated (1.6 fold), suggesting that ChI activity may also be increased in Dlx-CKO mice.

Discussion

These studies identify a core set of differentially expressed genes in the striatum of torsinA conditional knockout mice during postnatal CNS maturation. Despite the previously reported divergent phenotype between cell types (cholinergic neurodegeneration vs. GABAergic neuron survival (41)), both ChI soma and non-cholinergic striatum samples demonstrated a discrete set of gene expression changes consistent with the role of torsinA in the secretory pathway. Striatum samples also displayed expression changes of genes regulating synaptic transmission and an upregulation of activity-dependent immediate early genes. Consistent with our RNAseq analyses, striatal spiny projection neurons in adult mice demonstrated significantly higher spine density, suggesting that surviving striatal neurons exhibit increased excitability during striatal maturation and increased afferent inputs in adulthood.

We isolated either ChAT-GFP+ ChI somas or GFP negative striatal tissue containing mainly spiny projection neuron somas, as well as GABAergic interneuron somas, glia, and neural projections using laser microdissection (see Figure 1A for a summary of the laser microdissection approach). The ChI soma samples were therefore highly enriched in a single cell type, while striatum samples contained mostly GABAergic neurons in a mixture of cell types and compartments, mainly comprising spiny projection neurons. This is reflected in our analyses as a cholinergic marker enrichment of 193.7 fold vs. GABAergic marker enrichment of up to 2.8 fold. Differential expression analyses of both sample types were overrepresented for genes encoding factors that are secreted to the extracellular space. Several neuropeptides were overrepresented in Dlx-CKO ChI soma samples, including Pdyn (upregulated), Vip, Npy, Cartpt, and Sst (downregulated). These factors were previously found to be enriched in GABAergic striatal neurons (56-61), but our enrichment protocol may have enabled measurement of sparse neuropeptide expression. The differential expression of genes encoding extracellular proteins and neuropeptides are consistent with a central role of torsinA in the secretory pathway (21, 22), as suggested by its localization in the endoplasmic reticulum lumen (3, 62).

Dlx-CKO striatum samples demonstrated a suite of gene expression differences consistent with a structural or functional change in striatal synapses. Whether the synaptic changes of GABAergic neurons reflect intrinsic responses to torsinA deficiency or a compensation consequent to neighboring cholinergic neurodegeneration remains unknown. Striatal cholinergic signaling matures postnatally and begins to dynamically regulate the synaptic activity of other striatal neurons as skilled motor function develops (63). The second postnatal week (when samples were collected in this study) is a maturational period during which corticostriatal synaptogenesis and spinogenesis begins and progresses (reviewed in (64)) as activity induced factors shape the connectivity of striatal neurons (65, 66). Several differentially expressed genes identified in this study modulate striatal spiny projection neuron spine density. The nuclear receptor *Nr4a1* (upregulated 1.83 fold in Dlx-CKO) is enriched in spiny projection neurons (67), where its activity-induced expression alters spine density as part of a transcriptional program that regulates density and distribution

of dendritic spines (68, 69) and promotes spiny projection neuron maturation (67). *Npas4* (upregulated 2.51 fold) is a transcription factor that regulates GABAergic synaptic function (70) and is important for synaptic formation, function and ongoing plasticity (71). Knockdown of *Npas4* reduces dendritic spine density on D1 receptor-expressing spiny projection neurons (72). Expression of the cytoskeleton associated protein Arc (upregulated 2-fold in Dlx-CKO striatum) increases spine density *in vivo* (73, 74). IGF-1 (upregulated 2.19-fold in Dlx-CKO striatum) administration rescues spine density (75) or spine motility (76) in Mecp2 mutant mice and knockdown of IGF-1 decreases spine density of purkinje cells (77). The upregulation of these factors during striatal maturation is consistent with changes to synaptic structure, as evidenced by significantly increased spine density of Golgi-Cox-stained spiny projection neurons in the present study.

Our differential expression analyses also suggest functional synaptic changes in Dlx-CKO mice. *Doc2g* (upregulated 2.24 fold in Dlx-CKO) is a member of the DOC2 family of proteins that modulates spontaneous synaptic transmission (78). Knockdown of DOC2 proteins triggers excitatory synaptic scaling without altering action potential dependent activity (79). *Cnih3* (downregulated 1.84 fold in Dlx-CKO) is an AMPA receptor auxiliary subunit that functions in the endoplasmic reticulum and remains associated with the AMPA receptor complex at the synapse (80). CNIH3 regulates AMPA receptor trafficking and gating properties by determining the subunit composition of heteromeric AMPA receptors (81) and controlling the export of AMPA receptors from the endoplasmic reticulum (82). The structure of the interface between CNIH3 and AMPA receptors suggests that lipids play a role in the assembly of these complexes (83). The endoplasmic reticulum localization of CNIH3 and its interplay with lipids in complex with AMPA receptors suggests that it could be one link between torsinA function and the synaptic plasticity differences observed in animal models (24,35-37) and in people with dystonia (31-34). The synapse-related gene expression changes identified in torsinA null striatal neurons during maturation may therefore contribute to long lasting enhancement of spiny projection neuron synaptic structure and function.

To our knowledge, spine density has not been assessed previously in torsinA null mice. Heterozygous *Tor1a*$^{\Delta E/+}$ mice have reduced spiny projection neuron spine density at P26 (29), but no difference at P60 (29), consistent with other spine density studies in adult *Tor1a*$^{\Delta E/+}$ mice (27, 84). Spine density on distal dendrites of cerebellar purkinje neurons is reduced in 3 month old *Tor1a*$^{\Delta E/+}$ animals (28). However, motor behavior is not altered in these mice (85).

Surprisingly, despite glial enrichment, Gfap (encoding Glial Fibrillary Acidic Protein) was upregulated in both ChI soma and non-cholinergic striatum samples of Dlx-CKO mice. ChI soma sample *Gfap* expression could reflect "contamination" with adjacent or (synapsed) astrocytes, as increased neuronal activity increases expression of glial *Gfap* (86). However, astrogliosis is not observed in Dlx-CKO striatum (41). Neurons can express Gfap in neurodegenerative disease (87), but we observed robust Gfap expression in both control and Dlx-CKO samples. Some neuronal *Gfap* expression is observed in the normal mouse brain ((47); brainrnaseq.org). Fate mapping studies demonstrate that *Gfap*-expressing progenitors give rise to some neurons, including in the striatum (88), suggesting that we may be observing physiological ChI expression of *Gfap* during striatal maturation.

Six genes were differentially expressed in *both* ChI soma and non-cholinergic striatum samples. *Fos*, *Pdlim3*, and *Pdyn* were all upregulated to similar extents in both sample types, suggesting that these genes could represent common responses to torsinA loss of function or striatal circuit changes. In contrast, *Ptgds*, *Tuba1c*, and *Gfap* were downregulated in ChI somas, but upregulated in non-cholinergic striatum, suggesting a role in differential vulnerability of striatal neurons to cell death or cell type specific responses to torsinA loss of function. *Tuba1c* reduction (35.71 fold decreased in ChI) may reflect microtubule disruption or active degeneration of ChI, while its increase in non-cholinergic striatum (6.98 fold increased) could reflect compensatory neurite outgrowth or axon elongation in surviving cells (89). Only a single tubulin isoform was altered in this study, suggesting that torsinA loss of function caused a highly specific change rather than broad disruption of microtubule structure. Microtubule dynamics contribute to dendritic spine development, morphology, and synaptic plasticity (90-93). Increased *Tuba1c* expression may therefore reflect or contribute to the spine density increases we observed in Dlx-CKO spiny projection neurons.

Ptgds encodes lipocalin type prostaglandin D2 synthase, which catalyzes the conversion of prostaglandin H2 to the neuromodulatory prostaglandin D2 in the brain (94-96). Prostaglandin D2 is neuroprotective in contexts such as hypoxia-ischemic injuries, excitotoxicity, and oxidative stress (97,98,99,100,101). Prostaglandin D2 synthase (also called β-trace) itself is a neuroprotective chaperone that inhibits Aβ aggregation (102, 103), and alterations to its expression may be a biomarker of several neurological disorders (104). In the present study, *Ptgds* was 14.08 fold decreased in ChI soma and 6.56 fold increased in non-cholinergic striatum. Ptgds upregulation could contribute to the selective survival of non-cholinergic neurons in the striatum of Dlx-CKO mice. Further investigations would be required to determine whether this association is causative.

This study supports a developmental role for torsinA in the secretory pathway and demonstrates abnormal synaptic development in the torsinA deficient striatum. These transcriptomic datasets are freely available as a resource for future hypothesis driven work exploring the consequences of torsinA loss for striatal structure and function.

Data availability statement

All raw RNAseq data from this study is included as Supplementary Material and all differentially expressed genes are listed within the main article. Further inquiries can be directed to the corresponding author.

Ethics statement

The animal study was reviewed and approved by the UT Southwestern Institutional Animal Care and Use Committee.

Author contributions

DY—Analyzed data and edited manuscript. SO—Analyzed data and edited manuscript. WD—Edited manuscript. SP—Conducted experiments, analyzed data, wrote and edited manuscript.

Funding

This research was supported in part by the Dystonia Medical Research Foundation DMRF-MCMD-2022-2 (to DY), National Institute of Neurological Disorders and Stroke R01NS110853 and R01NS109227 (to WD).

Conflict of interest

The authors declare that the research was conducted in the absence of any commercial or financial relationships that could be construed as a potential conflict of interest.

Acknowledgments

We thank Drs. Phillip Kish and Alon Kahana for providing access and training for their laser microdissection microscope.

Supplementary material

The Supplementary Material for this article can be found online at: https://www.frontierspartnerships.org/articles/10.3389/dyst.2022.10892/full#supplementary-material.

SUPPLEMENTARY TABLE S1
Cell type markers control vs. Dlx-CKO (internal control).

SUPPLEMENTARY TABLE S2
Filtered genes removed from analysis.

SUPPLEMENTARY TABLE S3
Cross reference with the COMPARTMENTS database.

SUPPLEMENTARY TABLE S4
Cross reference with the Human Secretome.

SUPPLEMENTARY TABLE S5
Gene ontology analysis using DAVID: over-representation of genes encoding secreted proteins.

SUPPLEMENTARY TABLE S6
Gene ontology analysis using geneontology.org: over-representation of genes encoding proteins regulating synaptic structure and function.

SUPPLEMENTARY TABLE S7
Chl soma raw count data matrix.

SUPPLEMENTARY TABLE S8
Striatum raw count data matrix.

SUPPLEMENTARY TABLE S9
Aligned reads for each sample.

References

1. Albanese A, Bhatia K, Bressman SB, Delong MR, Fahn S, Fung VS, et al. Phenomenology and classification of dystonia: A consensus update. *Mov Disord* (2013) 28(7):863–73. doi:10.1002/mds.25475

2. Ozelius L, Hewett J, Page C, Bressman S, Kramer P, Shalish C, et al. The early-onset torsion dystonia gene (DYT1) encodes an ATP-binding protein. *Nat Genet* (1997) 17(1):40–8. doi:10.1038/ng0997-40

3. Goodchild RE, Dauer WT. The AAA+ protein torsinA interacts with a conserved domain present in LAP1 and a novel ER protein. *J Cel Biol* (2005) 168(6):855–62. doi:10.1083/jcb.200411026

4. Goodchild R, Buchwalter A, Naismith T, Holbrook K, Billion K, Dauer W, et al. Access of torsinA to the inner nuclear membrane is activity dependent and regulated in the endoplasmic reticulum. *J Cel Sci* (2015) 128(15):2854–65. doi:10.1242/jcs.167452

5. Demircioglu FE, Sosa BA, Ingram J, Ploegh HL, Schwartz TU. Structures of TorsinA and its disease-mutant complexed with an activator reveal the molecular basis for primary dystonia. *Elife* (2016) 5:e17983. doi:10.7554/eLife.17983

6. Sosa BA, Demircioglu FE, Chen JZ, Ingram J, Ploegh HL, Schwartz TU. How lamina-associated polypeptide 1 (LAP1) activates Torsin. *Elife* (2014) 3:e03239. doi:10.7554/eLife.03239

7. Brown R, Zhao C, Chase A, Wang J, Schlieker C. The mechanism of Torsin ATPase activation. *Proc Natl Acad Sci U S A* (2014) 111(45):E4822–31. doi:10.1073/pnas.1415271111

8. Zhao C, Brown RSH, Chase AR, Eisele MR, Schlieker C. Regulation of torsin ATPases by LAP1 and LULL1. *Proc Natl Acad Sci U S A* (2013) 110(17):E1545–54. doi:10.1073/pnas.1300676110

9. Naismith T, Heuser J, Breakefield X, Hanson P. TorsinA in the nuclear envelope. *Proc Natl Acad Sci U S A* (2004) 101(20):7612–7. doi:10.1073/pnas.0308760101

10. Goodchild RE, Dauer WT. Mislocalization to the nuclear envelope: An effect of the dystonia-causing torsinA mutation. *Proc Natl Acad Sci U S A* (2004) 101(3):847–52. doi:10.1073/pnas.0304375101

11. Naismith T, Dalal S, Hanson P. Interaction of torsinA with its major binding partners is impaired by the dystonia-associated DeltaGAG deletion. *J Biol Chem* (2009) 284(41):27866–74. doi:10.1074/jbc.M109.020164

12. Zhu L, Millen L, Mendoza JL, Thomas PJ. A unique redox-sensing sensor II motif in TorsinA plays a critical role in nucleotide and partner binding. *J Biol Chem* (2010) 285(48):37271–80. doi:10.1074/jbc.M110.123471

13. Li J, Kim S, Pappas SS, Dauer WT. CNS critical periods: Implications for dystonia and other neurodevelopmental disorders. *JCI Insight* (2021) 6(4):e142483. doi:10.1172/jci.insight.142483

14. Li J, Levin DS, Kim AJ, Pappas SS, Dauer WT. TorsinA restoration in a mouse model identifies a critical therapeutic window for DYT1 dystonia. *J Clin Invest* (2021) 131(6). doi:10.1172/jci139606

15. Goodchild RE, Kim CE, Dauer WT. Loss of the dystonia-associated protein torsinA selectively disrupts the neuronal nuclear envelope. *Neuron* (2005) 48(6): 923–32. doi:10.1016/j.neuron.2005.11.010

16. Tanabe L, Liang C, Dauer W. Neuronal nuclear membrane budding occurs during a developmental window modulated by torsin paralogs. *Cell Rep* (2016) 16(12):3322–33. doi:10.1016/j.celrep.2016.08.044

17. Pappas SS, Liang CC, Kim S, Rivera CO, Dauer WT. TorsinA dysfunction causes persistent neuronal nuclear pore defects. *Hum Mol Genet* (2018) 27(3): 407–20. doi:10.1093/hmg/ddx405

18. VanGompel M, Nguyen K, Hall D, Dauer W, Rose L. A novel function for the *Caenorhabditis elegans* torsin OOC-5 in nucleoporin localization and nuclear import. *Mol Biol Cel* (2015) 26(9):1752–63. doi:10.1091/mbc.E14-07-1239

19. Lodin Z, Blumajer J, Mares V. Nuclear pore complexes in cells of the developing mouse cerebral cortex. *Acta Histochem* (1978) 63(1):74–9. doi:10.1016/S0065-1281(78)80009-9

20. Nery F, Armata I, Farley J, Cho J, Yaqub U, Chen P, et al. TorsinA participates in endoplasmic reticulum-associated degradation. *Nat Commun* (2011) 2:393. doi:10.1038/ncomms1383

21. Hewett J, Nery F, Niland B, Ge P, Tan P, Hadwiger P, et al. siRNA knock-down of mutant torsinA restores processing through secretory pathway in DYT1 dystonia cells. *Hum Mol Genet* (2008) 17(10):1436–45. doi:10.1093/hmg/ddn032

22. Hewett J, Tannous B, Niland B, Nery F, Zeng J, Li Y, et al. Mutant torsinA interferes with protein processing through the secretory pathway in DYT1 dystonia cells. *Proc Natl Acad Sci U S A* (2007) 104(17):7271–6. doi:10.1073/pnas.0701185104

23. Chen P, Burdette A, Porter J, Ricketts J, Fox S, Nery F, et al. The early-onset torsion dystonia-associated protein, torsinA, is a homeostatic regulator of endoplasmic reticulum stress response. *Hum Mol Genet* (2010) 19(18):3502–15. doi:10.1093/hmg/ddq266

24. Rittiner J, Caffall Z, Hernández-Martinez R, Sanderson S, Pearson J, Tsukayama K, et al. Functional genomic analyses of mendelian and sporadic disease identify impaired eIF2α signaling as a generalizable mechanism for dystonia. *Neuron* (2016) 92(6):1238–51. doi:10.1016/j.neuron.2016.11.012

25. Beauvais G, Bode N, Watson J, Wen H, Glenn K, Kawano H, et al. Disruption of protein processing in the endoplasmic reticulum of DYT1 knock-in mice implicates novel pathways in dystonia pathogenesis. *J Neurosci* (2016) 36(40): 10245–56. doi:10.1523/JNEUROSCI.0669-16.2016

26. Beauvais G, Rodriguez-Losada N, Ying L, Zakirova Z, Watson JL, Readhead B, et al. Exploring the interaction between eIF2α dysregulation, acute endoplasmic reticulum stress and DYT1 dystonia in the mammalian brain. *Neuroscience* (2018) 371:455–68. doi:10.1016/j.neuroscience.2017.12.033

27. Song C, Bernhard D, Bolarinwa C, Hess E, Smith Y, Jinnah H. Subtle microstructural changes of the striatum in a DYT1 knock-in mouse model of dystonia. *Neurobiol Dis* (2013) 54:362–71. doi:10.1016/j.nbd.2013.01.008

28. Song C, Bernhard D, Hess E, Jinnah H. Subtle microstructural changes of the cerebellum in a knock-in mouse model of DYT1 dystonia. *Neurobiol Dis* (2014) 62: 372–80. doi:10.1016/j.nbd.2013.10.003

29. Maltese M, Stanic J, Tassone A, Sciamanna G, Ponterio G, Vanni V, et al. Early structural and functional plasticity alterations in a susceptibility period of DYT1 dystonia mouse striatum. *Elife* (2018) 7:e33331. doi:10.7554/eLife.33331

30. Vanni V, Puglisi F, Bonsi P, Ponterio G, Maltese M, Pisani A, et al. Cerebellar synaptogenesis is compromised in mouse models of DYT1 dystonia. *Exp Neurol* (2015) 271:457–67. doi:10.1016/j.expneurol.2015.07.005

31. Quartarone A, Hallett M. Emerging concepts in the physiological basis of dystonia. *Mov Disord* (2013) 28(7):958–67. doi:10.1002/mds.25532

32. Quartarone A, Pisani A. Abnormal plasticity in dystonia: Disruption of synaptic homeostasis. *Neurobiol Dis* (2011) 42(2):162–70. doi:10.1016/j.nbd.2010.12.011

33. Edwards M, Huang Y, Mir P, Rothwell J, Bhatia K. Abnormalities in motor cortical plasticity differentiate manifesting and nonmanifesting DYT1 carriers. *Mov Disord* (2006) 21(12):2181–6. doi:10.1002/mds.21160

34. Quartarone A, Ghilardi MF. Neuroplasticity in dystonia: Motor symptoms and beyond. *Handb Clin Neurol* (2022) 184:207–18. doi:10.1016/B978-0-12-819410-2.00031-X

35. Martella G, Maltese M, Nistico R, Schirinzi T, Madeo G, Sciamanna G, et al. Regional specificity of synaptic plasticity deficits in a knock-in mouse model of DYT1 dystonia. *Neurobiol Dis* (2014) 65C:124–32. doi:10.1016/j.nbd.2014.01.016

36. Martella G, Tassone A, Sciamanna G, Platania P, Cuomo D, Viscomi M, et al. Impairment of bidirectional synaptic plasticity in the striatum of a mouse model of DYT1 dystonia: Role of endogenous acetylcholine. *Brain* (2009) 132(9):2336–49. doi:10.1093/brain/awp194

37. Grundmann K, Glockle N, Martella G, Sciamanna G, Hauser TK, Yu L, et al. Generation of a novel rodent model for DYT1 dystonia. *Neurobiol Dis* (2012) 47(1): 61–74. doi:10.1016/j.nbd.2012.03.024

38. Burke R, Fahn S, Marsden C. Torsion dystonia: A double-blind, prospective trial of high-dosage trihexyphenidyl. *Neurology* (1986) 36(2):160–4. doi:10.1212/wnl.36.2.160

39. Hallett M. Neurophysiology of dystonia: The role of inhibition. *Neurobiol Dis* (2011) 42(2):177–84. doi:10.1016/j.nbd.2010.08.025

40. Eskow Jaunarajs K, Bonsi P, Chesselet M, Standaert D, Pisani A. Striatal cholinergic dysfunction as a unifying theme in the pathophysiology of dystonia. *Prog Neurobiol* (2015) 127-128:91–107. doi:10.1016/j.pneurobio.2015.02.002

41. Pappas SS, Darr K, Holley SM, Cepeda C, Mabrouk OS, Wong JM, et al. Forebrain deletion of the dystonia protein torsinA causes dystonic-like movements and loss of striatal cholinergic neurons. *Elife* (2015) 4:e08352. doi:10.7554/eLife.08352

42. Li J, Liang CC, Pappas SS, Dauer WT. TorsinB overexpression prevents abnormal twisting in DYT1 dystonia mouse models. *Elife* (2020) 9:e54285. doi:10.7554/eLife.54285

43. Pisani A, Bernardi G, Ding J, Surmeier D. Re-emergence of striatal cholinergic interneurons in movement disorders. *Trends Neurosci* (2007) 30(10):545–53. doi:10.1016/j.tins.2007.07.008

44. Langmead B, Trapnell C, Pop M, Salzberg SL. Ultrafast and memory-efficient alignment of short DNA sequences to the human genome. *Genome Biol* (2009) 10(3):R25. doi:10.1186/gb-2009-10-3-r25

45. Trapnell C, Hendrickson DG, Sauvageau M, Goff L, Rinn JL, Pachter L. Differential analysis of gene regulation at transcript resolution with RNA-seq. *Nat Biotechnol* (2013) 31(1):46–53. doi:10.1038/nbt.2450

46. Trapnell C, Pachter L, Salzberg SL. TopHat: Discovering splice junctions with RNA-seq. *Bioinformatics* (2009) 25(9):1105–11. doi:10.1093/bioinformatics/btp120

47. Zhang Y, Chen K, Sloan SA, Bennett ML, Scholze AR, O'Keeffe S, et al. An RNA-sequencing transcriptome and splicing database of glia, neurons, and vascular cells of the cerebral cortex. *J Neurosci* (2014) 34(36):11929–47. doi:10.1523/JNEUROSCI.1860-14.2014

48. Binder JX, Pletscher-Frankild S, Tsafou K, Stolte C, O'Donoghue SI, Schneider R, et al. Compartments: Unification and visualization of protein subcellular localization evidence. *Database* (2014) 2014:bau012. doi:10.1093/database/bau012

49. Uhlen M, Karlsson MJ, Hober A, Svensson AS, Scheffel J, Kotol D, et al. The human secretome. *Sci Signal* (2019) 12(609):eaaz0274. doi:10.1126/scisignal.aaz0274

50. Huang da W, Sherman BT, Lempicki RA. Systematic and integrative analysis of large gene lists using DAVID bioinformatics resources. *Nat Protoc* (2009) 4(1): 44–57. doi:10.1038/nprot.2008.211

51. Ashburner M, Ball CA, Blake JA, Botstein D, Butler H, Cherry JM, et al. Gene ontology: Tool for the unification of biology. The gene ontology consortium. *Nat Genet* (2000) 25(1):25–9. doi:10.1038/75556

52. Gene Ontology C. The gene ontology resource: Enriching a GOld mine. *Nucleic Acids Res* (2021) 49(D1):D325–D334. doi:10.1093/nar/gkaa1113

53. Sharpe N, Tepper J. Postnatal development of excitatory synaptic input to the rat neostriatum: An electron microscopic study. *Neuroscience* (1998) 84(4): 1163–75. doi:10.1016/s0306-4522(97)00583-6

54. Tepper J, Sharpe N, Koos T, Trent F. Postnatal development of the rat neostriatum: Electrophysiological, light- and electron-microscopic studies. *Dev Neurosci* (1998) 20(2-3):125–45. doi:10.1159/000017308

55. Tepper J, Trent F. *In vivo* studies of the postnatal development of rat neostriatal neurons. *Prog Brain Res* (1993) 99:35–50. doi:10.1016/s0079-6123(08)61337-0

56. Gerfen CR, Young WS, 3rd. Distribution of striatonigral and striatopallidal peptidergic neurons in both patch and matrix compartments: An *in situ* hybridization histochemistry and fluorescent retrograde tracing study. *Brain Res* (1988) 460(1):161–7. doi:10.1016/0006-8993(88)91217-6

57. Theriault E, Landis DM. Morphology of striatal neurons containing VIP-like immunoreactivity. *J Comp Neurol* (1987) 256(1):1–13. doi:10.1002/cne.902560102

58. Munoz-Manchado AB, Bengtsson Gonzales C, Zeisel A, Munguba H, Bekkouche B, Skene NG, et al. Diversity of interneurons in the dorsal striatum revealed by single-cell RNA sequencing and PatchSeq. *Cel Rep* (2018) 24(8): 2179–90. doi:10.1016/j.celrep.2018.07.053

59. Ibanez-Sandoval O, Tecuapetla F, Unal B, Shah F, Koos T, Tepper JM. A novel functionally distinct subtype of striatal neuropeptide Y interneuron. *J Neurosci* (2011) 31(46):16757–69. doi:10.1523/JNEUROSCI.2628-11.2011

60. Gokce O, Stanley GM, Treutlein B, Neff NF, Camp JG, Malenka RC, et al. Cellular taxonomy of the mouse striatum as revealed by single-cell RNA-seq. *Cel Rep* (2016) 16(4):1126–37. doi:10.1016/j.celrep.2016.06.059

61. Figueredo-Cardenas G, Morello M, Sancesario G, Bernardi G, Reiner A. Colocalization of somatostatin, neuropeptide Y, neuronal nitric oxide synthase and NADPH-diaphorase in striatal interneurons in rats. *Brain Res* (1996) 735(2): 317–24. doi:10.1016/0006-8993(96)00801-3

62. Vander Heyden A, Naismith T, Snapp E, Hodzic D, Hanson P. LULL1 retargets TorsinA to the nuclear envelope revealing an activity that is impaired by the DYT1 dystonia mutation. *Mol Biol Cel* (2009) 20(11):2661–72. doi:10.1091/mbc.e09-01-0094

63. McGuirt AF, Post MR, Pigulevskiy I, Sulzer D, Lieberman OJ. Coordinated postnatal maturation of striatal cholinergic interneurons and dopamine release dynamics in mice. *J Neurosci* (2021) 41(16):3597–609. doi:10.1523/JNEUROSCI.0755-20.2021

64. Kuo HY, Liu FC. Synaptic wiring of corticostriatal circuits in basal ganglia: Insights into the pathogenesis of neuropsychiatric disorders. *eNeuro* (2019) 6(3): ENEURO0076–192019. doi:10.1523/ENEURO.0076-19.2019

65. West AE, Greenberg ME. Neuronal activity-regulated gene transcription in synapse development and cognitive function. *Cold Spring Harb Perspect Biol* (2011) 3(6):a005744. doi:10.1101/cshperspect.a005744

66. Kozorovitskiy Y, Peixoto R, Wang W, Saunders A, Sabatini BL. Neuromodulation of excitatory synaptogenesis in striatal development. *Elife* (2015) 4:e10111. doi:10.7554/eLife.10111

67. Cirnaru MD, Melis C, Fanutza T, Naphade S, Tshilenge KT, Muntean BS, et al. Nuclear receptor Nr4a1 regulates striatal striosome development and dopamine D1 receptor signaling. *eNeuro* (2019) 6(5):ENEURO0305–192019. doi:10.1523/ENEURO.0305-19.2019

68. Chen Y, Wang Y, Erturk A, Kallop D, Jiang Z, Weimer RM, et al. Activity-induced Nr4a1 regulates spine density and distribution pattern of excitatory synapses in pyramidal neurons. *Neuron* (2014) 83(2):431–43. doi:10.1016/j.neuron.2014.05.027

69. Jeanneteau F, Barrere C, Vos M, De Vries CJM, Rouillard C, Levesque D, et al. The stress-induced transcription factor NR4A1 adjusts mitochondrial function and synapse number in prefrontal cortex. *J Neurosci* (2018) 38(6):1335–50. doi:10.1523/JNEUROSCI.2793-17.2017

70. Lin Y, Bloodgood BL, Hauser JL, Lapan AD, Koon AC, Kim TK, et al. Activity-dependent regulation of inhibitory synapse development by Npas4. *Nature* (2008) 455(7217):1198–204. doi:10.1038/nature07319

71. Fu J, Guo O, Zhen Z, Zhen J. Essential functions of the transcription factor Npas4 in neural circuit development, plasticity, and diseases. *Front Neurosci* (2020) 14:603373. doi:10.3389/fnins.2020.603373

72. Lissek T, Andrianarivelo A, Saint-Jour E, Allichon MC, Bauersachs HG, Nassar M, et al. Npas4 regulates medium spiny neuron physiology and gates cocaine-induced hyperlocomotion. *EMBO Rep* (2021) 22(12):e51882. doi:10.15252/embr.202051882

73. Lyford GL, Yamagata K, Kaufmann WE, Barnes CA, Sanders LK, Copeland NG, et al. Arc, a growth factor and activity-regulated gene, encodes a novel cytoskeleton-associated protein that is enriched in neuronal dendrites. *Neuron* (1995) 14(2):433–45. doi:10.1016/0896-6273(95)90299-6

74. Peebles CL, Yoo J, Thwin MT, Palop JJ, Noebels JL, Finkbeiner S. Arc regulates spine morphology and maintains network stability *in vivo*. *Proc Natl Acad Sci U S A* (2010) 107(42):18173–8. doi:10.1073/pnas.1006546107

75. Tropea D, Giacometti E, Wilson NR, Beard C, McCurry C, Fu DD, et al. Partial reversal of Rett Syndrome-like symptoms in MeCP2 mutant mice. *Proc Natl Acad Sci U S A* (2009) 106(6):2029–34. doi:10.1073/pnas.0812394106

76. Landi S, Putignano E, Boggio EM, Giustetto M, Pizzorusso T, Ratto GM. The short-time structural plasticity of dendritic spines is altered in a model of Rett syndrome. *Sci Rep* (2011) 1:45. doi:10.1038/srep00045

77. Nieto-Bona MP, Garcia-Segura LM, Torres-Aleman I. Transynaptic modulation by insulin-like growth factor I of dendritic spines in Purkinje cells. *Int J Dev Neurosci* (1997) 15(6):749–54. doi:10.1016/s0736-5748(97)00021-x

78. Pang ZP, Bacaj T, Yang X, Zhou P, Xu W, Sudhof TC. Doc2 supports spontaneous synaptic transmission by a Ca(2+)-independent mechanism. *Neuron* (2011) 70(2):244–51. doi:10.1016/j.neuron.2011.03.011

79. Ramirez DMO, Crawford DC, Chanaday NL, Trauterman B, Monteggia LM, Kavalali ET. Loss of doc2-dependent spontaneous neurotransmission augments glutamatergic synaptic strength. *J Neurosci* (2017) 37(26):6224–30. doi:10.1523/JNEUROSCI.0418-17.2017

80. Schwenk J, Harmel N, Zolles G, Bildl W, Kulik A, Heimrich B, et al. Functional proteomics identify cornichon proteins as auxiliary subunits of AMPA receptors. *Science* (2009) 323(5919):1313–9. doi:10.1126/science.1167852

81. Herring BE, Shi Y, Suh YH, Zheng CY, Blankenship SM, Roche KW, et al. Cornichon proteins determine the subunit composition of synaptic AMPA receptors. *Neuron* (2013) 77(6):1083–96. doi:10.1016/j.neuron.2013.01.017

82. Brockie PJ, Jensen M, Mellem JE, Jensen E, Yamasaki T, Wang R, et al. Cornichons control ER export of AMPA receptors to regulate synaptic excitability. *Neuron* (2013) 80(1):129–42. doi:10.1016/j.neuron.2013.07.028

83. Nakagawa T. Structures of the AMPA receptor in complex with its auxiliary subunit cornichon. *Science* (2019) 366(6470):1259–63. doi:10.1126/science.aay2783

84. Dang M, Yokoi F, Cheetham C, Lu J, Vo V, Lovinger D, et al. An anticholinergic reverses motor control and corticostriatal LTD deficits in Dyt1 ΔGAG knock-in mice. *Behav Brain Res* (2012) 226(2):465–72. doi:10.1016/j.bbr.2011.10.002

85. Tanabe LM, Martin C, Dauer WT. Genetic background modulates the phenotype of a mouse model of DYT1 dystonia. *PLoS One* (2012) 7(2):e32245. doi:10.1371/journal.pone.0032245

86. Steward O, Torre ER, Tomasulo R, Lothman E. Neuronal activity up-regulates astroglial gene expression. *Proc Natl Acad Sci U S A* (1991) 88(15):6819–23. doi:10.1073/pnas.88.15.6819

87. Hol EM, Roelofs RF, Moraal E, Sonnemans MA, Sluijs JA, Proper EA, et al. Neuronal expression of GFAP in patients with Alzheimer pathology and identification of novel GFAP splice forms. *Mol Psychiatry* (2003) 8(9):786–96. doi:10.1038/sj.mp.4001379

88. Casper KB, McCarthy KD. GFAP-positive progenitor cells produce neurons and oligodendrocytes throughout the CNS. *Mol Cel Neurosci* (2006) 31(4):676–84. doi:10.1016/j.mcn.2005.12.006

89. Miller KE, Suter DM. An integrated cytoskeletal model of neurite outgrowth. *Front Cel Neurosci* (2018) 12:447. doi:10.3389/fncel.2018.00447

90. Hu X, Viesselmann C, Nam S, Merriam E, Dent EW. Activity-dependent dynamic microtubule invasion of dendritic spines. *J Neurosci* (2008) 28(49): 13094–105. doi:10.1523/JNEUROSCI.3074-08.2008

91. Gu J, Firestein BL, Zheng JQ. Microtubules in dendritic spine development. *J Neurosci* (2008) 28(46):12120–4. doi:10.1523/JNEUROSCI.2509-08.2008

92. Jaworski J, Kapitein LC, Gouveia SM, Dortland BR, Wulf PS, Grigoriev I, et al. Dynamic microtubules regulate dendritic spine morphology and synaptic plasticity. *Neuron* (2009) 61(1):85–100. doi:10.1016/j.neuron.2008.11.013

93. Schatzle P, Esteves da Silva M, Tas RP, Katrukha EA, Hu HY, Wierenga CJ, et al. Activity-dependent actin remodeling at the base of dendritic spines promotes microtubule entry. *Curr Biol* (2018) 28(13):2081–93. doi:10.1016/j.cub.2018.05.004

94. Abdel-Halim MS, Hamberg M, Sjoquist B, Anggard E. Identification of prostaglandin D2 as a major prostaglandin in homogenates of rat brain. *Prostaglandins* (1977) 14(4):633–43. doi:10.1016/0090-6980(77)90190-3

95. Urade Y, Hayaishi O. Biochemical, structural, genetic, physiological, and pathophysiological features of lipocalin-type prostaglandin D synthase. *Biochim Biophys Acta* (2000) 1482(1-2):259–71. doi:10.1016/s0167-4838(00)00161-8

96. Urade Y, Fujimoto N, Hayaishi O. Purification and characterization of rat brain prostaglandin D synthetase. *J Biol Chem* (1985) 260(23):12410–5. doi:10.1016/s0021-9258(17)38889-0

97. Iwasa K, Yamamoto S, Yagishita S, Maruyama K, Yoshikawa K. Excitotoxicity-induced prostaglandin D2 production induces sustained microglial activation and delayed neuronal death. *J Lipid Res* (2017) 58(4): 649–55. doi:10.1194/jlr.M070532

98. Yoshikawa K, Kita Y, Kishimoto K, Shimizu T. Profiling of eicosanoid production in the rat hippocampus during kainic acid-induced seizure: Dual phase regulation and differential involvement of COX-1 and COX-2. *J Biol Chem* (2006) 281(21):14663–9. doi:10.1074/jbc.M511089200

99. Taniguchi H, Mohri I, Okabe-Arahori H, Aritake K, Wada K, Kanekiyo T, et al. Prostaglandin D2 protects neonatal mouse brain from hypoxic ischemic injury. *J Neurosci* (2007) 27(16):4303–12. doi:10.1523/JNEUROSCI.0321-07.2007

100. Fukuhara A, Yamada M, Fujimori K, Miyamoto Y, Kusumoto T, Nakajima H, et al. Lipocalin-type prostaglandin D synthase protects against oxidative stress-induced neuronal cell death. *Biochem J* (2012) 443(1):75–84. doi:10.1042/BJ20111889

101. Saleem S, Shah ZA, Urade Y, Dore S. Lipocalin-prostaglandin D synthase is a critical beneficial factor in transient and permanent focal cerebral ischemia. *Neuroscience* (2009) 160(1):248–54. doi:10.1016/j.neuroscience.2009.02.039

102. Kannaian B, Sharma B, Phillips M, Chowdhury A, Manimekalai MSS, Adav SS, et al. Abundant neuroprotective chaperone Lipocalin-type prostaglandin D synthase (L-PGDS) disassembles the Amyloid-beta fibrils. *Sci Rep* (2019) 9(1): 12579. doi:10.1038/s41598-019-48819-5

103. Kanekiyo T, Ban T, Aritake K, Huang ZL, Qu WM, Okazaki I, et al. Lipocalin-type prostaglandin D synthase/beta-trace is a major amyloid beta-chaperone in human cerebrospinal fluid. *Proc Natl Acad Sci U S A* (2007) 104(15):6412–7. doi:10.1073/pnas.0701585104

104. Lescuyer P, Gandini A, Burkhard PR, Hochstrasser DF, Sanchez JC. Prostaglandin D2 synthase and its post-translational modifications in neurological disorders. *Electrophoresis* (2005) 26(23):4563–70. doi:10.1002/elps.200500292

DYSTONIA

TYPE Original Research
PUBLISHED 16 February 2023
DOI 10.3389/dyst.2023.11053

OPEN ACCESS

EDITED BY
Roy Sillitoe,
Baylor College of Medicine,
United States

*CORRESPONDENCE
Nicole Calakos,
nicole.calakos@dm.duke.edu

RECEIVED 14 November 2022
ACCEPTED 02 February 2023
PUBLISHED 16 February 2023

CITATION
King CS, Caffall ZF, Soderblom EJ and Calakos N (2023), DYT-TOR1A genotype alters extracellular vesicle composition in murine cell model and shows potential for biomarker discovery.
Dystonia 2:11053.
doi: 10.3389/dyst.2023.11053

DYT-TOR1A genotype alters extracellular vesicle composition in murine cell model and shows potential for biomarker discovery

Connor S. King[1], Zachary F. Caffall[1], Erik J. Soderblom[2,3] and Nicole Calakos[1,2,4,5]*

[1]Department of Neurology, Duke University Medical Center, Durham, NC, United States, [2]Department of Cell Biology, Duke University Medical Center, Durham, NC, United States, [3]Proteomics and Metabolomics Shared Resource, Department of Biostatistics and Bioinformatics, Duke University Medical Center, Durham, NC, United States, [4]Department of Neurobiology, Duke University Medical Center, Durham, NC, United States, [5]Duke Institute for Brain Sciences, Duke University, Durham, NC, United States

Introduction: Biomarkers that can be used to identify patient subgroups with shared pathophysiology and/or that can be used as pharmacodynamic readouts of disease state are valuable assets for successful clinical trial design. In translational research for brain diseases, extracellular vesicles (EVs) have become a high-priority target for biomarker discovery because of their ubiquity in peripheral biofluids and potential to indicate brain state.

Materials and methods: Here, we applied unbiased quantitative proteomics of EVs isolated from DYT-TOR1A knockin mouse embryonic fibroblasts and littermate controls to discover candidates for protein biomarkers. We further examined the response of genotype perturbations to drug treatment conditions to determine their pharmacodynamic properties.

Results: We found that many DYT-TOR1A MEF EV differences were significantly corrected by ritonavir, a drug recently shown to correct DYT-TOR1A phenotypes in cell and mouse disease models. We also used tool compounds to explore the effect of the integrated stress response (ISR), which regulates protein synthesis and is implicated in dystonia pathogenesis. Integrated stress response inhibition in WT cells partially phenocopied the effects of DYT-TOR1A on EV proteome composition, and ISR potentiation in DYT-TOR1A caused changes that paralleled ritonavir treatment.

Conclusion: These results collectively show that DYT-TOR1A genotype alters EV protein composition, and these changes can be dynamically modulated by a candidate therapeutic drug and ISR activity state. These mouse model findings provide proof-of-concept that EVs may be a useful source of biomarkers in human populations and further suggest specific homologs to evaluate in cross-species validation.

KEYWORDS

dystonia, biomarkers, proteomics, DYT1, extracellular vesicles, ritonavir

Introduction

Dystonia is a movement disorder characterized by sustained muscle contractions with abnormal twisting movements (1). DYT-TOR1A is a rare inherited dystonia caused by a mutation in *TOR1A* (n. delGAG, p. ΔE) leading to a childhood-onset form of the disease that often involves most of the body (e.g., early-onset, generalized dystonia) (2). Currently, there is substantial unmet clinical need for DYT-TOR1A dystonia treatment. Oral medications are limited by narrow therapeutic windows and side effects, typically leaving deep brain stimulation surgery as the major alternative treatment option (3). To fill these treatment gaps, drug discovery efforts are underway to identify highly effective, well tolerated, and orally bioavailable small molecules. We have previously demonstrated that ritonavir, an HIV protease inhibitor, rescues diverse disease phenotypes in DYT-TOR1A preclinical models (4). However, translating effective treatments from the bench into the clinic is especially difficult for neurological diseases, which have a below average success rate in all clinical trial phases compared to other body systems (5, 6). One strategy to improve clinical trial design is identifying and measuring biomarkers before and during the treatment intervention. Biomarkers have multiple classifications depending on their clinical context of use. These include predictive biomarkers, which can be used to stratify patient subpopulations and enrich recruitment for subjects most likely to respond to the given intervention, and pharmacodynamic/response biomarkers, which track physiological changes throughout treatment to assess successful target engagement (7, 8). The incorporation of such biomarkers into clinical trials can double the likelihood of success from Phase I through final regulatory approval (5). Thus, biomarkers are a valuable asset, especially for rare and neurological diseases.

Peripheral biofluids are an easily accessible source of molecular biomarkers, such as proteins, lipids, and miRNAs (9–11). In a variety of clinical settings, these 'liquid biopsies' are now performed routinely to measure disease processes that often occur quite distal to the puncture collection site (9, 10). For example, tumor-derived DNA circulating in blood can reveal mutations that predict response to particular chemotherapies (12), and hemoglobin A1C in diabetes is both a diagnostic biomarker during initial screening and a pharmacodynamic/response biomarker for monitoring blood glucose after treatment (7). However, in diseases of the CNS like dystonia, peripheral biomarkers for brain state are more challenging to isolate because of the blood brain barrier (BBB). Extracellular vesicles (EVs) have been found to be a promising source for CNS disease biomarkers, since they can cross the BBB and carry protein and RNA cargo secreted by brain cells (13). As one example, neurofilament light chain in plasma EVs has been studied in X-linked dystonia-parkinsonism and other neurodegenerative diseases as a biomarker for brain axonal degeneration (14, 15). Thus, EVs are often considered to provide a view into the physiological state of their cells of origin.

In this study, we first sought to determine whether the DYT-TOR1A genotype altered EV composition, a finding that would open the possibility to use EVs as biomarkers in this disease. We focused on obtaining proof-of-concept in cell lines which also secrete EVs because DYT-TOR1A is a rare genetic disease with geographically isolated human subject populations (16, 17). While we considered DYT-TOR1A patient-derived cell lines (14, 18), we chose to use murine embryonic fibroblasts (MEFs) derived from the Tor1a$^{\Delta GAG/+}$ knockin mouse model of DYT-TOR1A (19) because it has construct validity and also provides a uniform genetic background to reduce variability in a proof-of-concept experiment. We examined the effects of DYT-TOR1A on EV protein composition using quantitative LC-MS/MS proteomics. Once putative genotype-modified candidates were identified, we next explored their behavior in response to pharmacological manipulations: therapeutic treatment with a candidate dystonia drug, ritonavir, and modulation of a conserved signaling pathway perturbed in multiple dystonias, the integrated stress response (ISR) (20). Lastly, we combined our experimental observations with pragmatic criteria for ideal clinical biomarkers to put forth candidates with the highest potential for future tests of DYT-TOR1A EV biomarkers in human subjects.

Results

DYT-TOR1A MEF EVs show altered protein composition

Immortalized murine embryonic fibroblast (MEF) cell lines were prepared from heterozygous knockin mice bearing the DYT-TOR1A mutation (Tor1a$^{\Delta GAG/+}$ genotype hereafter abbreviated as DYT-TOR1A or DYT) (19) and wildtype (WT) littermate embryos according to standard methodology (Methods). Three independent cell lines for each genotype were used. Genotype and all drug treatment conditions were tested in a blinded experimental design and in parallel by splitting the parental cell line flask into separate flasks for each condition. EVs produced during the 24-h period following media exchange with an EV-depleted media were isolated from the conditioned media by ultracentrifugation (21). Protein was isolated from the resultant EV pellet. DYT-TOR1A did not significantly modify recovery of total protein or amount of the constitutive EV marker, TSG101 (Figures 1B, C). Specific EV enrichment was confirmed by Western blot for TSG101 compared to non-EV markers (calnexin, actin) (Figures 1C, D) (22). Samples were then subjected to unbiased, quantitative LC-MS/MS proteomics analysis. Quantitative proteomic measurements also demonstrated that EV protein abundances of classic EV markers (TSG101 and the

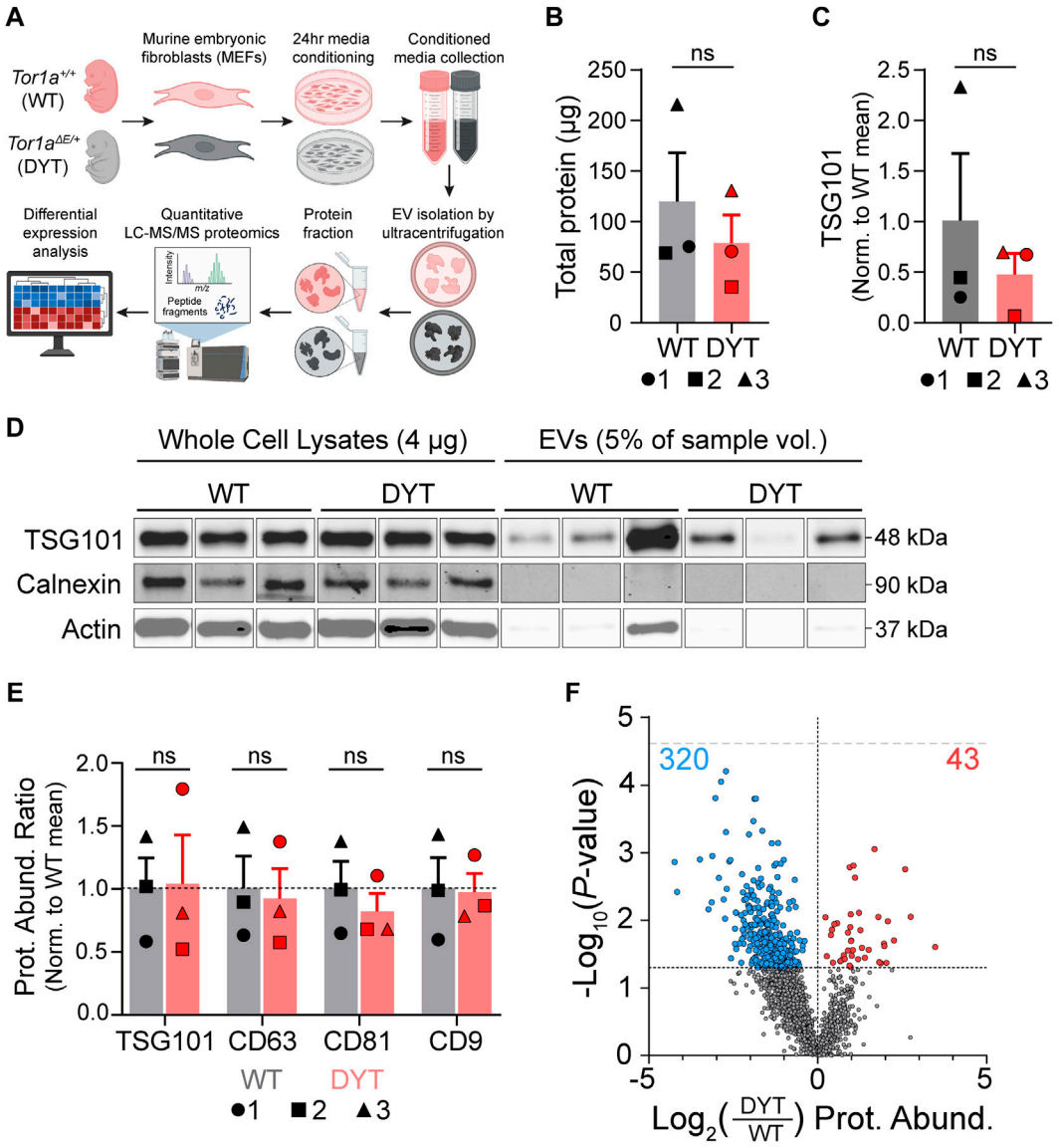

FIGURE 1
Quantitative proteomics shows DYT-TOR1A-dependent changes in protein composition of EVs isolated from murine embryonic fibroblasts. **(A)** Experimental workflow schematic. **(B)** Total protein in EV samples quantified by BCA. 1, 2, and 3 indicate specific biological replicates. **(C)** Quantification of TSG101 from Western blot in **(D)** normalized to the mean WT abundance. 1, 2, and 3 indicate specific biological replicates. **(D)** Western blot of whole cell lysates (4 µg protein) and EV samples (5% of total EV sample by volume) for TSG101 (EV marker), calnexin (ER marker), and actin. See Supplementary Figure S1 for complete blot images. **(E)** Mass spectrometry protein abundances (Prot. Abund.) of EV markers normalized to WT mean abundance. 1, 2, and 3 indicate specific biological replicates. Significance testing in **(B,C,E)** by unpaired Student's t tests. **(F)** Volcano plot comparing protein abundances of 1974 detected EV proteins between DYT-TOR1A and WT. Symbol color of data points indicate proteins significantly ($p \leq 0.05$) more (red dots) or less (blue dots) abundant in DYT-TOR1A relative to WT. Lower horizontal dashed line indicates p-value of 0.05 threshold. Upper gray horizontal dashed line indicates Bonferroni-adjusted p-value threshold of 2.5e-5. Differences in abundance are represented as fold change (using $\log_2$ transformation) and p-value is calculated by unpaired t-test for each protein ($n = 3$ biological replicates).

tetraspanins CD9, CD81, and CD63) were not modified by genotype (Figure 1E).

We characterized the EV proteome to identify genotype-dependent changes in EV protein abundances between DYT-TOR1A and WT EV samples. Following alignment of peptide signals to unique identifying peptides (UIPs) and removal of proteins with fewer than two detected UIPs, 1974 proteins were detected across all cell lines. Using a Bonferroni-adjusted p-value threshold for multiple hypothesis testing ($p < 2.5e-5$) (23), no significant genotype effects were identified. We next used this

discovery dataset to identify putative DYT biomarkers for testing in follow-on experiments. Using an uncorrected p-value cutoff of less than 0.05, we identified 363 of 1974 proteins with significantly different abundances in DYT-TOR1A versus WT EVs (Figure 1F). This differential subset of 363 is more than 3.5 times larger than would be predicted by chance (e.g., 99 proteins from the total of 1974, based on the expected proportion $\alpha = 0.05$).

We further noted that among the 363 differential proteins, there was an asymmetric distribution of genotype effects. The DYT-TOR1A effects showed a bias towards decreased abundances, with 320 proteins being significantly less abundant compared to only 43 being more abundant in DYT-TOR1A relative to WT (two-tailed binomial sign test, $p < 0.0001$). This skewed distribution was also maintained across all EV proteins (1491 less, 483 more; two-tailed binomial sign test, $p < 0.0001$).

We therefore considered technical reasons that could artifactually cause such a distribution bias, e.g., lower EV yields and/or detection thresholds not being met preferentially in DYT samples. As Figure 1E demonstrates, there were no significant genotype-dependent differences in abundance of EV constituents detected in the LC-MS/MS data. Secondly, when a protein is not detected in a sample, an imputed value is given as described in Methods prior to sample loading normalization. We therefore examined whether the DYT genotype effects came preferentially from proteins with multiple imputed values. Instead, we observed that hits were distributed proportionally across proteins with 0, 1, 2 or 3 imputed values and the vast majority of hits came from proteins with no imputed values (Supplementary Figure S2). These observations rule out LC-MS/MS detection thresholds as a systematic confound. In summary, we have performed proteomic analysis of MEF culture-derived EV preparations and identify 363 candidate proteins for DYT-TOR1A genotype biomarkers.

Ritonavir shows corrective effects on DYT-TOR1A EV protein composition

Recent studies have shown corrective effects of the HIV protease inhibitor ritonavir on cell and brain phenotypes in DYT-TOR1A preclinical models (4). For translation to human clinical trials, it is desirable to have pharmacodynamic biomarkers to aid early dose-finding studies and to assess target engagement (7, 8, 11). To explore the potential for the DYT-TOR1A genotype-associated EV changes that we identified to be used as pharmacodynamic biomarkers of disease state, we exposed DYT-TOR1A MEF cultures to 20 µM ritonavir throughout the 24 h of media conditioning preceding EV isolation. EV protein fractions were analyzed by quantitative LC-MS/MS proteomics performed in the same batch run as all conditions reported in this study.

Of the subset of 363 proteins significantly disrupted by DYT-TOR1A genotype basally, we found that >60% (230/363) had significant changes in abundance following ritonavir treatment at a threshold of $p \leq 0.05$. This number of hits is 12 times greater than would be predicted by chance if ritonavir had no true effect on the genotype-dependent hits (18.15 proteins by $\alpha = 0.05$). We further noticed that when examining the behavior of the 363 putative DYT biomarkers independent of p-value, the overwhelming majority of proteins showed ritonavir effects on protein abundance that were in the corrective direction (344/363) (Figure 2A). The putative DYT biomarker subset of proteins also showed strong and inverse correlations between genotype and ritonavir effects (Pearson $r = -0.78$, $p < 0.0001$) (Figure 2B). Noticing the very large number of proteins modified by ritonavir, we further examined the relationship between DYT genotype disruptions and DYT+RTV effects across the entire proteome and found that the strong inverse correlation was maintained ($n = 1974$, Pearson $r = -0.74$, $p < 0.0001$) (Figure 2B). Proteome-wide, ritonavir significantly modified 29% of the DYT EV proteome (uncorrected $p \leq 0.05$, 582/1974) in a direction that was opposite to the genotype effect, with an asymmetric distribution toward increasing abundances for both significant and non-significant abundance changes (two-tailed binomial sign test: 508/582, with $\log_2$ fold change >0, $p < 0.0001$; 1372/1974 with $\log_2$ fold change >0, $p < 0.0001$). Lastly, we deployed hierarchical clustering to evaluate ritonavir's effects on the putative DYT-TOR1A genotype biomarker proteins ($n = 363$). This analysis showed that ritonavir-treated DYT-TOR1A EV samples clustered more closely with WT than DYT-TOR1A samples (Figure 2C).

In summary, DYT-TOR1A genotype disruptions of EV protein composition show potential as pharmacodynamic markers of disease state. Ritonavir treatment acutely modified a substantial fraction of DYT-TOR1A genotype-dependent protein disruptions (95%) and caused dendrogram clustering of the EV proteome to become more closely related to WT samples than the DYT-TOR1A genotype.

Influence of the integrated stress response pathway on EV composition in WT and DYT-TOR1A

DYT-TOR1A and other dystonias show dysfunction in a biochemical pathway, the integrated stress response (ISR), that has wide-reaching effects on the proteome because it regulates global protein synthesis (20). This prompted us to ask how the broad EV compositional differences we observed in the previous 2 experiments were related to ISR pathway effects.

We used ISR tool compounds to modify ISR activity. Our prior studies established the corrective directionality of the eIF2α phosphatase inhibitor salubrinal in DYT-TOR1A cell and mouse model phenotypes and sufficiency of the ISR inhibitor ISRIB to

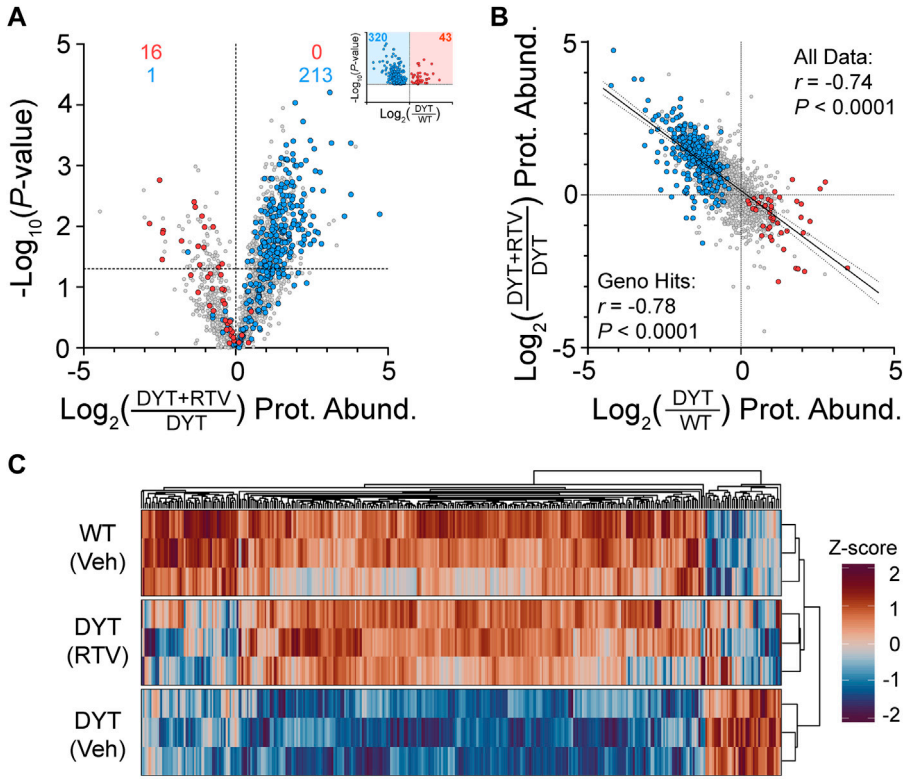

FIGURE 2
Effects of ritonavir treatment on protein composition of EVs isolated from DYT-TOR1A MEF cultures. **(A)** Volcano plot comparing protein abundances (Prot. Abund.) between EVs isolated from DYT-TOR1A MEF cultures treated with ritonavir (DYT+RTV) vs. vehicle (DYT). For **(A,C)**, differences in protein abundance are represented as fold change (using $\log_2$ transform) and p-value is calculated by unpaired t-test for each protein (n = 3 biological replicates). Horizontal dashed line indicates uncorrected p-value of 0.05. Color-coded data points indicate the original genotype disrupted proteins from Figure 1F with coloring showing the protein's genotype effect (red being increased and blue being decreased in DYT/WT. Inset shows genotype results from Figure 1F). **(B)** Comparison of genotype (DYT/WT) and ritonavir (DYT+RTV/DYT) effects on protein abundances ($\log_2$ transformed). **(C)** Hierarchical clustering heatmap of WT, DYT, and DYT+RTV protein abundances for proteins significantly different in DYT relative to WT (n = 363).

mimic DYT-TOR1A phenotypes (4, 20, 24). We therefore hypothesized that ISRIB-induced EV composition changes in WT MEF EVs would reproduce DYT-TOR1A genotype differences that were related to ISR dysregulation and that salubrinal treatment of DYT-TOR1A MEF EVs would cause normalizing shifts in genotype differences if they were related to ISR dysregulation.

WT MEFs were treated with 50 nM ISRIB to inhibit ISR pathway output for 24 h prior to EV harvest from the conditioned media. ISRIB treatment of WT cells disrupted fewer proteins at the statistical threshold of $p \leq 0.05$ than were observed between DYT and WT samples (103/1974 (5%) vs. 363/1974 (18%)) and only 7% of the genotype-disrupted proteins (26/363) were reproduced by ISRIB at the statistical threshold ($p \leq 0.05$). However, an examination of proteome-wide effects independent of p-value thresholds showed protein abundance directionality (greater or lesser) to be non-randomly distributed (Fisher's exact test, $p < 0.0001$) and in a directionality similar to the DYT genotype effects (Figure 3A). A Pearson's correlation analysis showed a positive correlation between DYT genotype effects and ISRIB effects, supporting the hypothesis that ISRIB treatment of WT cells mimics DYT genotype effects (Pearson $r = 0.40$, $p < 0.0001$)(Figure 3B). Interestingly, as was observed with ritonavir effects, this correlation was also maintained when the entire proteome was evaluated (Pearson $r = 0.37$, $p < 0.0001$).

To augment ISR activity in DYT-TOR1A MEFs, cell cultures were treated with 20 μM salubrinal during the 24 h conditioning period prior to EV harvest from the media. Salubrinal is a specific inhibitor of eIF2α phosphatases, CReP and GADD34 (25). Salubrinal treatment of DYT samples significantly modified 9% of the total proteins (169/1974) and caused significant corrective effects on 13% of DYT disrupted proteins (46/363) (Figure 3C). Like ISRIB, secondary analyses of effects independent of p-value thresholds showed that DYT disrupted proteins were not randomly distributed (Fisher's exact test, $p <$

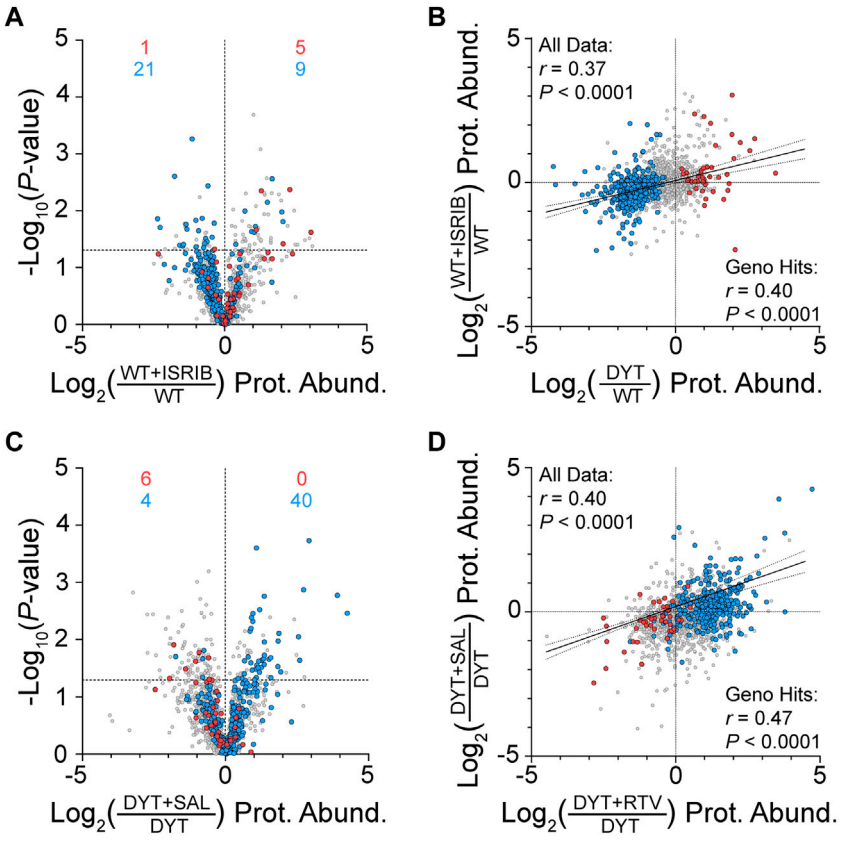

FIGURE 3
Effects of ISR tool compounds on MEF EV protein composition. **(A)** Volcano plot shows ISRIB effects on protein abundances in WT MEFs. For **(A–D)**, color-coded data points indicate proteins significantly increased (red) or decreased (blue) in DYT-TOR1A MEF EVs compared to WT experiment shown in Figure 1F. Differences in protein abundance are represented as fold change (using $\log_2$ transform) and p-value is calculated by unpaired t-test for each protein (n = 3 biological replicates). Horizontal dashed line indicates p-value of 0.05. **(B)** Correlation of protein abundance fold changes between DYT genotype effects (DYT/WT) and ISRIB effects (WT+ISRIB/WT). **(C)** Volcano plot showing the effect of salubrinal treatment of DYT MEFs (DYT+SAL) on EV protein abundances compared to vehicle control (DYT). **(D)** Correlation between ritonavir and salubrinal treatment effects on protein abundances in DYT MEF EVs.

0.0001) and showed directionality biases supporting the hypothesis that salubrinal has corrective effects on DYT disruptions (Figure 3C). Lastly, we examined the concordance of drug effects between salubrinal and ritonavir on DYT-TOR1A MEF EV protein abundances, given that both drugs augment ISR activity (4, 25, 26). Ritonavir and salubrinal effects on the putative DYT-TOR1A biomarker proteins were positively correlated (Pearson r = 0.47, p < 0.0001) (Figure 3D). This result is consistent with a degree of shared mechanism of action between salubrinal and ritonavir.

In summary, ISR tool compound experiments demonstrate that ISR activity effects correlate with DYT-TOR1A genotype disruptions and ritonavir corrective effects on MEF EV protein composition. These results support the hypothesis that DYT-TOR1A genotype disruptions of MEF EV protein abundances and the corrective effects of ritonavir treatment are related, at least in part, to ISR pathway activity.

Stratification of EV components for biomarker potential in human samples

In this study, we have taken advantage of the benefits of control over biological variables that an animal model system affords to generate initial proteomic discovery datasets for putative biomarkers of DYT-TOR1A. To guide translation to dystonia biomarker discovery in future patient-derived cell line or human plasma and CSF samples, we considered the results from our three experimental tests alongside human biospecimen datasets to prioritize candidates with the greatest potential.

Our stratification process considered the following features. First, we identified protein candidates that have been previously detected in human plasma (27). This criterion identified 164 of the 363 genotype-disrupted proteins. Second, we identified candidates that showed conserved directionality of effects across two drug perturbations, independent of effect size or

p-value (Ritonavir-DYT, ISRIB-WT) (Supplementary Data Sheet S1 Columns 5,6). This criterion identified 121 of 164 proteins. Then, we created a composite score of genotype and ritonavir effect sizes by summing the absolute value of their respective Cohen's *d* score. The results of this analysis are compiled in Supplementary Data Sheet S1. Overall, a third of the DYT-TOR1A genotype disrupted proteins show favorable characteristics according to these prioritizations.

Discussion

Here we used a discovery proteomics approach to determine whether DYT-TOR1A alters EV composition by comparing EVs isolated from DYT-TOR1A heterozygous knockin MEF cultures to those from wildtype littermate controls. We identified a subset of 363 proteins with significant genotype effects. We then tested their pharmacodynamic responsivity to candidate drugs and found that ritonavir has a strikingly broad corrective effect on the EV proteome, and that at least a subset of these changes further correlates with ISR activity. Altogether, the results of this study provide preclinical proof-of-principle for the potential to use EVs in DYT-TOR1A for predictive and pharmacodynamic biomarker applications and define a prioritized list of candidate biomarkers based on follow-on testing and human bioinformatic data.

A significant takeaway from this exploratory study is that in DYT-TOR1A, rather than identifying one or a handful of candidate biomarkers, we found broad proteome-wide disruptions and corrections. We hypothesize at least three mechanisms that could cause the widespread EV composition disturbances we observed in DYT-TOR1A. First, in previous *in vitro* studies of DYT-TOR1A, patient-derived dermal fibroblasts exhibit secretion deficits through the ER-to-Golgi secretory pathway (20, 28), which regulates trafficking to a variety of intracellular locations prior to extracellular release (29). EVs are a heterogeneous population of vesicles produced by distinct biogenesis mechanisms—exosomes form as intraluminal vesicles within late endosomes and are released when these multivesicular bodies fuse with the plasma membrane, while microvesicles arise from direct outward budding of the plasma membrane (29–31). However, both carry cargo sorted and transported by the ER-to-Golgi pathway, and the ultracentrifugation EV isolation method used in this study likely includes a mixed EV population (32, 33). Broad-based changes in DYT-TOR1A EV composition may reflect upstream disruptions in these intracellular trafficking pathways. Second, ΔE-TorsinA abnormally localizes to the nuclear envelope relative to TorsinA's usual predominance in the ER, and this mislocalization is likely to influence trafficking through the nuclear envelope (19, 34–37). A third mechanism that could cause broad EV compositional changes is the influence of ISR dysregulation on protein synthesis in DYT-TOR1A. ISR dysfunction is implicated in the pathogenesis of DYT-TOR1A and other dystonias (20). The ISR regulates mRNA translation at the level of translation initiation (38). ISR activity markedly and globally reconfigures which proteins are translated (38–40). In addition, HIV protease inhibitors (including ritonavir) activate the ISR (4, 26) and show corrective effects on several DYT-TOR1A phenotypes (4). Therefore, the influence of the ISR on global proteostasis could contribute to the EV proteome genotype effects and ritonavir effects we observed. Although EV cargo loading is a regulated process, rather than a simple stochastic loading of nearby proteins (31, 41), a sufficiently large change in proteostasis could be reflected across multiple subcellular compartments, including EVs. Future studies examining the intracellular dynamics of the DYT-TOR1A candidate biomarkers identified in this study could further test these three candidate pathophysiological mechanisms.

It was striking that the strongest and broadest drug effect identified in this study was caused by ritonavir and not ISR-targeting tool compounds. In measuring the pharmacodynamic responsivity of DYT-TOR1A genotype-disrupted proteins to ritonavir, we found that 63% of these proteins (230/363) were significantly different in DYT-TOR1A following ritonavir treatment and 95% of these changes were in the corrective direction toward WT. This is best illustrated by unsupervised hierarchical clustering of each sample showing that all three ritonavir-treated DYT-TOR1A samples cluster closer to WT cell lines than their DYT vehicle-treated corresponding cell lines. These results identify a proteomic "signature" that could be used as a measure of pharmacodynamic response.

Many of the differentially abundant EV proteins identified in this study show strong cross-species homology and are detected in human plasma. Since similar mouse-to-human predictive approaches have proven useful in other diseases (42), we aimed to generate a prioritized candidate biomarker set using the advantages of the mouse model system to guide pharmacodynamic biomarker discovery in human patients with this rare disease.

Identifying a DYT-TOR1A biomarker signature also has implications for other forms of dystonia beyond DYT-TOR1A that may benefit from predictive biomarkers. While DYT-TOR1A has a recognizable clinical manifestation and is readily diagnosed by genotype testing, sporadic dystonias with no known genetic etiology are the most common form of dystonia. We have previously shown that ~4% of sporadic cervical dystonia patients had mutations in ATF4, the main effector protein of the ISR, and several other inherited dystonias also have ISR involvement (20, 43–46). We therefore anticipate that EV biomarkers may be useful not only for pharmacodynamic monitoring but also for identifying dystonia subpopulations with shared pathophysiology. Such predictive biomarkers could help identify sporadic dystonia patients who are most likely to respond to ritonavir or other ISR-modifying treatments in future clinical trials. Finally, a common but poorly understood feature of many inherited

dystonias is that they show reduced penetrance. Current DYT-TOR1A genetic mouse models are not suited to address whether EV biomarkers may also have prognostic value because the model does not reproduce the dystonia phenotype. Future human studies will be needed to determine whether DYT-TOR1A EV biomarkers vary based on symptom manifestation and can be used to predict disease penetrance. Our results provide proof-of-concept that DYT-TOR1A genotype disrupts EV composition and its pharmacodynamic responsiveness under the more optimal homogenous conditions afforded by mouse models. We hope that these findings will accelerate future biomarker discovery.

Materials and methods

Experimental blinding, power, and statistical approach

Sample size was arbitrarily set *a priori* at three samples per group. Experimenters were blinded to MEF cell line genotype and drug treatment prior to cell culture experiments, and proteomics were performed on these blinded sample groups. Experimenters were unblinded after initial differential abundance analyses were completed. For differences in protein abundances, statistical testing used unpaired Student's t tests between $n = 3$ WT and $n = 3$ DYT samples without correction for multiple hypothesis testing or with Bonferroni correction where noted (23). Two-tailed binomial sign test was performed using a null probability $p = 0.5$. Fisher's Exact Test was performed on contingency tables for overlaps of the 363 significantly different proteins between conditions using abundances greater than or less than zero $\log_2$ fold change.

Animals

ΔE Torsin1a knockin (courtesy of Dr. W. Dauer, UTSW; IMSR_JAX:025637) (19) mice on C57BL/6 background were bred in standard housing conditions with food and water provided *ad libitum*. All procedures were approved by the Duke University Institutional Animal Care and Use Committee (IACUC).

Cell lines and cell culture

Mouse embryonic fibroblasts were harvested as previously described (37) from E14 *TOR1A*$^{\Delta E/+}$ mice and immortalized *via* SV40 transfection. MEFs were maintained in sterile-filtered MEF media [DMEM (Thermo Fisher Scientific, #11995-065) + 10% fetal bovine serum (Hyclone, #SH0071.03) + 1X GlutaMAX (Gibco, #35050-061) + 1% penicillin/streptomycin/amphotericin (Gibco, #15240062) + 1% Non-Essential Amino Acids (Gibco, #11140050)+ 55 nM β-Mercaptoethanol (Gibco, #21985023)] at 37°C/5% CO_2.

MEF EV-conditioned media collection

EV-depleted (dEV) media was prepared by spinning 10% FBS MEF media for 18 h at 100,000 x g (Beckman L8-55M ultracentrifuge; SW27 rotor; 23,600 rpm; 4°C) (47). MEFs were seeded at 5.8×10^5 cells into one 15 cm dish per line. At 90% confluence, cells were passaged 1:10 into four 15 cm dishes per line and when each line reached ~50% confluence, media was exchanged for dEV media containing 1% dEV FBS and the given drug treatment. Ritonavir (Tocris Biosciences, #5856), ISRIB (Sigma, #SML0843), and salubrinal (Tocris Biosciences, #2347) were dissolved in DMSO (100 mg/mL) and frozen in aliquots at −20°C. On the day of each treatment, these aliquots were thawed and added to dEV media containing 1% FBS to final concentrations (0.04% DMSO vehicle, 50 nM ISRIB, 20 μM ritonavir, or 20 μM salubrinal). After 24 h in dEV media, the EV-conditioned media and cells were collected separately.

EV protein isolation

EV-conditioned media was centrifuged at 4°C for 20 min at 2000 x g (Sorvall HS-4, 3500 rpm). Supernatant was transferred to a new tube and centrifuged at 4°C for 30 min at 8000 x g (Sorvall HS-4, 6500 rpm). Final clarified supernatant was stored at −80°C. Media was thawed in room temperature water bath and 36 mL per sample was ultra-centrifuged in Ultra-Clear tubes (Beckman Coulter, #344058) for 16 h at 100,000 x g (Beckman L8-55M ultracentrifuge; SW27 rotor; 23,600 rpm; 4°C) to isolate EVs (21). The supernatant was discarded and protein was extracted from the pellet. Protein was extracted by adding 50 μL modified RIPA buffer [1% Triton X-100, 0.5% SDS, 0.5% deoxycholic acid, 50 mM $NaPO_4$ at pH 7.4, 150 mM NaCl, 2 mM EDTA, 50 mM NaF, 10 mM sodium pyrophosphate, 1 mM sodium orthovanadate, and protease inhibitor cocktail (Roche, #04693159001)], vortexing on low speed for 15 s, and shaking on an orbital shaker for 1 h at 4°C. Cell lysates were prepared in 1 mL modified RIPA buffer by rotating on a Nutator for 2 h. Lysates were then sonicated and centrifuged for 10 min at 10,000 x g to remove insoluble material, and the supernatant was taken as the whole cell lysate protein fraction.

Immunoblotting

Total EV protein concentrations were quantified using a Micro BCA™ Protein Assay Kit (Thermo Fisher Scientific, #23235) and cell lysate protein concentrations were quantified by Pierce™ BCA assay (Thermo Fisher Scientific, #23225). Proteins were resolved on 4%–15% TGX gels (BioRad, #5671085), transferred to nitrocellulose membrane, blocked in TBS-T (0.1% Tween-20) with 5% BSA, and probed as indicated. Densitometry was quantified using ImageJ (48). The following primary antibodies and dilution ratios were used for

immunoblotting experiments: anti-Actin—1:5000 (Millipore, #MAB1501); anti-TSG101—1:1000 (Abcam, #ab30871); anti-calnexin—1:1000 (Proteintech, #10427-2-AP).

Quantitative mass spectrometry proteomics

Sample Preparation: The Duke Proteomics and Metabolomics Core Facility (DPMCF) received 18 samples (3 biological replicates each of six conditions). Methods are as described in (37) with minor modifications and restated here for convenience: "Samples were first normalized to 20 µg and spiked with undigested casein at a total of 40, 80, or 160 fmol/µg, then reduced with 10 mM dithiolthreitol for 30 min at 80°C and alkylated with 20 mM iodoacetamide for 30 min at room temperature. Next, they were supplemented with a final concentration of 1.2% phosphoric acid and 741 µL of S-Trap (Protifi) binding buffer (90% MeOH/100 mM triethylammonium bicarbonate). Proteins were trapped on the S-Trap, digested using 20 ng/µL sequencing grade trypsin (Promega) for 1 h at 47°C, and eluted using 50 mM triethylammonium bicarbonate, followed by 0.2% formic acid, and lastly using 50% acetonitrile/0.2% formic acid All samples were then lyophilized to dryness and resuspended in 40 µL 1% trifluoracetic acid/2% acetonitrile containing 12.5 fmol/µL yeast alcohol dehydrogenase (ADH_YEAST). A Sample Pool QC (SPQC) was created from 3 uL of each sample. SPQCs were run periodically throughout the acquisition period.

Quantitative Analysis Methods: Quantitative LC-MS/MS was performed on 2 µL of each sample, using a nanoAcquity UPLC system (Waters Corp) coupled to a Thermo Orbitrap Fusion Lumos high resolution accurate mass tandem mass spectrometer (Thermo) *via* a nano-electrospray ionization source. Briefly, the sample was first trapped on a Symmetry C18 20 mm × 180 µm trapping column (5 µL/min at 99.9/0.1 v/v water/acetonitrile), after which the analytical separation was performed using a 1.8 µm Acquity HSS T3 C18 75 µm × 250 mm column (Waters Corp.) with a 90-min linear gradient of 5%–30% acetonitrile with 0.1% formic acid at a flow rate of 400 nL/min with a column temperature of 55°C. Data collection on the Fusion Lumos mass spectrometer was performed in a data-dependent acquisition (DDA) mode of acquisition with a r = 120,000 (at m/z 200) full MS scan from m/z 375 – 1500 with a target automatic gain control (AGC) value of 2e5 ions. MS/MS scans were acquired at Rapid scan rate (Ion Trap) with an AGC target of 5e3 ions and a max injection time of 25 m. The total cycle time between full MS scans was 2 s. A 20 s dynamic exclusion was employed to increase depth of coverage.

Proteomics Data Analysis: Following 22 total UPLC-MS/MS analyses (including 4 SPQC injections) were imported into Proteome Discoverer 2.3 (Thermo Scientific Inc.), and analyses were aligned based on the accurate mass and retention time of detected ions ("features") using Minora Feature Detector algorithm in Proteome Discoverer. Relative peptide abundance was calculated based on area-under-the-curve (AUC) of the selected ion chromatograms of the aligned features across all runs. The MS/MS data was searched against the SwissProt *M. musculus* database, SwissProt *bovine* database (downloaded Sept 2019) and an equal number of reversed sequence "decoys" for false discovery rate determination. Mascot Distiller and Mascot Server (v 2.5, Matrix Sciences) were utilized to produce fragment ion spectra and to perform the database searches. Database search parameters included fixed modification on Cys (carbamidomethyl) and variable modifications on Meth (oxidation) and Asn and Gln (deamidation). Full trypsin enzyme rules were selected with 2 ppm precursor and 0.8 Da product ion mass tolerances. Peptide Validator and Protein FDR Validator nodes in Proteome Discoverer were used to annotate the data at a maximum 1% protein false discovery rate.

Following data alignment and AUC quantitation, missing values were imputed in the following manner. If less than half of the values are missing within any one treatment group, values are imputed with an intensity derived from a normal distribution defined by measured values within the same intensity range (20 bins). If greater than half values are missing for a peptide in a group and a peptide intensity is > 5e6, then it was concluded that peptide was misaligned and its measured intensity is set to 0. All remaining missing values are imputed with the lowest 5% of all detected values. These data were then subjected to a sample loading normalization in which the total signals were summed and those summed values were used as normalizing factors across all samples. All peptide AUCs belonging to the same protein were then summed together to generate a protein level intensity" (37).

Data were analyzed using GraphPad Prism v9 and R v4.2.0. Hierarchical clustering was performed in R using Euclidean distance measures and average-linkage clustering (49).

Potential candidate biomarker criteria

For proteins, our DYT-TOR1A genotype-dependent subset of 363 differential proteins were annotated as "In Human Plasma" based on their presence in a public database, the Human Plasma Proteome Project (HPPP) (50, 51). The HPPP is a set of >3500 proteins that have been detected with varying degrees of evidence in different mass spectrometry studies. We focused on HPPP proteins that were detected in a minimum of 3 distinct studies. This criterion identified 164 of the 363 genotype-disrupted proteins.

We next used Cohen's *d* as a standardized effect size for each genotype and drug treatment condition. This was calculated using the formulas below (52), where n_1 and n_2 are group sample sizes, s_1 and s_2 are group standard deviations, and s^2_{pooled} is a pooled variance calculated using both groups' features.

$$\text{Cohen's } d = \frac{\bar{X}_{Exp.} - \bar{X}_{Control}}{s_{\text{pooled}}}$$

$$s^2_{\text{pooled}} = \sqrt{\frac{(n_1 - 1){s_1}^2 + (n_2 - 1){s_2}^2}{n_1 + n_2 - 2}}$$

To rank candidate proteins by their genotype and ritonavir-treatment effect sizes, the absolute value of Cohen's *d* for each condition was summed to make a combined score, "Absolute Cohen's *d* Sum (Geno+RTV)." Candidate biomarkers were filtered based on the directionality of their pharmacodynamic response to ritonavir and ISRIB being concordant with genotype predictions (ritonavir opposing genotype directionality, ISRIB reproducing genotype directionality). These criteria were then combined to stratify biomarker subsets as displayed in Supplemental Data Sheet S1.

Data availability statement

All raw data and Protein Discoverer results files that support this study are publicly available in MassIVE.ucsd.edu under the identifier MSV000090835.

Ethics statement

The animal study was reviewed and approved by Duke University IACUC.

Author contributions

CSK led and executed the majority of the experiments and analyses and generated initial drafts of manuscript and figures. ZFC, NC, and CSK jointly developed the project idea. ZFC and NC provided oversight and critical discussions throughout. NC provided funding and final oversight of data, analyses and publication materials. EJS provided expert consultation on sample preparation, oversaw execution of quantitative proteomic experiments in core facility and generation of the initial processing of the peptide results. All authors reviewed the final manuscript.

Funding

This work was supported by a Sponsored Research Agreement with Neurocrine Biosciences Inc. (to NC), Tyler's Hope for a Dystonia Cure Foundation (to NC), Department of Defense grant W81XWH1910018 (to NC), and the Dean's Summer Research Fellowship from Duke University's Trinity College (to CSK).

Conflict of interest

NC, CSK, and ZFC are co-inventors on W.I.P.O. patent application no. PCT/US2021/050296 entitled "Biomarker signatures for dystonia and uses thereof." NC and ZC are co-inventors on U.S. patent no. 10,857,145B2 entitled "Compositions and Methods for Identifying and Treating Dystonia Disorders." NC is a principal investigator on a biomarker research support agreement with Neurocrine Biosciences Inc. and served on the Medical and Scientific Advisory Council for the Dystonia Medical Research Foundation and scientific advisory boards for LabCorp Inc. and the Collaborative Center for X-Linked Dystonia Parkinsonism at Massachusetts General Hospital.

The remaining author declares that the research was conducted in the absence of any commercial or financial relationships that could be construed as a potential conflict of interest.

Acknowledgments

We thank Kunal Shroff, Miranda Shipman, Greg Waitt, Tricia Ho, and Michael Lutz for technical and analytical assistance. We thank the Duke University School of Medicine for the use of the Proteomics and Metabolomics Core Facility, which provided LC-MS/MS proteomics services. Figure 1A was created with BioRender. We are grateful to the reviewers for providing insightful suggestions to improve the manuscript.

Supplementary material

The Supplementary Material for this article can be found online at: https://www.frontierspartnerships.org/articles/10.3389/dyst.2023.11053/full#supplementary-material.

References

1. Balint B, Mencacci NE, Valente EM, Pisani A, Rothwell J, Jankovic J, et al. Dystonia. *Nat Rev Dis Prim* (2018) 4:25. doi:10.1038/s41572-018-0023-6

2. Ozelius LJ, Hewett JW, Page CE, Bressman SB, Kramer PL, Shalish C, et al. The early-onset torsion dystonia gene (DYT1) encodes an ATP-binding protein. *Nat Genet* (1997) 17(1):40–8. doi:10.1038/ng0997-40

3. Lungu C, Ozelius L, Standaert D, Hallett M, Sieber BA, Swanson-Fisher C, et al. Defining research priorities in dystonia. *Neurology* (2020) 94(12):526–37. doi:10.1212/wnl.0000000000009140

4. Caffall ZF, Wilkes BJ, Hernandez-Martinez R, Rittiner JE, Fox JT, Wan KK, et al. The HIV protease inhibitor, ritonavir, corrects diverse brain phenotypes across development in mouse model of DYT-TOR1A dystonia. *Sci Transl Med* (2021) 13(607):1–14. doi:10.1126/scitranslmed.abd3904

5. PharmaIntelligence. *Clinical development success rates and contributing factors*. PharmaIntelligence Rep (2020).

6. Takebe T, Imai R, Ono S. The current status of drug discovery and development as originated in United States academia: The influence of industrial and academic

collaboration on drug discovery and development. *Clin Transl Sci* (2018) 11(6): 597–606. doi:10.1111/cts.12577

7. FDA-NIH Biomarker Working Group. *BEST (biomarkers, EndpointS, and other tools) resource* (2021).

8. Califf RM. Biomarker definitions and their applications. *Exp Biol Med* (2018) 243(3):213–21. doi:10.1177/1535370217750088

9. Mateescu B, Jones JC, Alexander R, Alsop E, An JY, Asghari M, et al. Phase 2 of extracellular RNA communication consortium charts next-generation approaches for extracellular RNA research. *iScience* (2022) 25(8):104653. doi:10.1016/j.isci.2022.104653

10. Shah R, Patel T, Freedman J. Circulating extracellular vesicles in human disease. *N Engl J Med* (2018) 379(10):958–66. doi:10.1056/NEJMra1704286

11. Kraus VB. Biomarkers as drug development tools: discovery, validation, qualification and use. *Nat Rev Rheumatol* (2018) 14(6):354–62. doi:10.1038/s41584-018-0005-9

12. Fountzilas E, Tsimberidou AM, Vo HH, Kurzrock R. Clinical trial design in the era of precision medicine. *Genome Med* (2022) 14:101. doi:10.1186/s13073-022-01102-1

13. Hornung S, Dutta S, Bitan G. CNS-derived blood exosomes as a promising source of biomarkers: Opportunities and challenges. *Front Mol Neurosci* (2020) 13: 38. doi:10.3389/fnmol.2020.00038

14. Al Ali J, Vaine CA, Shah S, Campion L, Hakoum A, Supnet ML, et al. *TAF1* transcripts and neurofilament light chain as biomarkers for X-linked dystonia-parkinsonism. *Mov Disord* (2021) 36(1):206–15. doi:10.1002/mds.28305

15. Gaetani L, Blennow K, Calabresi P, Di Filippo M, Parnetti L, Zetterberg H. Neurofilament light chain as a biomarker in neurological disorders. *J Neurol Neurosurg Psychiatry* (2019) 90(8):870–81. doi:10.1136/jnnp-2018-320106

16. Defazio G, Abbruzzese G, Livrea P, Berardelli A. Epidemiology of primary dystonia. *Lancet Neurol* (2004) 3(11):673–8. doi:10.1016/S1474-4422(04)00907-X

17. Ozelius L, Lubarr N. *DYT1 early-onset isolated dystonia*. Seattle: University of Washington (2016). GeneReviews®.

18. Cruz L, György B, Cheah PS, Kleinstiver BP, Eimer WA, Garcia SP, et al. Mutant allele-specific CRISPR disruption in DYT1 dystonia fibroblasts restores cell function. *Mol Ther Nucleic Acids* (2020) 21:1–12. doi:10.1016/j.omtn.2020.05.009

19. Goodchild RE, Kim CE, Dauer WT. Loss of the dystonia-associated protein torsinA selectively disrupts the neuronal nuclear envelope. *Neuron* (2005) 48(6): 923–32. doi:10.1016/j.neuron.2005.11.010

20. Rittiner JE, Caffall ZF, Hernández-Martinez R, Sanderson SM, Pearson JL, Tsukayama KK, et al. Functional genomic analyses of mendelian and sporadic disease identify impaired eIF2α signaling as a generalizable mechanism for dystonia. *Neuron* (2016) 92(6):1238–51. doi:10.1016/j.neuron.2016.11.012

21. Théry C, Amigorena S, Raposo G, Clayton A. Isolation and characterization of exosomes from cell culture supernatants and biological fluids. *Curr Protoc Cel Biol* (2006) Chapter 3:Unit 3.22–9. doi:10.1002/0471143030.cb0322s30

22. Théry C, Witwer KW, Aikawa E, Jose Alcaraz M, Anderson JD, Jay SM, et al. Minimal information for studies of extracellular vesicles 2018 (MISEV2018): A position statement of the international society for extracellular vesicles and update of the MISEV2014 guidelines. *J Extracell Vesicles* (2018) 7:1535750. doi:10.1080/20013078.2018.1535750

23. Armstrong RA. When to use the Bonferroni correction. *Ophthalmic Physiol Opt* (2014) 34(5):502–8. doi:10.1111/opo.12131

24. Helseth AR, Hernandez-Martinez R, Hall VL, Oliver ML, Turner BD, Caffall ZF, et al. Cholinergic neurons constitutively engage the ISR for dopamine modulation and skill learning in mice. *Science* (2021) 372(6540):eabe1931. doi:10.1126/science.abe1931

25. Boyce M, Bryant KF, Jousse C, Long K, Harding HP, Scheuner D, et al. A selective inhibitor of eIF2alpha dephosphorylation protects cells from ER stress. *Science* (2005) 307(5711):935–9. doi:10.1126/science.1101902

26. De Gassart A, Bujisic B, Zaffalon L, Decosterd LA, Di Micco A, Frera G, et al. An inhibitor of HIV-1 protease modulates constitutive eIF2α dephosphorylation to trigger a specific integrated stress response. *Proc Natl Acad Sci U S A* (2016) 113(2): E117–26. doi:10.1073/pnas.1514076113

27. Schwenk JM, Omenn GS, Sun Z, Campbell DS, Baker MS, Overall CM, et al. The human plasma proteome draft of 2017: Building on the human plasma PeptideAtlas from mass spectrometry and complementary assays. *J Proteome Res* (2017) 16(12):4299–310. doi:10.1021/acs.jproteome.7b00467

28. Hewett JW, Tannous B, Niland BP, Nery FC, Zeng J, Li Y, et al. Mutant torsinA interferes with protein processing through the secretory pathway in DYT1 dystonia cells. *Proc Natl Acad Sci* (2007) 104(17):7271–6. doi:10.1073/pnas.0701185104

29. Pettersen Hessvik N, Llorente A. Current knowledge on exosome biogenesis and release. *Cell Mol Life Sci* (2018) 75:193–208. doi:10.1007/s00018-017-2595-9

30. Yáñez-Mó M, Siljander PR-M, Andreu Z, Bedina Zavec A, Borràs FE, Buzas EI, et al. Biological properties of extracellular vesicles and their physiological functions. *J Extracell Vesicles* (2015) 4(1):27066. doi:10.3402/jev.v4.27066

31. Tricarico C, Clancy J, D'souza-Schorey C. Biology and biogenesis of shed microvesicles. *Small GTPases* (2017) 8(4):220–32. doi:10.1080/21541248.2016.1215283

32. Zhang Q, Higginbotham JN, Jeppesen DK, Yang YP, Li W, McKinley ET, et al. Transfer of functional cargo in exomeres. *Cell Rep* (2019) 27(3):940–54. doi:10.1016/j.celrep.2019.01.009

33. Théry C, Amigorena S, Raposo G, Clayton A. Isolation and characterization of exosomes from cell culture supernatants and biological fluids. In: *Current protocols in cell biology*. John Wiley & Sons (2006). p. 3.22.1–3.22.29.

34. Naismith TV, Heuser JE, Breakefield XO, Hanson PI. TorsinA in the nuclear envelope. *Proc Natl Acad Sci* (2004) 101(20):7612–7. doi:10.1073/pnas.0308760101

35. Jokhi V, Ashley J, Nunnari J, Noma A, Ito N, Wakabayashi-Ito N, et al. Torsin mediates primary envelopment of large ribonucleoprotein granules at the nuclear envelope. *Cel Rep* (2013) 3(4):988–95. doi:10.1016/j.celrep.2013.03.015

36. Rampello AJ, Laudermilch E, Vishnoi N, Prophet SM, Shao L, Zhao C, et al. Torsin ATPase deficiency leads to defects in nuclear pore biogenesis and sequestration of MLF2. *J Cel Biol* (2020) 219(6):e201910185. doi:10.1083/jcb.201910185

37. Shroff K, Caffall ZF, Calakos N. DYT-TOR1A subcellular proteomics reveals selective vulnerability of the nuclear proteome to cell stress. *Neurobiol Dis* (2021) 158:105464. doi:10.1016/j.nbd.2021.105464

38. Pakos-Zebrucka K, Koryga I, Mnich K, Ljujic M, Samali A, Gorman AM. The integrated stress response. *EMBO Rep* (2016) 17(10):1374–95. doi:10.15252/embr.201642195

39. Vattem KM, Wek RC. Reinitiation involving upstream ORFs regulates ATF4 mRNA translation in mammalian cells. *Proc Natl Acad Sci* (2004) 101(31):11269–74. doi:10.1073/pnas.0400541101

40. Wek RC. Role of eIF2α kinases in translational control and adaptation to cellular stress. *Cold Spring Harb Perspect Biol* (2018) 10(7):a032870. doi:10.1101/cshperspect.a032870

41. Villarroya-Beltri C, Baixauli F, Gutiérrez-Vázquez C, Sánchez-Madrid F, Mittelbrunn M. Sorting it out: regulation of exosome loading. *Semin Cancer Biol* (2014) 28:3–13. doi:10.1016/j.semcancer.2014.04.009

42. Eninger T, Müller SA, Bacioglu M, Schweighauser M, Lambert M, Maia LF, et al. Signatures of glial activity can be detected in the CSF proteome. *Proc Natl Acad Sci* (2022) 119(24):e2119804119. doi:10.1073/pnas.2119804119

43. Musacchio T, Zech M, Reich MM, Winkelmann J, Volkmann J. A recurrent EIF2AK2 missense variant causes autosomal-dominant isolated dystonia. *Ann Neurol* (2021) 89(6):1257–8. doi:10.1002/ana.26081

44. Kuipers DJS, Mandemakers W, Lu CS, Olgiati S, Breedveld GJ, Fevga C, et al. EIF2AK2 missense variants associated with early onset generalized dystonia. *Ann Neurol* (2021) 89(3):485–97. doi:10.1002/ana.25973

45. Burnett SB, Vaughn LS, Sharma N, Kulkarni R, Patel RC. Dystonia 16 (DYT16) mutations in PACT cause dysregulated PKR activation and eIF2α signaling leading to a compromised stress response. *Neurobiol Dis* (2020) 146: 105135. doi:10.1016/j.nbd.2020.105135

46. Zakirova Z, Fanutza T, Bonet J, Readhead B, Zhang W, Yi Z, et al. Mutations in THAP1/DYT6 reveal that diverse dystonia genes disrupt similar neuronal pathways and functions. *PLOS Genet* (2018) 14(1):e1007169. doi:10.1371/journal.pgen.1007169

47. Guha D, Lorenz DR, Misra V, Chettimada S, Morgello S, Gabuzda D. Proteomic analysis of cerebrospinal fluid extracellular vesicles reveals synaptic injury, inflammation, and stress response markers in HIV patients with cognitive impairment. *J Neuroinflammation* (2019) 16(1):254. doi:10.1186/s12974-019-1617-y

48. Schneider CA, Rasband WS, Eliceiri KW. NIH image to ImageJ: 25 years of image analysis. *Nat Methods* (2012) 9(7):671–5. doi:10.1038/nmeth.2089

49. Crameri F. *Scientific colour maps*. Zenodo (2021).

50. Ignjatovic V, Geyer PE, Palaniappan K, Chaaban J, Omenn G, Baker M, et al. Mass spectrometry-based plasma proteomics: Considerations from sample collection to achieving translational data. *J Proteome Res* (2019) 18:4085–97. doi:10.1021/acs.jproteome.9b00503

51. Deutsch EW, Omenn GS, Sun Z, Maes M, Pernemalm M, Palaniappan KK, et al. Advances and utility of the human plasma proteome. *J Proteome Res* (2021) 20(12):5241–63. doi:10.1021/acs.jproteome.1c00657

52. Lee DK. Alternatives to P value: confidence interval and effect size. *Korean J Anesthesiol* (2016) 69(6):555–62. doi:10.4097/kjae.2016.69.6.555

DYSTONIA

Dystonia is the official journal of
the Dystonia Medical Research Foundation

The mission of the DMRF is to advance research for more treatments and ultimately a cure, to promote awareness and education, and to support the needs and well being of affected individuals and families.

Discover more of our Special Issues

See more →

fro.ntiers.in/special-issue
frontierspartnerships.org

Contact

+41 (0) 21 510 17 40
dystonia@frontierspartnerships.org